Mon. Not. R. Astron. Soc. **000**, 1–43 (2014) Printed 18 June 2015 (MN LATEX style file v2.2)

Spatial distribution of Galactic Wolf-Rayet stars and implications for the global population

C. K. Rosslowe⋆ and P. A. Crowther
Dept of Physics and Astronomy, University of Sheffield, Hicks Building, Hounsfield Road, S3 7RH, United Kingdom

arXiv:1412.0699v2 [astro-ph.SR] 17 Jun 2015

ABSTRACT

We construct revised near-infrared absolute magnitude calibrations for 126 Galactic Wolf-Rayet (WR) stars at known distances, based in part upon recent large scale spectroscopic surveys. Application to 246 WR stars located in the field, permits us to map their Galactic distribution. As anticipated, WR stars generally lie in the thin disk (∼40 pc half width at half maximum) between Galactocentric radii 3.5–10 kpc, in accordance with other star formation tracers. We highlight 12 WR stars located at vertical distances of $\geqslant$300 pc from the midplane. Analysis of the radial variation in WR subtypes exposes a ubiquitously higher N_{WC}/N_{WN} ratio than predicted by stellar evolutionary models accounting for stellar rotation. Models for non-rotating stars or accounting for close binary evolution are more consistent with observations. We consolidate information acquired about the known WR content of the Milky Way to build a simple model of the complete population. We derive observable quantities over a range of wavelengths, allowing us to estimate a total number of 1200^{+300}_{-100} Galactic WR stars, implying an average duration of ~ 0.25 Myr for the WR phase at the current Milky Way star formation rate. Of relevance to future spectroscopic surveys, we use this model WR population to predict follow-up spectroscopy to $K_S \simeq 13$ mag will be necessary to identify 95% of Galactic WR stars. We anticipate that ESA's *Gaia* mission will make few additional WR star discoveries via low-resolution spectroscopy, though will significantly refine existing distance determinations. Appendix A provides a complete inventory of 322 Galactic WR stars discovered since the VIIth catalogue (313 including Annex), including a revised nomenclature scheme.

Key words: stars: Wolf-Rayet - stars: evolution - stars: massive - stars: distances - infrared: stars - Galaxy: disc

1 INTRODUCTION

Massive stars exert a major influence on their immediate surroundings, and play a dominant role in the evolution of their host galaxies. Wolf-Rayet (WR) stars represent the ultimate, short-lived (< 1Myr) evolutionary phase of only the most massive ($M_i > 25\,M_\odot$) O-stars (see Crowther 2007). They possess dense and fast stellar winds, giving them characteristic strong and broad emission line spectra. Their distinctive spectral appearance befits them as effective tracers of high-mass star formation both in the Galaxy (e.g., Kurtev et al. 2007; Davies et al. 2012) and at extra-galactic distances (Schaerer & Vacca 1998). Through their powerful winds and likely fate as Type Ib/c supernovae, they are important sources of nuclear processed material to the interstellar medium (ISM; Esteban & Peimbert 1995; Dray et al. 2003), and are capable of influencing further episodes of star formation on local (Shetty & Ostriker 2008; Kendrew et al. 2012) and galactic (Hopkins, Quataert & Murray 2011) scales. However, the postulated link between WR stars and H-free Type Ib/c SN remains unestablished (Eldridge et al. 2013), hence it is crucial we better our knowledge of the uniquely resolvable population in the Milky Way.

Strong mass-loss in WR stars proceeds to unveil successive layers of nuclear processed material, such that examples are seen with spectra dominated by nitrogen (WN), carbon (WC), and oxygen (WO). WC and WO stars are universally H-free and He-rich, whereas the surface H mass fraction of WN stars varies from zero to $X_H \simeq 50\%$. A subset of H-rich WN stars display weak hydrogen emission and *intrinsic* hydrogen absorption lines, referred to here as WNha stars (see Crowther & Walborn 2011). These stars are almost uniquely found in young clusters, suggesting current masses $>65\,M_\odot$ from cluster turn-offs and higher luminosities than their core He-burning counterparts (Crowther et al. 1995a), and hence are very rare. They differ from 'classical' He core-burning WR stars in that they represent an extension of the upper

⋆ Email: chris.rosslowe@sheffield.ac.uk

© 2014 RAS

main-sequence, and are thought to be H-burning. We treat these objects separately from other WN stars when calibrating absolute magnitudes.

Our knowledge of the Galaxy's Wolf-Rayet content rests on the successive achievements of tailored imaging surveys. The use of narrow-band selection techniques was pioneered by Massey & Conti (1983) and Moffat & Shara (1983) to identify extra-galactic WR stars, taking advantage of strong WR star emission lines at optical wavelengths. Shara et al. (1991, 1999) applied similar methods to push the extent of the known Galactic population beyond 5 kpc from the Sun, and extension to near-IR wavelengths has facilitated yet deeper investigation of the Galactic disk (Shara et al. 2009, 2012). Another distinctive feature of WR stars - the near-IR excess caused by free-free emission in their winds - has been exploited to yield further discoveries (Homeier et al. 2003; Hadfield et al. 2007; Mauerhan, Van Dyk & Morris 2011). These efforts, alongside several serendipitous discoveries (e.g., Clark et al. 2005, Mauerhan et al. 2010a), have brought the recognised Galactic WR star population to ∼635 as of March 2014[1].

Several attempts have been made to determine the total number of WR stars in the Galaxy. Maeder & Lequeux (1982) used the then-known 157 WR stars to arrive at a total of ∼1,200 by assuming the surface density of WR stars to vary with Galactocentric radius (R_G) in the same way as giant HII-regions, including a dearth at $R_G \lesssim 3$kpc. To emphasise the need for IR investigation, Shara et al. (1999) created a model WR star population featuring a stellar disk of exponentially increasing density towards $R_G = 0$. From this they inferred a total of 2,500 Galactic WR stars, or 1,500 if few WR stars inhabit the region $R_G \lesssim 3$kpc, as the decline in gas density suggests (barring the inner 500 pc). van der Hucht (2001) arrived at a much higher 6,500 WR stars by extrapolating the surface density of local WR stars (7kpc$< R_G <$ 12kpc) across the entire disk, neglecting the decrease in star formation rate interior to $R_G \sim 3$kpc. Most recently, in the light of numerous WR star discoveries in IR surveys, Shara et al. (2009) presented an updated population model - still featuring an exponential disk of stars - yielding a total of 6,400. The same work also suggested that observations of WR stars as faint as $K \simeq 15.5$ mag are necessary to achieve a completeness of 95%.

The Galaxy provides a range of environments over which to test various predictions of massive star evolution, which has long been expected to depend on metallicity (Z). As the winds of hot stars are driven by the transfer of photon momentum to metal-lines (see Puls, Vink & Najarro (2008) for a recent review), and mass-loss dominates the evolutionary fate of the most massive stars, we expect to observe differences between the population of evolved massive stars in the metal-rich Galactic Centre (GC) regions, and that of the metal-poor outer Galaxy. Smith (1968) first observationally demonstrated evidence for differences in WR populations between the Milky Way and Magellanic Clouds. Crowther et al. (2002) showed that WC subtype variations are primarily a consequence of denser stellar winds at higher metallicity, while WN stars have long been known to be a more heterogeneous group. Increased mass-loss is predicted to have two main effects of WR surface properties; more efficient removal of outer (hydrogen-rich) layers will lead to quicker progression through post main-sequence evolutionary phases i.e., from WN to WC stages, and the accelerated spin-down of a star due to loss of angular momentum will inhibit various internal mixing processes, with implications for the lifetimes of evolutionary phases (Maeder & Meynet 2000). Systematic testing of such predictions requires statistically significant, unbiased samples of evolved massive stars, currently only available through IR investigation of the Galactic disk.

An improved set of IR tools are necessary to reveal and characterise the full Galactic WR population, allowing accurate distances and classifications to be obtained. In Section 2 we introduce improved near-IR absolute magnitude-spectral type calibrations for WR stars. In Section 3 these calibrations are applied to estimate distances to the majority of the known WR population, from which the radial variation of WR subtypes is obtained, allowing a comparison with evolutionary model predictions. In Section 4 we develop a toy model to estimate the global WR population of the Milky Way. Finally, we make predictions about the detectability of WR stars, which may be of interest to those planning future surveys. Our findings are summarised in Section 5. Appendix A lists all 322 Galactic Wolf-Rayet stars discovered since the VIIth catalogue of van der Hucht (2001) and its Annex (van der Hucht 2006).

2 CALIBRATION OF IR ABSOLUTE MAGNITUDES FOR WR STARS

van der Hucht (2001) reviewed and updated the v-band absolute magnitude for Galactic Wolf-Rayet stars. However, the accuracy and usefulness of this relation is limited by the relatively small number of WR stars observable at optical wavelengths. Recent discoveries of visibly obscured WR stars provide a much larger sample, from which broad-band calibrations in the near-IR may be obtained. In this section we present a calibration of absolute magnitudes over the wavelength range 1–8μm for each WR spectral type, extending earlier results by Crowther et al. (2006b) via additional WR stars located within star clusters that have been identified within the past decade.

2.1 Calibration sample

Adopted distances and spectral types for the WR stars used for our IR absolute magnitude calibration are shown in Tables 1, 2 & 3 for WC/WO stars, WN stars, and WR stars in binary systems with OB companions respectively. This sample is drawn from an updated online catalogue of Galactic WR stars[1] and totals 126, with 91 inhabiting clusters, 26 in OB associations and 9 appearing 'isolated'. By subtype, 85 of these are Nitrogen (WN) type, 40 Carbon (WC) type, and 1 Oxygen (WO) type. For OB associations that have been historically well studied at optical wavelengths, membership is taken from Lundström & Stenholm (1984). For WR stars in visually obscured clusters we generally accept the membership conclusions of the discovering author(s), except where noted.

For most star clusters and associations considered, there

[1] http://pacrowther.staff.shef.ac.uk/WRcat/

is typically more than one distance measurement to be found in the literature. Where these measurements are in general agreement we favour methods of OB-star spectrophotometry over main-sequence fitting. A small number of WR stars, in relative isolation, have kinematic distances derived from velocity measurements of an associated nebula; we accept these distances but remain wary of kinematic distance estimates in general because of their sensitivity to the assumed Galactic rotation curve.

Where multiple consistent distance estimates are found in the literature we take an average of the reported distances - weighted by the square of the inverse uncertainty reported on each (e.g., Westerlund 1 and Car OB1) - indicated by multiple references in Tables 1 – 3. Cases in which inconsistent distances have been reported in the literature are discussed further in Appendix B.

Table 1. Apparently single dust-free WO and WC stars, and dust-producing WC stars of known distance used to calibrate near-IR absolute magnitudes by spectral type. New nomenclature is explained in Appendix A.

Sp. Type	WR#	Cluster	Association	Distance (kpc)	Ref	J	H	K_S	Ref	$A^J_{K_S}$	$A^H_{K_S}$	$\bar{A}_{K_S}$	M_{K_S}
WO2	142	Berkeley 87		1.23 ± 0.04	1	9.54	8.89	8.60	a,a,a	0.40	0.41	0.41 ± 0.01	-2.26 ± 0.07
WC4	144		Cyg OB2	1.40 ± 0.08	2	9.41	8.59	7.71	a,a,a	0.51	0.43	0.48 ± 0.02	-3.50 ± 0.13
WC5	111		Sgr OB1	1.9 ± 0.2	3, 4	7.28	7.14	6.51	a,a,a	0.07	0.07	0.07 ± 0.01	-4.95 ± 0.23
	114		Ser OB1	2.05 ± 0.09	5, 6	8.98	8.43	7.61	a,a,a	0.36	0.34	0.35 ± 0.02	-4.30 ± 0.10
WC6	23		Car OB1	2.6 ± 0.2	7, 8	7.89	7.60	7.06	a,a,a	0.10	...	0.10 ± 0.03	-5.12 ± 0.17
	*48-4	Danks 1		4.16 ± 0.60	9	13.16	11.82	10.78	a,a,a	0.84	0.65	0.75 ± 0.03	-3.06 ± 0.32
	154		Cep OB1	3.5 ± 1.0	10	9.30	9.01	8.29	a,a,a	0.19	0.20	0.19 ± 0.01	-4.62 ± 0.62
WC7	14		Anon Vel a	2.0 ± 0.1	11	7.49	7.25	6.61	a,a,a	0.12	0.07	0.11 ± 0.01	-5.00 ± 0.11
	68		Cir OB1	3.6 ± 0.3	12	9.90	9.39	8.75	a,a,a	0.25	0.08	0.20 ± 0.02	-4.23 ± 0.18
WC8	48-3	(G305.4+0.1)/Danks 1		4.16 ± 0.60	9	10.75	9.57	8.77	a,a,a	0.74	0.59	0.67 ± 0.03	-4.99 ± 0.32
	48-2	Danks 2		4.16 ± 0.60	9	10.83	9.83	8.98	a,a,a	0.67	0.66	0.67 ± 0.03	-4.78 ± 0.32
	77g	Westerlund 1		4.0 ± 0.2	13, 14	11.81	10.40	9.53	b,b,b	0.88	0.69	0.81 ± 0.04	-4.29 ± 0.13
	102k	Quintuplet		8.00 ± 0.25	15, 16	16.71	13.45	11.19	d,d,a	2.49	2.55	2.50 ± 0.08	-5.83 ± 0.12
	*124-1	Glimpse 20		4.45 ± 0.65	17	...	10.38	9.19	a,a	...	1.14	1.14 ± 0.10	-5.20 ± 0.33
	135		Cyg OB3	1.9 ± 0.2	18	7.23	7.11	6.66	a,a,a	0.07	0.10	0.08 ± 0.01	-4.81 ± 0.23
WC9	77p	Westerlund 1		4.0 ± 0.2	13, 14	10.12	9.09	8.29	b,b,b	0.76	0.76	0.76 ± 0.05	-5.48 ± 0.16
	101f	GC		8.00 ± 0.25	15, 16	18.78	15.43	13.11	e,e,e	2.65	2.78	2.72 ± 0.04	-4.12 ± 0.08
	101oa	GC		8.00 ± 0.25	15, 16	18.48	15.43	13.01	e,e,e	2.56	2.92	2.72 ± 0.04	-4.23 ± 0.08
	102h	Quintuplet		8.00 ± 0.25	15, 16	16.62	13.51	11.34	d,d,a	2.47	2.58	2.50 ± 0.08	-5.68 ± 0.12
WC8d	53			4.00 ± 1.00	19	8.75	7.92	6.84	a,a,a	...	...	$0.29 \pm 0.09^{\ddagger}$	-6.43 ± 0.55
	102e	Quintuplet		8.00 ± 0.25	15, 16	17.5	13.3	10.4	d,d,d	...	...	$3.1 \pm 0.5^{\dagger}$	-7.22 ± 0.51
	102f	Quintuplet		8.00 ± 0.25	15, 16	...	...	10.4	c	...	...	$3.1 \pm 0.5^{\dagger}$	-7.22 ± 0.51
	113			2.0 ± 0.2	20	7.02	6.28	5.49	a,a,a	...	...	$0.38 \pm 0.01^{\ddagger}$	-6.37 ± 0.22
WC9d	65		Cir OB1	3.6 ± 0.3	12	8.46	7.28	6.17	a,a,a	...	...	$0.91 \pm 0.04^{\ddagger}$	-7.45 ± 0.19
	77aa	Westerlund 1		4.00 ± 0.25	13,14	10.04	8.21	6.72	b,b,b	...	...	$1.01 \pm 0.14^{\dagger}$	-7.30 ± 0.20
	77b	Westerlund 1		4.00 ± 0.25	13,14	9.69	7.84	6.41	b,b,b	...	...	$1.01 \pm 0.14^{\dagger}$	-7.61 ± 0.20
	77i	Westerlund 1		4.00 ± 0.25	13,14	10.13	7.64	6.90	b,b,b	...	...	$1.01 \pm 0.14^{\dagger}$	-7.12 ± 0.22
	77l	Westerlund 1		4.00 ± 0.25	13,14	10.31	8.56	7.38	b,b,b	...	...	$1.01 \pm 0.14^{\dagger}$	-6.64 ± 0.20
	77m	Westerlund 1		4.00 ± 0.25	13,14	11.26	9.51	8.23	b,b,b	...	...	$1.01 \pm 0.14^{\dagger}$	-5.79 ± 0.20
	77n	Westerlund 1		4.00 ± 0.25	13,14	9.85	7.97	7.28	b,b,b	...	...	$1.01 \pm 0.14^{\dagger}$	-6.74 ± 0.20
	95	Trumpler 27		2.5 ± 0.5	21	8.29	6.67	5.27	a,a,a	...	...	$0.66 \pm 0.03^{\dagger b}$	-7.38 ± 0.44
	101ea	GC		8.00 ± 0.25	15,16	17.79	13.46	10.50	f,f,f	...	...	3.2 ± 0.2	-7.22 ± 0.22
	102-2	Quintuplet		8.00 ± 0.25	15,16	...	...	10.30	c	...	...	$3.1 \pm 0.5^{\dagger}$	-7.32 ± 0.51
	102-3	Quintuplet		8.00 ± 0.25	15,16	15.49	11.71	9.32	d,d,d	...	...	$3.1 \pm 0.5^{\dagger}$	-8.30 ± 0.51
	104			2.6 ± 0.7	4	6.67	4.34	2.42	a,a,a	...	...	$0.86 \pm 0.02^{\ddagger}$	-10.44 ± 0.64

Continued on next page...

© 2014 RAS, MNRAS **000**, 1–43

Continued from previous page

Sp. Type	WR#	Cluster	Association	Distance (kpc)	Ref	J	H	K_S	Ref	$A^J_{K_S}$	$A^H_{K_S}$	$\bar{A}_{K_S}$	M_{K_S}
	111a	SGR 1806-20		8.70 ± 1.65	22	...	13.76	11.60	g,g	...	...	$3.0 \pm 0.3^{\dagger}$	-6.10 ± 0.51
	118-1	Quartet		6.3 ± 0.2	17	13.22	10.14	8.09	a,a,a	...	...	$1.6 \pm 0.4^{\dagger}$	-7.51 ± 0.41

*Indicates updated spectral types based on an improved near-IR classification scheme.
Distance references: (1)Turner et al. (2006), (2)Rygl et al. (2012), (3)Mel'Nik & Dambis (2009), (4)Tuthill et al. (2008), (5)Hillenbrand et al. (1993), (6)Djurašević et al. (2001), (7)Smith (2006), (8)Hur, Sung & Bessell (2012), (9)Davies et al. (2012a), (10)Cappa et al. (2010), (11)Lundström & Stenholm (1984), (12)Vazquez et al. (1995), (13)Kothes & Dougherty (2007), (14)Koumpia & Bonanos (2012), (15)Reid et al. (2009), (16)Gillessen et al. (2013), (17)Messineo et al. (2009), (18)Reid et al. (2011), (19)Martín, Cappa & Testori (2007), (20)Esteban & Rosado (1995), (21)Crowther et al. (2006b), (22)Bibby et al. (2008).
Photometry references: (a)2MASS, (b)Crowther et al. (2006b), (c)Liermann, Hamann & Oskinova (2009), (d)Figer, McLean & Morris (1999), (e)Dong, Wang & Morris (2012), (f)Eikenberry et al. (2004), (g)Bibby et al. (2008).
Extinction: †Average of parent cluster, ‡A_v taken from van der Hucht (2001) and converted using $A_K = 0.12A_v$.

Table 2. Apparently single WN stars (and those with an insignificant companion contribution at IR wavelengths) of known distance used to calibrate near-IR absolute magnitudes by spectral type. New nomenclature is explained in Appendix A.

Spect Type	WR#	Cluster	Association	Distance(kpc)	Ref	J	H	K_S	Ref	$A^J_{K_S}$	$A^H_{K_S}$	$\bar{A}_{K_S}$	M_{K_S}
WN2b	2		Cas OB1	2.4 ± 0.8	23	10.04	9.78	9.45	a,a,a	0.33	0.52	0.40 ± 0.02	-2.86 ± 0.72
WN3b	46		Cru OB4	4.00 ± 0.85	24, 25	10.20	10.08	9.83	a,a,a	0.23	0.39	0.27 ± 0.01	-3.45 ± 0.46
WN4b	1		Cas OB7	2.3 ± 0.5	3	8.21	7.86	7.48	a,a,a	0.17	0.15	0.17 ± 0.01	-4.49 ± 0.47
	6			1.80 ± 0.27	26	6.35	6.23	5.89	a,a,a	0.04	0.09	0.05 ± 0.01	-5.44 ± 0.33
	7			5.5 ± 0.5	27	9.97	9.67	9.27	a,a,a	0.16	0.19	0.17 ± 0.01	-4.60 ± 0.20
	18		Car OB1	2.6 ± 0.2	7, 8	8.57	8.21	7.68	a,a,a	0.25	0.36	0.27 ± 0.02	-4.67 ± 0.17
	35b	Sher 1		10.0 ± 1.4	28	10.95	10.35	9.76	a,a,a	0.39	0.46	0.41 ± 0.03	-5.65 ± 0.31
WN6b	*102c	Quintuplet		8.00 ± 0.25	15, 16	...	13.12	11.53	d,d	...	1.78	1.78 ± 0.38	-4.77 ± 0.44
	111c	SGR 1806-20		8.70 ± 1.65	22	...	14.03	12.16	f,f	...	2.25	2.25 ± 0.15	-4.79 ± 0.44
	134		Cyg OB3	1.9 ± 0.2	18	6.72	6.52	6.13	a,a,a	0.10	0.17	0.12 ± 0.01	-5.39 ± 0.23
	136		Cyg OB1	1.3 ± 0.2	29	6.13	5.90	5.56	a,a,a	0.09	0.10	0.09 ± 0.01	-5.10 ± 0.33
WN7b	77sc	Westerlund 1		4.0 ± 0.2	13, 14	10.34	9.11	8.37	b,b,b	0.76	0.66	0.74 ± 0.05	-5.38 ± 0.16
	111-2	Cl 1813-178		3.6 ± 0.7	30	9.62	8.60	7.94	a,a,a	0.62	0.55	0.59 ± 0.03	-5.44 ± 0.42
WN3	152		Cep OB1	3.5 ± 1.0	10	10.49	10.32	10.04	a,a,a	0.26	0.43	0.31 ± 0.02	-2.99 ± 0.62
WN5	77e	Westerlund 1		4.0 ± 0.2	13, 14	11.70	10.30	9.70	b,b,b	0.87	0.62	0.79 ± 0.06	-4.10 ± 0.16
	77q	Westerlund 1		4.0 ± 0.2	13, 14	11.92	10.84	10.26	b,b,b	0.70	0.59	0.67 ± 0.04	-3.42 ± 0.13
	77sd	Westerlund 1		4.0 ± 0.2	13, 14	12.36	11.08	10.25	b,b,b	0.92	0.94	0.93 ± 0.04	-3.69 ± 0.13
WN6	67	Pismis 20	Cir OB1	3.6 ± 0.3	12	9.28	8.86	8.45	a,a,a	0.31	0.35	0.32 ± 0.02	-4.65 ± 0.18
	77sb	Westerlund 1		4.0 ± 0.2	13, 14	11.00	9.98	9.45	b,b,b	0.65	0.52	0.61 ± 0.04	-4.17 ± 0.12
	77a	Westerlund 1		4.0 ± 0.2	13, 14	11.72	10.67	10.00	b,b,b	0.73	0.72	0.73 ± 0.04	-3.74 ± 0.13
	77s	Westerlund 1		4.0 ± 0.2	13, 14	10.77	9.72	9.20	b,b,b	0.66	0.51	0.61 ± 0.04	-4.42 ± 0.12
	85			2.8 ± 1.1	31	...	7.94	7.48	a,a	...	0.43	0.43 ± 0.16	-5.19 ± 0.87
	*101o	GC		8.00 ± 0.25	15, 16	17.94	14.13	11.60	e,e,e	3.00	3.20	3.11 ± 0.04	-6.02 ± 0.08
	115		Ser OB1	2.05 ± 0.09	5, 6	7.99	7.42	6.95	a,a,a	0.41	0.44	0.42 ± 0.02	-5.03 ± 0.10
WN7	75ba			4.1 ± 0.4	32	10.22	9.29	8.91	a,a,a	0.56	0.39	0.51 ± 0.04	-4.67 ± 0.23
	77r	Westerlund 1		4.0 ± 0.2	13, 14	11.63	10.31	9.61	b,b,b	0.90	0.83	0.87 ± 0.04	-4.27 ± 0.13
	77j	Westerlund 1		4.0 ± 0.2	13, 14	11.36	9.97	9.28	b,b,b	0.93	0.82	0.89 ± 0.04	-4.62 ± 0.13
	77d	Westerlund 1		4.0 ± 0.2	13, 14	11.06	9.83	9.26	b,b,b	0.80	0.65	0.74 ± 0.04	-4.49 ± 0.13
	*77sa	Westerlund 1		4.0 ± 0.2	13, 14	12.11	10.75	10.04	b,b,b	0.92	0.85	0.89 ± 0.04	-3.86 ± 0.13
	78	NGC 6231	Sco OB1	1.64 ± 0.03	33	5.44	5.27	4.98	a,a,a	0.16	0.25	0.18 ± 0.01	-6.27 ± 0.05
	87	Halven-Moffat 1		3.3 ± 0.3	34	8.00	7.45	7.09	a,a,a	0.37	0.36	0.37 ± 0.02	-5.88 ± 0.20
	*101ai	GC		8.00 ± 0.25	15, 16	...	14.33	12.12	e,e	...	2.84	2.84 ± 0.07	-5.23 ± 0.10
	*111-4	Cl 1813-178		3.6 ± 0.7	30	10.31	9.27	8.66	a,a,a	0.72	0.70	0.71 ± 0.03	-4.84 ± 0.42
WN8	12•	Bochum 7		4.2 ± 2.1	35	8.62	8.26	7.87	a,a,a	0.29	0.40	0.32 ± 0.02	-5.57 ± 1.09
	*48-7	Danks 1		4.16 ± 0.60	9	9.81	8.48	7.65	a,a,a	0.97	1.01	0.99 ± 0.04	-6.43 ± 0.32
	66		Cir OB1	3.6 ± 0.3	12	8.93	8.48	8.15	a,a,a	0.31	0.31	0.31 ± 0.02	-4.94 ± 0.18

Continued on next page...

Continued from previous page

Spect Type	WR#	Cluster	Association	Distance(kpc)	Ref	J	H	K_S	Ref	$A^J_{K_S}$	$A^H_{K_S}$	$\bar{A}_{K_S}$	M_{K_S}
	77c	Westerlund 1		4.0 ± 0.2	13, 14	10.89	9.57	8.86	b,b,b	0.90	0.85	0.88 ± 0.04	-5.03 ± 0.13
	77h	Westerlund 1		4.0 ± 0.2	13, 14	10.75	9.42	8.76	b,b,b	0.89	0.77	0.84 ± 0.04	-5.09 ± 0.13
	89	Halven-Moffat 2		3.3 ± 0.3	34	7.39	6.96	6.58	a,a,a	0.32	0.39	0.34 ± 0.02	-6.36 ± 0.20
	101b	GC		8.00 ± 0.25	15, 16	...	13.53	11.43	e,e	...	2.69	2.69 ± 0.06	-5.77 ± 0.09
	101nc	GC		8.00 ± 0.25	15, 16	17.38	14.23	11.91	e,e,e	2.60	2.99	2.79 ± 0.04	-5.40 ± 0.08
	*101oc	GC		8.00 ± 0.25	15, 16	18.66	14.93	12.61	e,e,e	2.89	2.99	2.94 ± 0.04	-4.85 ± 0.08
	*101dd	GC		8.00 ± 0.25	15, 16	18.96	15.43	13.01	e,e,e	2.84	3.12	2.98 ± 0.04	-4.49 ± 0.08
	102a	Arches		8.00 ± 0.25	15, 16	17.17	13.26	11.02	h,a,a	2.94	2.88	2.91 ± 0.05	-6.40 ± 0.10
	*102ae	Arches		8.00 ± 0.25	15, 16	15.43	12.40	10.62	i,i,i	2.28	2.25	2.27 ± 0.02	-6.16 ± 0.07
	*102af	Arches		8.00 ± 0.25	15, 16	15.97	12.81	10.88	i,i,i	2.42	2.46	2.44 ± 0.03	-6.08 ± 0.07
	*102ah	Arches		8.00 ± 0.25	15, 16	15.23	12.03	10.07	i,i,i	2.45	2.50	2.48 ± 0.03	-6.92 ± 0.07
	*102al	Arches		8.00 ± 0.25	15, 16	15.11	12.09	10.24	i,i,i	2.31	2.34	2.33 ± 0.02	-6.60 ± 0.07
	124			3.35 ± 0.67	36	8.58	8.18	7.73	a,a,a	0.34	0.47	0.39 ± 0.02	-5.28 ± 0.44
WN9	*48-6	(G305.4+0.1)/Danks 1		4.16 ± 0.60	9	10.21	8.57	7.58	a,a,a	1.19	1.24	1.21 ± 0.05	-6.73 ± 0.32
	*48-10	Danks 1		4.16 ± 0.60	9	9.42	8.15	7.48	a,a,a	0.86	0.79	0.83 ± 0.04	-6.45 ± 0.32
	48-9	Danks 1		4.16 ± 0.60	9	8.26	7.27	6.61	a,a,a	0.72	0.77	0.74 ± 0.03	-7.22 ± 0.32
	77k	Westerlund 1		4.0 ± 0.2	13, 14	9.08	7.72	7.19	b,b,b	0.84	0.59	0.75 ± 0.04	-6.57 ± 0.13
	*101m	GC		8.00 ± 0.25	15, 16	16.58	13.53	11.32	e,e,e	2.50	2.84	2.67 ± 0.03	-5.86 ± 0.08
	*101e	GC		8.00 ± 0.25	15, 16	15.87	12.73	10.41	e,e,e	2.60	2.99	2.79 ± 0.04	-6.90 ± 0.08
	*102aa	Arches		8.00 ± 0.25	15, 16	...	...	11.18	j	...	...	$2.48 \pm 0.37^{\dagger}$	-5.82 ± 0.39
	*102ad	Arches		8.00 ± 0.25	15, 16	15.86	12.44	10.35	i,i,i	2.63	2.69	2.66 ± 0.03	-6.83 ± 0.08
	*102ag	Arches		8.00 ± 0.25	15, 16	15.67	12.45	10.46	i,i,i	2.48	2.55	2.52 ± 0.03	-6.58 ± 0.07
	*102ai	Arches		8.00 ± 0.25	15, 16	...	12.24	10.34	a,a	...	2.41	2.41 ± 0.19	-6.59 ± 0.22
	*102aj	Arches		8.00 ± 0.25	15, 16	16.55	13.56	11.79	i,i,i	2.26	2.24	2.25 ± 0.02	-4.98 ± 0.07
	*102bb	Arches		8.00 ± 0.25	15, 16	15.58	12.36	10.36	i,i,i	2.48	2.54	2.52 ± 0.03	-6.67 ± 0.07
	*102bc	Arches		8.00 ± 0.25	15, 16	...	13.14	11.20	i,i	...	2.47	2.47 ± 0.13	-5.79 ± 0.16
	102d	Quintuplet		8.00 ± 0.25	15, 16	15.58	12.40	10.50	d,d,c	2.41	2.42	2.42 ± 0.09	-6.43 ± 0.15
	102hb	Quintuplet		8.00 ± 0.25	15, 16	14.19	10.90	9.60	d,d,c	2.18	1.61	2.01 ± 0.09	-6.93 ± 0.15
	102i	Quintuplet		8.00 ± 0.25	15, 16	14.77	11.67	10.22	d,a,a	2.16	1.81	1.98 ± 0.05	-6.27 ± 0.10
	102j	Quintuplet		8.00 ± 0.25	15, 16	14.66	11.77	10.23	a,a,a	2.10	1.94	2.03 ± 0.03	-6.32 ± 0.08
	105		Sgr OB1	1.9 ± 0.2	3, 4	7.04	6.25	5.73	a,a,a	0.56	0.58	0.57 ± 0.02	-6.24 ± 0.23
WN6ha	20a1			8.0 ± 1.0	37	9.61	8.84	8.34	a,a,a	0.61	0.65	0.63 ± 0.03	-6.80 ± 0.38
	20a2			8.0 ± 1.0	37	9.61	8.84	8.34	a,a,a	0.61	0.65	0.63 ± 0.03	-6.80 ± 0.38
	24	Coll 228	Car OB1	2.6 ± 0.2	7, 8	6.10	6.01	5.82	a,a,a	0.14	0.23	0.16 ± 0.01	-6.42 ± 0.17
	25•	Trumpler 16	Car OB1	2.6 ± 0.2	7, 8	6.26	5.97	5.72	a,a,a	0.26	0.31	0.28 ± 0.02	-6.63 ± 0.17
	43A1	NGC 3603		7.6 ± 0.4	38	8.57	8.36	7.78	k,k,k	0.38	0.77	0.49 ± 0.05	-7.11 ± 0.16
	43A2	NGC 3603		7.6 ± 0.4	38	8.98	8.77	8.19	k,k,k	0.38	0.77	0.49 ± 0.04	-6.70 ± 0.14

Continued on next page...

Continued from previous page

Spect Type	WR#	Cluster	Association	Distance(kpc)	Ref	J	H	K_S	Ref	$A^J_{K_S}$	$A^H_{K_S}$	$\bar{A}_{K_S}$	M_{K_S}
	43B	NGC 3603		7.6 ± 0.4	38	7.78	7.70	7.08	k,k,k	0.34	0.83	0.47 ± 0.03	-7.80 ± 0.13
	43C•	NGC 3603		7.6 ± 0.4	38	8.49	8.13	7.81	k,k,k	0.33	0.41	0.35 ± 0.03	-6.95 ± 0.13
WN7ha	22•		Car	2.6 ± 0.2	7, 8	5.71	5.58	5.39	a,a,a	0.17	0.26	0.20 ± 0.03	-6.81 ± 0.17
	*125-3	Mercer 23		6.5 ± 0.3	39	8.65	7.84	7.33	l,l,l	0.64	0.70	0.67 ± 0.02	-7.40 ± 0.10
WN9ha	79a	NGC 6231	Sco OB1	1.64 ± 0.03	33	5.15	5.09	4.90	a,a,a	0.14	0.25	0.17 ± 0.02	-6.34 ± 0.05
	79b		KQ Sco	3.5 ± 0.5	40	6.76	6.62	6.48	a,a,a	0.16	0.19	0.17 ± 0.01	-6.41 ± 0.31

*Indicates updated spectral types based on an improved near-IR classification scheme.
•Spectroscopic binary systems with a dominant WR component at IR wavelengths ($F^{WR}/F^{sys} > 2/3$). Binary detections: (WR 12)Fahed & Moffat (2012), (WR 25)Gamen et al. (2006), (WR 43C)Schnurr et al. (2008), (WR 22)Schweickhardt et al. (1999).
Distance references (1-22 as in Table 1): (23)Arnal et al. (1999), (24)Crowther, Smith & Hillier (1995b), (25)Tovmassian, Navarro & Cardona (1996), (26)Howarth & Schmutz (1995), (27)Cappa et al. (1999), (28)Moffat, Shara & Potter (1991), (29)Garmany & Stencel (1992), (30)Messineo et al. (2011), (31)Vázquez et al. (2005), (32)Cohen, Parker & Green (2005), (33)Sana et al. (2006), (34)Vázquez & Baume (2001), (35)Corti, Bosch & Niemela (2007), (36)Marchenko, Moffat & Crowther (2010), (37)Rauw et al. (2007), (38)Melena et al. (2008), (39)Hanson et al. (2010), (40)Bohannan & Crowther (1999).
Photometry references (a-g as in Table 1): (h)Cotera et al. (1999), (i)Espinoza, Selman & Melnick (2009), (j)Martins et al. (2008), (k)Harayama, Eisenhauer & Martins (2008), (l)Hanson et al. (2010).
Extinction: †Average of parent cluster.

© 2014 RAS, MNRAS **000**, 1–43

Table 3. WR stars in confirmed binary systems (WR+non-WR) used for absolute magnitude-spectral type calibrations.

WR#	Spect Type	Cluster/Association	Distance(kpc)	Ref	JHK_S^{sys}	Ref	Flux ratio F^{WR}/F^{sys}	Extinction	M^{WR}
11	WC8+O7.5III		0.342 ± 0.035	41	$J = 2.12$	m	0.45 ± 0.32	0.00	$M_J = -4.68 \pm 0.81$
					$H = 2.17$	m	0.48 ± 0.30	0.00	$M_H = -4.70 \pm 0.72$
					$K_S = 1.98$	m	0.60 ± 0.23	0.00	$M_{K_S} = -5.14 \pm 0.48$
77o	WN7o+?	Westerlund 1	4.0 ± 0.2	13, 14	$J = 10.34$	b	0.59 ± 0.10	2.98 ± 0.20	$M_J = -5.08 \pm 0.26$
					$K_S = 8.37$	b	0.80 ± 0.10	0.96 ± 0.05	$M_{K_S} = -5.36 \pm 0.23$
79	WC7+O5-8V	Sco OB1	1.64 ± 0.03	33	$J = 5.96$	a	0.41 ± 0.05	0.48 ± 0.03	$M_J = -4.62 \pm 0.14$
					$K_S = 5.39$	a	0.45 ± 0.05	0.16 ± 0.01	$M_{K_S} = -4.97 \pm 0.13$
93	WC7+O7-9	Pismis 24	2.0 ± 0.2	tw.	$K_S = 5.87$	a	0.73 ± 0.72	$0.58 \pm 0.03^{\ddagger}$	$M_{K_S} = -5.88 \pm 1.10$
127	WN5+O8.5V	Vul OB2	4.41 ± 0.12	42	$J = 9.18$	a	0.58 ± 0.17	0.56 ± 0.09	$M_J = -4.00 \pm 0.65$
					$H = 9.02$	a	0.59 ± 0.13	0.31 ± 0.05	$M_H = -3.93 \pm 0.26$
					$K_S = 8.76$	a	0.67 ± 0.09	0.18 ± 0.03	$M_{K_S} = -4.21 \pm 0.16$
133	WN5+O9I	NGC 6871	2.14 ± 0.07	43	$J = 6.32$	a	0.22 ± 0.05	0.55 ± 0.05	$M_J = -3.86 \pm 0.19$
					$K_S = 6.25$	a	0.23 ± 0.05	0.18 ± 0.02	$M_{K_S} = -4.04 \pm 0.19$
137	WC7+O9	Cyg OB1	1.3 ± 0.2	29	$J = 7.00$	n	0.41 ± 0.12	0.59 ± 0.07	$M_J = -3.19 \pm 0.47$
					$K_S = 6.43$	n	0.46 ± 0.13	0.19 ± 0.02	$M_{K_S} = -3.49 \pm 0.46$
139	WN5+O6III-V	Cyg OB1	1.3 ± 0.2	29	$J = 6.70$	a	0.44 ± 0.06	0.59 ± 0.06	$M_J = -3.57 \pm 0.36$
					$K_S = 6.33$	a	0.50 ± 0.07	0.19 ± 0.02	$M_{K_S} = -3.69 \pm 0.36$
141	WN5+O5III-V	Cyg OB1	1.3 ± 0.2	29	$J = 7.34$	a	0.65 ± 0.07	$0.45 \pm 0.15^{\dagger}$	$M_J = -3.21 \pm 0.34$
157	WN5+?	Markarian 50	3.46 ± 0.35	44	$J = 8.22$	a	0.47 ± 0.10	0.90 ± 0.15	$M_J = -4.53 \pm 0.30$
					$K_S = 7.73$	a	0.68 ± 0.10	0.29 ± 0.04	$M_{K_S} = -4.88 \pm 0.36$

Distance references (1-40 as in Tables 1 & 2): (41)van Leeuwen (2007), (42)Turner (1980), (43)Malchenko & Tarasov (2009), (44)Baume, Vázquez & Carraro (2004).
Photometry references (a-l as in Tables 1 & 2): (m)Williams et al. (1990b), (n)Williams et al. (2001).
Spectral types: (WR 11) De Marco & Schmutz (1999), (WR 77o) Crowther et al. (2006b), (WR 79) Smith, Shara & Moffat (1990), (WR 93) Lortet, Testor & Niemela (1984), (WR 127) de La Chevrotière, Moffat & Chené (2011), (WR 133) Underhill & Hill (1994), (WR 137) Williams et al. (2001), (WR 139) Marchenko, Moffat & Koenigsberger (1994), (WR 141) Marchenko, Moffat & Eenens (1998), (WR 157) Smith et al. (1996).
Extinction: $^{\ddagger}A_v$ taken from van der Hucht (2001) and converted using $A_K = 0.12A_v$. †Average extinction taken from WR 136 and WR 139, also members of Cyg OB1.

2.2 Classification of WR stars from near-infrared spectra

Spectral types of approximately 50% of our calibration sample have been obtained from optical spectroscopy following Smith, Shara & Moffat (1996) for WN subtypes and Crowther, De Marco & Barlow (1998) for WC and WO subtypes. For the remaining objects, we reassess published spectral types based upon their near-IR (1–5μm) spectra, using an updated version of the scheme from Crowther et al. (2006b). Updated spectral types are shown in Tables 1–3. Diagnostics involve emission line equivalent width ratios drawn from adjacent ionisation stages of the same atomic species. Full details will be presented elsewhere, but we shall briefly discuss the methodology here.

2.2.1 WN diagnostics

For WN stars, ratios of He II/He I lines provide the primary classification diagnostics; particularly He II 1.012μm/He I 1.083μm in the J-band and He II+Brγ2.165μm/He II 2.189μm in the K-band. Degeneracies in these primary line ratios between spectral types are lifted by considering various weaker lines. For example, we find WN7–9 types can be distinguished by considering the strength of Si IV 1.190μm relative to He II 1.163μm, while an inspection of spectral morphology in the K-band permits WN4–6 stars to be distinguished using N V 2.100μm and N III 2.116μm.

2.2.2 WC diagnostics

For WC stars, ratios of C II-IV provide the primary classification diagnostics, with C IV 1.191μm/C III 0.972μm in the J-band permitting a consistent classification to optical lines. He II 1.012μm/He I 1.083μm also prove useful for classification, although the H-band contains little diagnostic information. However, we find the very strong C IV 1.736μm line to be useful for recognising the dilution effects of hot circumstellar dust (see Section 2.3.2). In the K-band, the ratio of C IV 2.070–2.084μm to C III+He I 2.112–2.114μm serves as a good ionisation diagnostic, but is incapable of discriminating between WC4–6 stars.

2.2.3 Accuracy of near IR spectral types

To gain an insight into the reliability of our revised near-IR classification scheme, we have carried out blind-tests using WR stars with optically derived spectral types, and find J and K-band diagnostics provide the highest level of consistency.

For WN stars, an exact 3D spectral type (Smith et al. 1996) can be achieved from low-resolution J through K spectra, with solely the J-band proving criteria for identifying the presence of Hydrogen. We find spectra in J or K alone yield spectral types with an accuracy of ± 1, and H-band diagnostics are accurate to ± 2.

For WC stars, we find an exact spectral type can be assigned solely from a J-band spectrum. Our K-band diagnostics are capable of ± 1 spectral type amongst early (WC4–6) types, and exact classification for late (WC7–9). We only find it possible to distinguish between WCE/WCL using spectra from H, L or M bands. For both WN and WC stars, ionisation types at either extreme (WN9,3,2; WC9) are conspicuous in spectral appearance, and can be identified with a higher degree of certainty, usually by inspection of the spectral morphology alone. Stars are only included in our calibration sample if we are confident within ± 1 of their spectral types.

Table 4. Intrinsic colours adopted for each type of WR star, primarily from Crowther et al. (2006b), supplemented with unpublished stellar atmospheric model results for additional types considered here (e.g. WO).

Sp. type	$(J–K_S)_0$	$(H–K_S)_0$
WO2	0.11	0.00
WC4–7	0.62	0.58
WC8	0.43	0.38
WC9	0.23	0.26
WN4–7b	0.37	0.27
WN2–4	–0.11	–0.03
WN5–6	0.18	0.16
WN7–9	0.13	0.11
WN5–6ha	–0.015	0.03
WN7–9ha	–0.04	0.005

2.3 Photometry and extinction

In general we take JHK$_S$ photometry for each WR star from the Two Micron All-Sky Survey (2MASS) point source catalogue (Skrutskie et al. 2006), plus IRAC [3.6]–[8.0](μm) photometry from the GLIMPSE survey (Benjamin et al. 2003) for sufficiently isolated sources in the surveyed field.

We require a minimum quality flag of C where 2MASS photometry is used. Many cluster and association members are located in fields too crowded for 2MASS to be useful. In such cases we turn to dedicated observations with higher spatial resolution of the stellar groupings in question (Tables 1–3).

We have attempted to ensure consistency in the near-IR photometry used. For example, observations of WR stars in the Galactic Centre region are assembled by Dong et al. (2012), consisting of Hubble Space Telescope snapshot imaging plus multiple ground-based observations. In this case, to maintain consistency with other assembled photometry, we construct and apply a simple algorithm to convert the Dong et al. JHK$_S$ values into the 2MASS photometric system (following their equations 7–9). However, in general we regard the slight differences between ground-based filter systems as insignificant, as they have a much smaller effect on calculated absolute magnitudes than that of distance uncertainties.

We calculate an extinction towards each calibration star by evaluating the colour excesses E_{J-K_S} and E_{H-K_S}, utilising intrinsic JHK$_S$ Wolf-Rayet colours given by Crowther et al. (2006b), updated in Table 4. Two values of K$_S$-band extinction follow;

$$A^J_{K_S} = E_{J-K_S} \times (\frac{A_J}{A_{K_S}} - 1)^{-1}, \quad (1)$$

and

$$A^H_{K_S} = E_{H-K_S} \times (\frac{A_H}{A_{K_S}} - 1)^{-1}. \quad (2)$$

Table 5. Calibrated near-IR absolute magnitudes for Galactic WR stars. The number of objects used to arrive at each value is indicated in adjacent parentheses. Two uncertainties are shown with each value; formal errors (parenthesised, Equation 5) do not account for the intrinsic spread in magnitude within a WR spectral type - estimated to be ~ 0.3 mag - which is incorporated into the final (nonparenthesised) uncertainty.

Sp. type	$\bar{M}_J$	(N)	$\bar{M}_H$	(N)	$\bar{M}_{K_S}$	(N)
WO2	$-2.15 \pm (0.08)\, 0.31$	(1)	$-2.26 \pm (0.08)\, 0.31$	(1)	$-2.26 \pm (0.07)\, 0.31$	(1)
WC4	$-2.88 \pm (0.13)\, 0.33$	(1)	$-2.92 \pm (0.13)\, 0.33$	(1)	$-3.50 \pm (0.13)\, 0.33$	(1)
WC5	$-3.80 \pm (0.27)\, 0.40$	(2)	$-3.84 \pm (0.27)\, 0.40$	(2)	$-4.40 \pm (0.25)\, 0.39$	(2)
WC6	$-4.03 \pm (0.61)\, 0.68$	(3)	$-4.06 \pm (0.62)\, 0.69$	(3)	$-4.66 \pm (0.61)\, 0.68$	(3)
WC7	$-4.21 \pm (0.20)\, 0.36$	(4)	$-4.25 \pm (0.20)\, 0.36$	(2)	$-4.84 \pm (0.21)\, 0.36$	(5)
WC8	$-4.26 \pm (0.24)\, 0.38$	(6)	$-4.35 \pm (0.22)\, 0.37$	(7)	$-5.04 \pm (0.28)\, 0.41$	(7)
WC9	$-4.42 \pm (0.39)\, 0.49$	(4)	$-4.17 \pm (0.32)\, 0.44$	(4)	$-4.57 \pm (0.38)\, 0.48$	(4)
WC8d	$-5.53 \pm (0.25)\, 0.39$	(3)	$-5.83 \pm (0.23)\, 0.38$	(3)	$-6.57 \pm (0.27)\, 0.41$	(4)
WC9d	$-6.34 \pm 0(.25)\, 0.39$	(12)	$-6.63 \pm (0.21)\, 0.37$	(13)	$-7.06 \pm (0.20)\, 0.36$	(14)
WN2b	$-2.97 \pm (0.73)\, 0.79$	(1)	$-2.89 \pm (0.73)\, 0.78$	(1)	$-2.86 \pm (0.72)\, 0.78$	(1)
WN3b	$-3.56 \pm (0.46)\, 0.55$	(1)	$-3.48 \pm (0.46)\, 0.55$	(1)	$-3.45 \pm (0.46)\, 0.55$	(1)
WN4b	$-4.48 \pm (0.23)\, 0.38$	(5)	$-4.58 \pm (0.23)\, 0.38$	(5)	$-4.85 \pm (0.23)\, 0.38$	(5)
WN5b	$-4.70 \pm (0.16)\, 0.34^a$	(0)	$-4.74 \pm (0.16)\, 0.34^a$	(0)	$-5.00 \pm (0.16)\, 0.34^a$	(0)
WN6b	$-4.93 \pm (0.23)\, 0.38$	(2)	$-4.90 \pm (0.22)\, 0.37$	(4)	$-5.16 \pm (0.22)\, 0.37$	(4)
WN7b	$-5.02 \pm (0.16)\, 0.34$	(2)	$-5.12 \pm (0.19)\, 0.36$	(2)	$-5.38 \pm (0.15)\, 0.34$	(2)
WN3	$-3.10 \pm (0.62)\, 0.69$	(1)	$-3.02 \pm (0.62)\, 0.69$	(1)	$-2.99 \pm (0.62)\, 0.69$	(1)
WN4	$-3.36 \pm (0.32)\, 0.44^a$	(0)	$-3.33 \pm (0.32)\, 0.44^a$	(0)	$-3.39 \pm (0.32)\, 0.44^a$	(0)
WN5	$-3.63 \pm (0.16)\, 0.34$	(8)	$-3.66 \pm (0.15)\, 0.34$	(4)	$-3.86 \pm (0.15)\, 0.34$	(7)
WN6	$-4.47 \pm (0.30)\, 0.43$	(6)	$-4.74 \pm (0.34)\, 0.45$	(7)	$-4.94 \pm (0.34)\, 0.46$	(7)
WN7	$-5.32 \pm (0.34)\, 0.45$	(9)	$-5.01 \pm (0.28)\, 0.41$	(9)	$-5.49 \pm (0.30)\, 0.42$	(10)
WN8	$-5.94 \pm (0.19)\, 0.35$	(15)	$-5.78 \pm (0.19)\, 0.36$	(16)	$-5.82 \pm (0.20)\, 0.36$	(16)
WN9	$-6.18 \pm (0.18)\, 0.35$	(15)	$-6.19 \pm (0.16)\, 0.34$	(17)	$-6.32 \pm (0.15)\, 0.33$	(18)
WN6ha	$-6.98 \pm (0.17)\, 0.34$	(8)	$-6.94 \pm (0.19)\, 0.36$	(8)	$-7.00 \pm (0.18)\, 0.35$	(8)
WN7ha	$-7.33 \pm (0.25)\, 0.39$	(2)	$-7.26 \pm (0.27)\, 0.40$	(2)	$-7.24 \pm (0.28)\, 0.41$	(2)
WN9ha	$-6.38 \pm (0.07)\, 0.31$	(2)	$-6.33 \pm (0.07)\, 0.31$	(2)	$-6.34 \pm (0.05)\, 0.30$	(2)

[a] Average of adjacent types since no stars of this type are available for calibration.

The second terms in Equations 1 and 2 require knowledge of the near-IR extinction law.

Due to the growing body of evidence suggesting a difference in dust properties toward the GC, we employ two different Galactic near-IR extinction laws. For stars in the GC region ($358^\circ < l < 2^\circ, |b| < 1^\circ$) we use the line-derived extinction law of Fritz et al. (2011) ($^A J/A_{K_S} = 3.05 \pm 0.07$, $^A H/A_{K_S} = 1.74 \pm 0.03$). For all other Galactic sight lines we use the law of Stead & Hoare (2009) ($^A J/A_{K_S} = 3.1 \pm 0.2$, $^A H/A_{K_S} = 1.71 \pm 0.09$) – an updated form of that provided by Indebetouw et al. (2005). For the purpose of calculating the absolute magnitude of each calibration star, we take an average, $\bar{A}_{K_S}$, from Equations 1 and 2. Since extinction in the IRAC bands is lower, we opt for a more straightforward approach and use the relations given by Indebetouw et al. (2005), independent of sight line.

A minority of stars in our calibration sample only have single-band photometry available, preventing an extinction calculation by colour excess. For these objects we resort to one of two alternatives; we adopt the average A_{K_S} calculated for other O or WR stars in the cluster/association if sufficient numbers are available, or we take A_v as listed in van der Hucht (2001) and convert this using $A_{K_S} \simeq 0.11 A_V \simeq 0.12 A_v$ (Rieke & Lebofsky 1985). If neither is possible we exclude the star from our sample.

2.3.1 Correction for binary companions

For cluster/OB association WR stars in spectroscopically confirmed binary systems, we attempt to correct for the contribution of companion(s) to systemic magnitudes, allowing an absolute magnitude calculation for the WR component. Depending on the information available about the companion star(s), we follow one of two methods to apply these corrections.

If the companion is an OB star of known spectral type, we use the synthetic photometry of Martins & Plez (2006), or *Hipparcos*-based absolute magnitudes (Wegner 2006), to correct for its contribution. Otherwise we determine a WR/companion continuum flux ratio by considering dilution of the WR emission lines in the bands that line measurements are available. The *single star* emission line strengths used to determine WR/companion continuum flux ratios are presented in Appendix C. If the companion is not an OB-star or is insufficiently bright to notably dilute WR emission lines, it will not make a significant contribution to the combined light. Ten of the WR stars in our calibration sample, detailed in Table 3, have been corrected by one of these methods.

Two systems in our calibration sample are WNha+WNha binaries. There are no known 'classical' WR+WR binaries, highlighting the sensitivity of post-MS evolution to initial mass. The fact that WNha+WNha

Table 6. Calibrated mid-IR (Spitzer IRAC filters) absolute magnitudes for Galactic WR stars. The number of objects used to arrive at each value is indicated in adjacent parentheses. Two uncertainties are shown with each value; formal errors (parenthesised, Equation 5) do not account for the intrinsic spread in magnitude within a WR spectral type - estimated to be ~ 0.3 mag - which is incorporated into the final (nonparenthesised) uncertainty.

WR Sp. type	$\bar{M}_{[3.6]}$	(N)	$\bar{M}_{[4.5]}$	(N)	$\bar{M}_{[5.8]}$	(N)	$\bar{M}_{[8.0]}$	(N)
WC5–6	$-4.34 \pm (0.35)\, 0.46$	(2)	$-4.75 \pm (0.35)\, 0.46$	(2)	$-5.02 \pm (0.28)\, 0.41$	(3)	$-5.32 \pm (0.29)\, 0.41$	(3)
WC7–9	$-5.96 \pm (0.29)\, 0.42$	(4)	$-6.27 \pm (0.33)\, 0.45$	(4)	$-6.06 \pm (0.33)\, 0.45$	(4)	$-6.27 \pm (0.34)\, 0.46$	(4)
WC8d	...		...		$-8.18 \pm (0.55)\, 0.63$	(1)	$-8.47 \pm (0.55)\, 0.63$	(1)
WC9d	$-6.88 \pm (0.48)\, 0.57$	(1)	$-7.25 \pm (0.50)\, 0.58$	(1)	$-9.29 \pm (0.16)\, 0.34$	(4)	$-9.36 \pm (0.16)\, 0.34$	(4)
WN3b	$-3.59 \pm (0.46)\, 0.55$	(1)	$-3.84 \pm (0.46)\, 0.55$	(1)	$-4.11 \pm (0.46)\, 0.55$	(1)	$-4.50 \pm (0.46)\, 0.55$	(1)
WN6–7b	$-5.51 \pm (0.41)\, 0.51$	(2)	$-5.88 \pm (0.40)\, 0.50$	(2)	$-6.14 \pm (0.38)\, 0.49$	(2)	$-6.41 \pm (0.44)\, 0.53$	(2)
WN4–6	$-4.18 \pm (0.13)\, 0.33$	(1)	$-4.42 \pm (0.14)\, 0.33$	(1)	$-4.71 \pm (0.15)\, 0.34$	(1)	$-5.05 \pm (0.15)\, 0.33$	(1)
WN7–9	$-5.96 \pm (0.39)\, 0.49$	(5)	$-6.23 \pm (0.36)\, 0.47$	(6)	$-6.53 \pm (0.28)\, 0.41$	(12)	$-6.79 \pm (0.30)\, 0.43$	(11)
WN7ha	...		$-7.74 \pm (0.12)\, 0.32$	(1)	$-7.87 \pm (0.12)\, 0.32$	(1)	$-8.22 \pm (0.12)\, 0.32$	(1)
WN9ha	...		...		$-6.79 \pm (0.31)\, 0.43$	(1)	$-6.90 \pm (0.31)\, 0.43$	(1)

binaries *are* observed emphasises their similarity to massive O-stars. We separate the light contributions of individual stars to each system by considering mass ratios derived by spectroscopic monitoring of their orbits. The stars making up WR 20a are of identical spectral type and have very similar masses (Rauw et al. 2005), hence we assume an equal light contribution from each star in the J, H and K_S-bands, and alter the systemic photometry accordingly. Similarly, WR 43A in the NGC 3603 cluster is comprised of two stars with very high measured masses, $116 \pm 31\,M_\odot$ and $89 \pm 16\,M_\odot$ ($q = 0.8 \pm 0.2$; Schnurr et al. 2008). Using the mass-luminosity relationship for very massive stars ($M > 80\,M_\odot$) provided by Yusof et al. (2013), we arrive at a light ratio of 1.46 ± 0.47 for this system in all bands, assuming identical spectral energy distributions (SEDs). We include the stars of WR 20a and WR 43A under the WN6ha spectral type in Table 2.

2.3.2 Treatment of dust-forming WC stars

The majority of WC9, and a diminishing fraction of earlier WC stars, show evidence of periodic or persistent circumstellar dust production (e.g. WR 140, Williams et al. 1990a). Episodes of dust formation occur at perihelion passage in eccentric WC+OB systems, whereas circular orbits allow persistent dust production, enhancing the near-IR flux of the system dramatically. For completeness, we perform near to mid-IR absolute magnitude calibrations for WC8d and WC9d spectral types based on the 18 stars at known distances. However, we do not make any attempt to remove the light contribution of potential companion stars; firstly because their K_S-band flux is usually insignificant compared to that of the hot circumstellar dust, and secondly because dust production seems to be inextricably linked to the presence of these companions (Crowther 2003).

Thermal emission from hot circumstellar dust dominates the IR colours of dusty WC systems, prohibiting extinction determination via near-IR colour excess. For the dusty systems in our calibration sample we either adopt an average A_{K_S} for the relevant cluster/association, or its A_v from van der Hucht (2001) and convert this to the K_S-band according to $A_{K_S} \simeq 0.12 A_v$.

We make an exception of WR 137 - a member of the Cyg OB1 association comprising WC7 and O9($\pm$0.5) type stars - which displays periodic dust formation episodes concurrent with its 13 yr orbit. Williams et al. (2001) present JHK_S photometry for this system during a quiescent phase (1992–4), allowing us to derive a K_S-band flux ratio ($F_{WR}/F_{sys} = 0.46 \pm 0.13$) using line strengths measured from spectra taken during quiescence (W.D. Vacca, priv. comm.), and remove the O-star light. The WC7 component is included in Table 3.

2.4 Callibration method and uncertainties

The results of our near-IR absolute magnitude calibrations are presented in Table 5, with mid-IR calibrations shown in Table 6. Figures 1 and 2 present the K_S-band absolute magnitudes for WN and WC stars, respectively. We use a weighted mean method to arrive at an average absolute magnitude for each WR spectral type, computed by

$$\bar{M} = \sum_{i=1}^{n} \frac{p_i M_i}{p}, \tag{3}$$

using weights

$$p_i = \frac{1}{s_i^2}, \qquad p = \sum_{i=1}^{n} p_i, \tag{4}$$

where s_i is the error in absolute magnitude (M_i) - invariably dominated by distance uncertainty - calculated for each of the n WR stars of that type. We calculate a formal error (σ) on each calibrated absolute magnitude value by combining two uncertainty estimates for weighted data:

$$\sigma = \sqrt{\sigma_1^2 + \sigma_2^2}, \tag{5}$$

where

$$\sigma_1 = \frac{1}{\sqrt{p}}, \tag{6}$$

and

$$\sigma_2 = \sqrt{\frac{\sum_{i=1}^{n} p_i (M_i - \bar{M})^2}{p(n-1)}}. \tag{7}$$

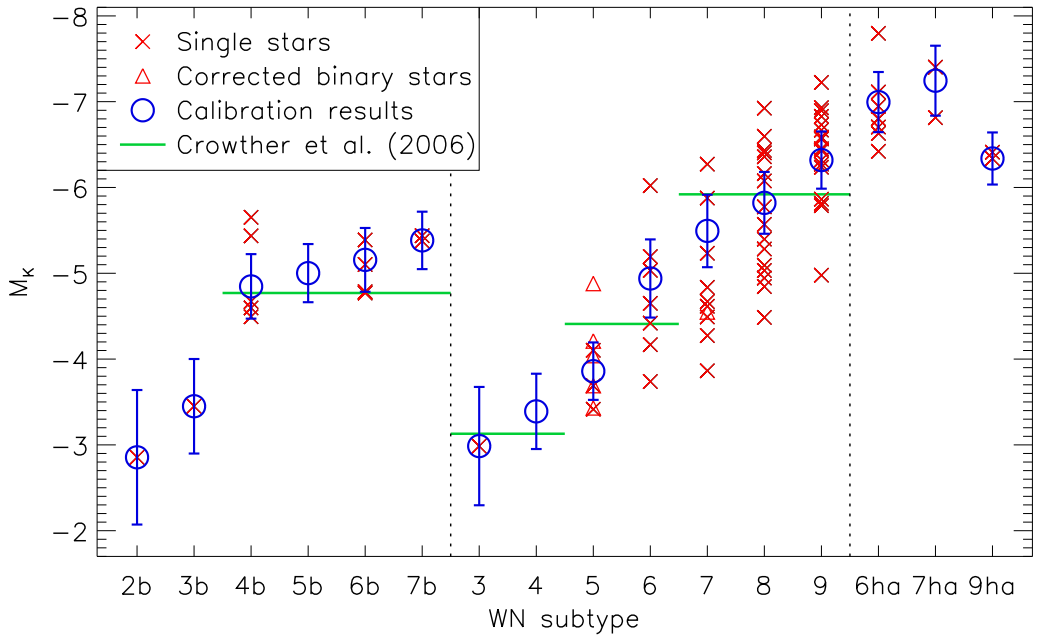

Figure 1. Calibration of M_{K_S} for WN spectral types. Broad-line stars are on the left, weak-line (including 'WN#o' and 'WN#h' stars) in the centre, and 'WN#ha' stars to the right. Individual single stars are represented by small (red) crosses, and stars that have been corrected for a companion(s) by (red) triangles. Larger (blue) symbols show the weighted average for each type with a combination of statistical error (Equations 5, 6 & 7) and the estimated intrinsic spread (0.3 mag) in M_{K_S} within a WR spectral type. Horizontal lines represent the previous calibrations of Crowther et al. (2006b).

This combination is chosen because σ_1 depends only on s_i and does not consider the spread in M_i, which is taken into consideration by σ_2.

This weighted average approach favours objects with the most accurately determined distances, but the formal uncertainty given by Equation 5 does not account for any *intrinsic* scatter in WR star luminosity within a spectral type. Such a scatter is expected as a WR spectral type does not represent a perfectly uniform class of objects, but the division of smoothly varying Wolf-Rayet properties at spectroscopically identifiable boundaries. Therefore one expects each subclass to encompass a range in mass, temperature and luminosity.

Westerlund 1, the Arches and the GC cluster individually contain enough stars of a single spectral type to evaluate some basic measures of spread, effectively eliminating the scatter introduced by distance uncertainties when considering one type across multiple clusters. In Table 7 we show the range and standard deviation in M_{K_S} within a WR spectral type. Ranges are typically < 1, although WN9 stars in the Arches cluster show a larger range due to the anomalously faint WR 102aj; we classify this star based on a K-band spectrum published by Martins et al. (2008) and thus can only claim a ± 1 accuracy on the WN9 spectral type. Typical standard deviations of 0.3–0.6 mag in M_{K_S} suggest that WR absolute magnitudes intrinsically vary by at least ± 0.3 within a spectral type. Following this result, we add an uncertainty of 0.3 mag in quadrature to the result of Equation 5 (see Tables 5 - 6), and recommend the adoption of this combined uncertainty when applying these calibrated absolute magnitudes to WR stars in the field.

Throughout the rest of this paper we favour discussion and application of the M_{K_S} calibration as these results are affected by lower (and more accurately determined) extinctions than those in J and H-bands, and are derived using the largest sample. For completeness, in the cases of WN4 and WN5b stars (unrepresented in our calibration sample), we take average values in each band from the adjacent ionisation types.

Table 7. Intrinsic scatter in absolute magnitude within a WR spectral type

Cluster	Stars (WR#)	M_{K_S} range	σ_{M_K}
	WN7		
Westerlund 1	77d, 77j, 77r, 77sa	0.76	0.33
	WN8		
Arches	102a, 102ae, 102af, 102ah, 102al	0.84	0.34
GC Cluster	101b, 101dd, 101nc, 101oc	1.28	0.57
	WN9		
Arches	102ad, 102ag, 102ai, 102aj, 102bb, 102bc	1.85	0.72

2.5 Results of near to mid-IR absolute magnitude calibrations

Both strong and weak-line WN stars show a monotonic increase in intrinsic near-IR brightness with ionisation type. This is largely due to cooler, late-type WN stars having smaller bolometric corrections. WN stars displaying intrinsic absorption features (the 'ha' stars) are the most luminous

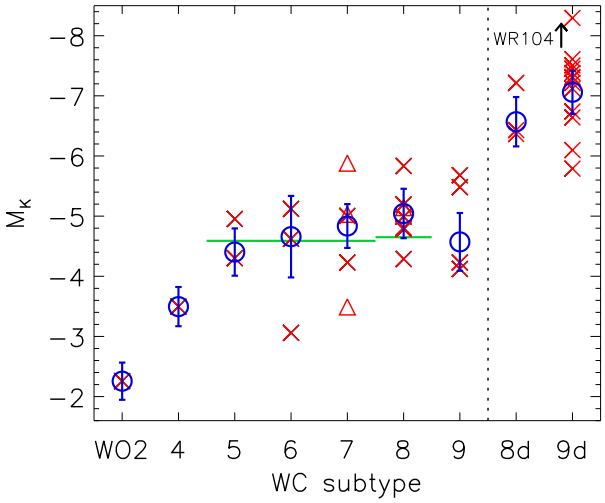

Figure 2. Calibration of M_{K_S} for WO and WC subtypes. To the right of the vertical dotted line are subtypes associated with circumstellar dust. WR 104 (WC9d+B) has $M_{K_S} = -10.4$, outside the range displayed here. Symbols same as Figure 1.

at these wavelengths, as a consequence of their high masses. Our results show good agreement with the calibrations of Crowther et al. (2006b) for weak-line WN stars, but suggest slightly higher IR luminosities for strong-line WN4–7b. We note that for ionisation types 6–7, strong and weak line stars have similar M_{K_S}. One would expect an enhanced contribution from free-free excess in the denser winds of 'b' stars to make them brighter at IR wavelengths than weak-line stars. However, the strong-line stars of these ionisation types have higher effective temperatures (Hamann et al. 2006), so the enhanced IR emission from free-free excess is counteracted by larger bolometric corrections at these subtypes.

The lower number of WC stars available reveal a less obvious variation in M_{K_S} with ionisation type, yet a monotonic increase in near-IR luminosity does appear to be present for WC4–8. As expected, dusty WC stars display a large range in M_{K_S} due to varying quantities of dust and the range of orbital phases sampled amongst periodic dust forming systems.

The limited area and resolution of the GLIMPSE survey results in far fewer stars available for absolute magnitude calibration at 3.6–8.0μm. Hence, in some cases spectral types showing only small differences in M_{K_S} are grouped together to provide more robust estimates. For all WR types with GLIMPSE coverage we observe a brightening across [3.6]–[8.0], gradual in most cases except dusty WC stars which exhibit a dramatic $\Delta M \sim 2$ between [4.5] and [5.8], owing to hot circumstellar dust emission.

2.5.1 *The effects of a different Galactic Center extinction law*

The results presented in this paper are produced by applying the line-derived Fritz et al. (2011) 1–19μm law - with $A \propto \lambda^{-\alpha}, \alpha = 2.13 \pm 0.08$ over the JHK$_S$ range - to WR stars residing in the GC ($358° < l < 2°, |b| < 1°$). Alternatively, Nishiyama et al. (2009) propose a shallower law ($\alpha = 2.0$). It can be seen in Equations 1 and 2 that a shallower law would lead to lower derived extinctions by the colour excess method. We perform a second set of absolute magnitude calibrations using the Nishiyama et al. law to quantify its effect on our results. The biggest change is seen in our calibrated absolute magnitudes for late-type WN and WC stars, as these dominate in the inner Galaxy. Compared to values presented in Table 5, adopting the Nishiyama et al. law changes $\bar{M}_J$, $\bar{M}_H$, and $\bar{M}_{K_S}$ of WN9 stars by −0.30, −0.31 and −0.30 mag, respectively; WN8 stars by −0.26, −0.31, −0.32 mag, and WC9 stars by −0.27, −0.32, −0.32 mag. All differences are within our adopted uncertainties (Table 5), and hence are not significant. However, as we proceed to obtain further results based on these values we monitor their effects and comment where discrepancies arise.

3 THE OBSERVED GALACTIC WR STAR DISTRIBUTION

The sample of WR stars involved in our absolute magnitude calibrations represents approximately 20% of the current known Galactic population. The remainder either have poorly defined spectral types, uncertain binary status, or in a majority of cases do not reside in an identified cluster or association for which a distance measurement is available. For convenience, we shall refer to any WR star not in our calibration sample (i.e., Tables 1–3) as a 'field' star.

Up until recently it was widely accepted that most stars formed in clusters (Lada & Lada 2003), so the low frequency of WR stars presently in clusters arose via dynamical ejection or rapid cluster dissolution. It is now recognised that a high fraction of star formation occurs in relatively low density regions (Bressert et al. 2010), so the low fraction of WR stars in clusters does not require an unusually high rate of ejection. Smith & Tombleson (2014) compare the association of WR stars (and Luminous Blue Variables) in the Milky Way and Magellanic Clouds with O stars. They find WR stars to be less clustered than O-type stars, with WC stars in particular showing weak spatial coincidence with O-stars and H-rich WN stars.

Our WN and WC calibration samples echo this finding, with approximately half as many WC stars residing in clusters or associations as WN stars. The typical velocity dispersion of cluster stars is not high enough to account for the isolation of WC stars considering their age. The relative isolation of WC stars challenges the commonly accepted evolutionary paradigm that this phase follows the WN phase in the lives of the most massive stars. Two alternative scenarios may explain the locations of WC stars; either they descend from a lower initial mass regime than other WR types (Sander et al. 2012), or the runaway fraction of WC and H-free WR stars in general is higher. Further detailed modelling of cluster collapse and the ejection of massive stars is needed to explain these emerging statistics.

In this section we present an analysis of the spatial distribution of WR stars, where distances to 246 field WR stars are obtained by application of our absolute magnitude calibrations. Runaway WR stars are discussed further in Section 3.2.3.

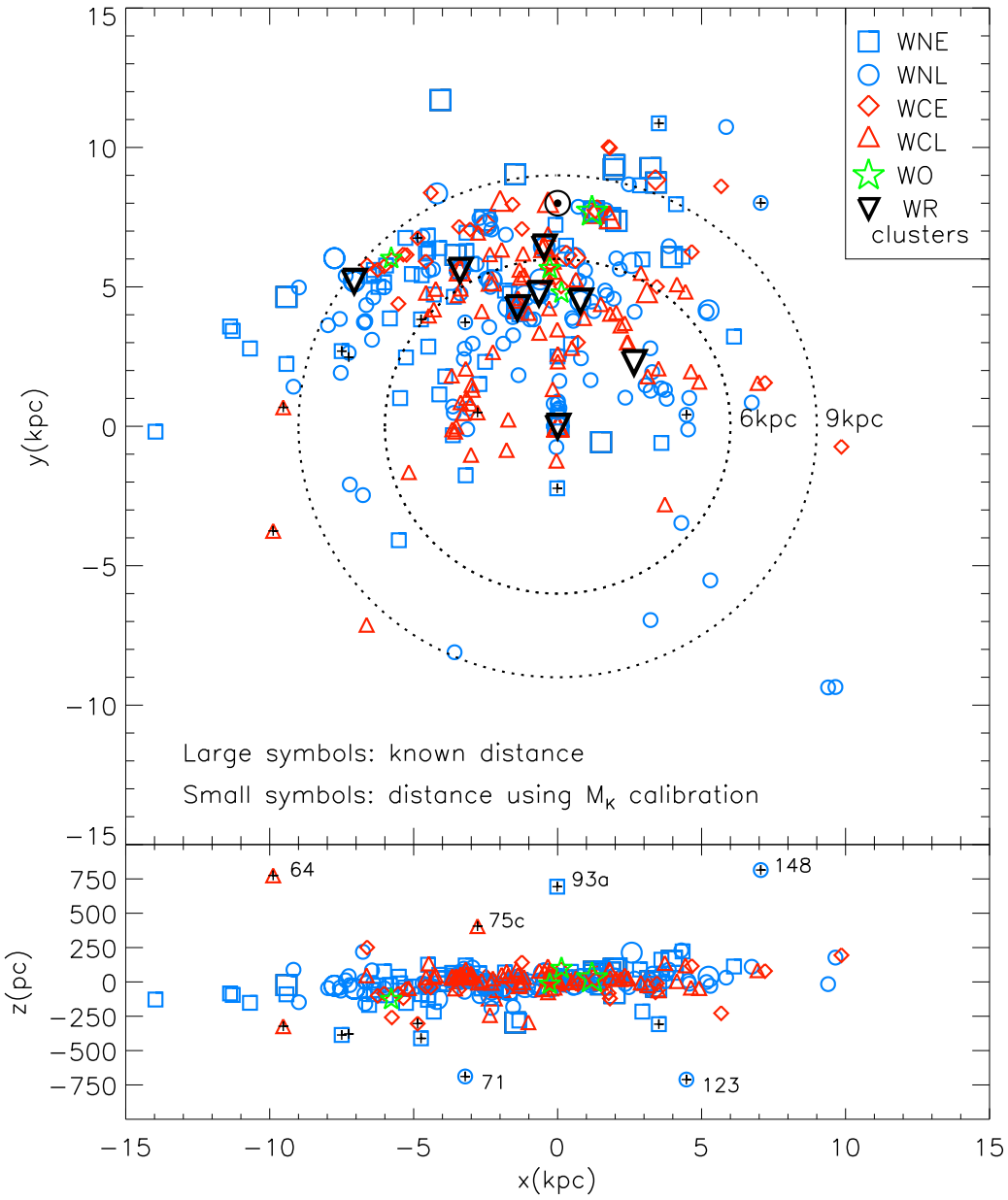

Figure 3. Positions of 354 WR stars projected on the Galactic plane (top) and viewed edge-on (bottom) in Cartesian coordinates, with the GC at (0,0,0). Galactic longitude increases anti-clockwise about the Sun, which is represented by the standard symbol. Stars with known distances (calibration sample) are represented by larger symbols, whereas those with photometric distances (field sample) are represented by smaller symbols. Black crosses indicate stars located at $|z| > 300$ kpc and the most extreme cases are labelled with WR number. Dotted lines at $R_G = 6$ kpc and 9 kpc delineate the three chosen metallicity zones. From left to right, the displayed clusters from which >1 WR stars are taken are: NGC 3603 [–7.07, 5.20], Danks 1&2 [–3.39, 5.59], Westerlund 1 [–1.40, 4.25], Havlen-Moffat 1&2 [–0.65, 4.76], NGC 6231 [–0.47, 6.43], GC [0.0, 0.0], Arches & Quintuplet [0.02, 0.0], Cl 1813-178 [0.79, 4.49] and Quartet [2.65, 2.29].

3.1 Applying M_{K_S} Calibrations

Photometry and the derived spatial information for 246 field WR stars is given in Tables 8–9. For any non-dusty field WR star with a well-defined spectral type and no evidence of a significant binary companion - either spectroscopically or through dilution of near-IR emission lines - we simply apply our M_{K_S} calibrations to obtain a distance. For these straightforward cases, we once again use 2MASS photometry and calculate extinctions by the method described in Section 2.3.

Regarding rare WO stars, although only one star (WR 142, WO2) is available for calibration, we apply the absolute magnitude of this star to the other three field WO stars in the Galaxy, spanning WO1–4 spectral types.

We find the spectral type and binary status of many field WR stars to be uncertain. The majority of the field sample are heavily reddened stars discovered by near-IR

Table 8. Calculated spatial locations of the 228 'field' WR stars showing no conclusive evidence for an IR-bright companion, to which our calibrated absolute magnitudes have been assigned. Shown for each object are the adopted spectral type, 2MASS photometry (unless stated), derived K_S-band extinction, heliocentric distance (d), Galactocentric radius (R_G) and vertical distance from the Galactic midplane (z). A full version of this table is available online, and further details of stars discovered following the VIIth catalogue (WRXXX-#) are provided in Appendix A.

WR#	Sp. Type	ref	J	H	K_S	$\bar{A}_{K_S}$	d(kpc)	R_G(kpc)	z(pc)
3	WN3ha	1	10.24	10.13	10.01	0.18 ± 0.02	4.53 ± 1.15	11.41 ± 1.18	-308 ± 83
4	WC5	2	8.75	8.57	7.88	0.13 ± 0.01	2.69 ± 0.49	10.15 ± 0.55	-121 ± 25
5	WC6	2	8.63	8.34	7.65	0.16 ± 0.02	2.69 ± 0.84	10.18 ± 0.88	-82 ± 32
13	WC6	2	10.14	9.64	8.86	0.29 ± 0.02	4.42 ± 1.38	9.46 ± 1.40	-40 ± 19
15	WC6	2	7.85	7.34	6.60	0.28 ± 0.02	1.57 ± 0.49	8.11 ± 0.55	-10 ± 9
16	WN8h	2	6.97	6.71	6.38	0.24 ± 0.02	2.77 ± 0.46	7.95 ± 0.52	-104 ± 20
17	WC5	2	9.93	9.74	9.17	0.07 ± 0.02	5.02 ± 0.91	8.31 ± 0.95	-303 ± 59
17-1	WN5b	3	11.73	10.38	9.53	0.85 ± 0.05	5.43 ± 0.86	8.58 ± 0.89	-41 ± 10
19	WC5+O9	4,5	9.75	9.13	8.53	0.20 ± 0.02	3.52 ± 0.64	7.93 ± 0.69	-54 ± 13
19a	WN7(h)	2	9.07	8.13	7.50	0.71 ± 0.04	2.41 ± 0.47	7.78 ± 0.53	-23 ± 8
...	...	...	...	...	...	...	...	...	...

Spectral types: (1)Marchenko et al. (2004), (2)van der Hucht (2001), (3) this work, (4)Crowther et al. (1998), (5)Williams, Rauw & van der Hucht (2009b), ...

Table 9. Calculated spatial locations of 18 binary 'field' WR stars to which our calibrated absolute magnitudes have been assigned. Shown for each object are the adopted spectral type(s), systemic 2MASS photometry (unless stated), calculated K_S-band (unless stated otherwise in parentheses) WR/system flux ratio, derived K_S-band extinction, heliocentric distance (d), Galactocentric radius (R_G) and vertical distance from the Galactic midplane (z).

WR#	Sp. Type	ref	J^{sys}	H^{sys}	K_S^{sys}	F^{WR}/F^{sys}	$\bar{A}_{K_S}$	d(kpc)	R_G(kpc)	z(pc)
29	WN7h+O5I	1	9.91	9.46	9.12	0.49 ± 0.16	0.51 ± 0.19	9.48 ± 2.56	10.27 ± 2.57	-148 ± 45
30	WC6+O6-8	2	10.06	9.76	9.21	$0.75^{+0.25}_{-0.66}$	$0.25^{+0.37}_{-0.25}$	6.11 ± 3.44	8.29 ± 3.45	-258 ± 157
30a	WO4+O5-5.5	3	10.25	9.83	9.56	0.13 ± 0.04	0.40 ± 0.04	5.67 ± 1.18	8.17 ± 1.21	-117 ± 28
31	WN4+O8V	2	9.17	8.96	8.69	0.46 ± 0.23	0.30 ± 0.22	3.34 ± 1.12	7.63 ± 1.15	21 ± 1
35a	WN6h+O8.5V	4	10.47	9.98	9.65	$0.80^{+0.20}_{-0.33}$	0.37 ± 0.14	7.81 ± 1.99	9.13 ± 2.00	12 ± 2
41	WC5+OB	2	11.53	10.98	10.12	$0.93^{+0.07}_{-0.53}$	0.47 ± 0.27	6.69 ± 2.06	8.40 ± 2.07	-101 ± 37
42	WC7+O7V	5	7.59	7.52	7.08	0.53 ± 0.10(J)	0.14 ± 0.03	2.96 ± 0.53	7.47 ± 0.58	-6 ± 5
47	WN6+O5.5	6	8.32	7.92	7.55	$0.93^{+0.07}_{-0.12}$(J)	0.37 ± 0.03	2.12 ± 0.44	7.10 ± 0.50	11 ± 2
50	WC7+OB	2	9.75	9.38	8.81	$0.86^{+0.14}_{-0.59}$	$0.21^{+0.37}_{-0.21}$	5.23 ± 2.18	6.49 ± 2.19	45 ± 11
51	WN4+OB?	2	10.90	10.33	9.89	$0.77^{+0.23}_{-0.30}$	$0.72^{+0.86}_{-0.72}$	3.70 ± 1.80	6.55 ± 1.82	35 ± 7
63	WN7+OB	2	8.60	8.07	7.64	$0.89^{+0.11}_{-0.44}$	0.43 ± 0.27	3.68 ± 1.23	5.85 ± 1.26	-6 ± 8
86	WC7+B0III	7	7.44	7.14	6.67	0.77 ± 0.26	0.31 ± 0.02	1.97 ± 0.47	6.05 ± 0.53	83 ± 15
125	WC7ed+O9III	2	9.26[8]	8.74[8]	8.25[8]	0.46 ± 0.07	0.25 ± 0.12	5.45 ± 1.05	6.56 ± 1.08	120 ± 19
138	WN5+OB	2	6.97	6.80	6.58	0.61 ± 0.11	0.27 ± 0.10	1.38 ± 0.26	7.76 ± 0.36	46 ± 5
143	WC4+Be	9	8.58	8.10	7.46	0.53 ± 0.17	0.60 ± 0.06	1.33 ± 0.30	7.82 ± 0.39	18 ± 1
151	WN4+O5V	2	9.76	9.36	9.01	0.73 ± 0.10	0.40 ± 0.11	2.93 ± 0.65	9.10 ± 0.70	91 ± 16
155	WN6+O9II-Ib	2	7.48	7.34	7.16	0.70 ± 0.07	0.14 ± 0.08	2.56 ± 0.56	9.02 ± 0.61	-38 ± 13
158	WN+OB?	2	8.64	8.20	7.81	$0.84^{+0.16}_{-0.28}$	0.40 ± 0.03	6.46 ± 1.38	12.23 ± 1.40	31 ± 3

(1)Gamen et al. (2009), (2)van der Hucht (2001), (3)Gosset et al. (2001), (4)Gamen et al. (2014), (5)Davis, Moffat & Niemela (1981), (6)Fahed & Moffat (2012), (7)Lépine et al. (2001), (8)Williams et al. (1992): average of quiescent photometry in 1989, (9)Varricatt&Ashok (2006).

surveys, with typically only a K-band (and occasionally H-band) spectrum available in the literature; inclusion of these stars in our analysis is subject to a spectral type being attributable by our near-IR classification scheme to the the required ± 1. Of the field WR stars included in this distribution analysis, we modify the previously claimed spectral types of ∼25% of those with *only* IR data available, indicated in Tables 8–9. For the remaining 75%, we either agree with previous spectral types based on near-IR spectra, or adopt optically assigned spectral types (always assumed to be reliable).

Further difficulty is encountered when trying to deter-

mine the binary status of each WR star, particularly late-WC stars, as IR line-dilution could be a result of thermal emission from circumstellar dust *or* the continuum of a bright companion. For WR stars of types other than WC7-9 showing evidence of binarity, if a flux ratio of the WR component to its companion is determinable in either J, H or K_S, it is straightforward to adjust the corresponding 2MASS photometry to that of the WR component alone. We follow one of two procedures to obtain near-IR flux ratios for suspected binary systems, depending on whether or not the companion responsible for line-dilution has been classified.

In the case of SB2 systems where both stars have been explicitly classified, we determine flux ratios in the JHK_S bands using the absolute magnitudes of Martins & Plez (2006) (O-stars) or Wegner (2006) (B-stars) along with our calibrated WR star absolute magnitudes. The advantage of this method is it enables us to correct photometry over all bands, allowing an extinction calculation by our favoured colour excess method. This method is also applicable to dusty WC stars, providing photometry is available from a quiescent period.

If a (non WC7-9) WR star shows diluted near-IR emission lines - but the nature of the diluting source is unclear - we estimate the flux ratio using single star emission line strengths (Appendix C). The dilution of optical lines can also be used, as the uniformity of OB-star intrinsic (V-K_S) colours (Martins & Plez 2006) makes it straightforward to translate a V-band flux ratio to the near-IR. However, the paucity of published line strengths typically results in a flux ratio only being determinable in one near-IR band. When this is the case, we either adopt A_v from the literature (indicated in Tables 8–9) or exclude the star from our analysis.

To determine the nature of late-WC stars displaying diluted emission lines, we incorporate photometry from the WISE all-sky survey (Wright et al. 2010) allowing us to construct a simplistic 1–22μm SED. We interpret a peak energy output at $\gtrsim 5\mu$m as evidence for circumstellar dust emission, and stars displaying this are excluded from our analysis as we cannot determine their distances accurately. We identify only one line-diluted late WC, WR 42 (WC7+O7V), to be conclusively dust-free, and include this star in the binary field sample (Table 9) with J-band photometry corrected for the companion.

Our field WR star sample consists of 246 objects; 18 of these are corrected for a companion by the line dilution technique, and 3 are corrected for a spectroscopically classified companion. We note that with the currently known population standing at $\sim$635, approximately 260 WR stars are unaccounted for in our calibration and field samples. Of these, the majority have uncertain spectral types, and lack spectra of sufficient quality (or spectral range) to obtain the required precision. Also excluded are stars with inconclusive evidence for a companion, and subtypes for which we cannot assign reliable near-IR absolute magnitudes (dusty WC stars, WN/C stars, WN10–11 stars).

A complete list of WR stars discovered between the Annex to the VIIth WR catalogue (van der Hucht 2001, 2006) and March 2014 is provided in Appendix A, which also highlights those for which distances have been obtained from the present study, together with an explanation of the revised nomenclature.

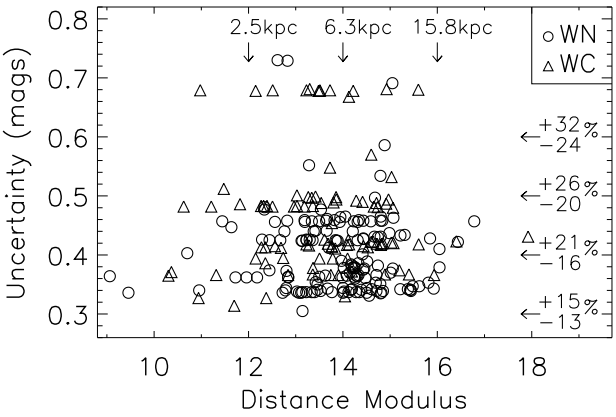

Figure 4. Distance modulus uncertainty for field WR stars, with equivalent distances indicated by vertical arrows and percentage errors by horizontal arrows.

3.2 Spatial properties

The Galactic locations of 354 WN and non-dusty WC stars comprising our calibration and field samples are shown in Figure 3. Uncertainties on distance moduli of field WR stars are displayed in Figure 4, where it can be seen that $\Delta DM \sim 0.4$ mag typically applies, and minimum distance uncertainties are approximately $\pm$14%.

3.2.1 Radial distribution

Figure 5 shows the radial distribution of 354 WR stars in the Milky Way. As expected, the majority of WR stars are located at Galactocentric distances of 3.5–10 kpc, with an additional peak at $R_G < 500$ pc owing to significant star formation within the central molecular zone (CMZ), reminiscent of OB-star forming regions (Bronfman et al. 2000).

Two conspicuous sub-peaks, consisting mostly of WN stars, occur at $R_G \sim 4.5$ kpc and ~ 7.5 kpc. Both may be viewed as superpositions on the underlying WR population, the innermost and outermost are largely attributable to the WR content of Westerlund 1 ($\sim$20 WR) and the nearby Cygnus star-forming region ($\sim$15 WR, $l \sim 75°$, $d = 1.3$–1.9 kpc) respectively.

3.2.2 z - distribution

Figure 6 shows that, as expected, WR stars are largely confined to the thin disk. This strict confinement to $z = 0$ resembles a Cauchy distribution. Indeed, a non-linear least squares fit of a Lorentzian function (Equation 8) matches well the distribution of vertical heights (z) of WR stars from the Galactic plane,

$$N(z) = A\Big[\frac{\gamma^2}{(z - z_o)^2 + \gamma^2}\Big], \qquad (8)$$

where γ is the half width at half maximum (HWHM), z_o is the location of the peak and A is an intensity. Assuming the Sun lies 20 pc above the Galactic plane (Humphreys & Larsen 1995), our fit yields $\gamma = 39.2$ pc and $z_o = 1.9$ pc (Figure 6).

Unlike other young stellar population tracers, we find

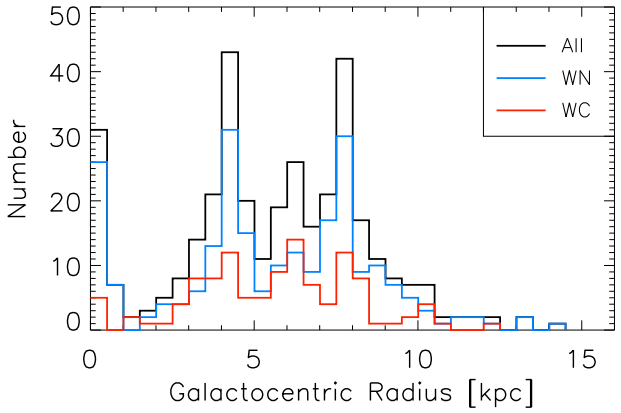

Figure 5. The distribution of Galactocentric radii for 354 WR stars, in 0.5 kpc bins

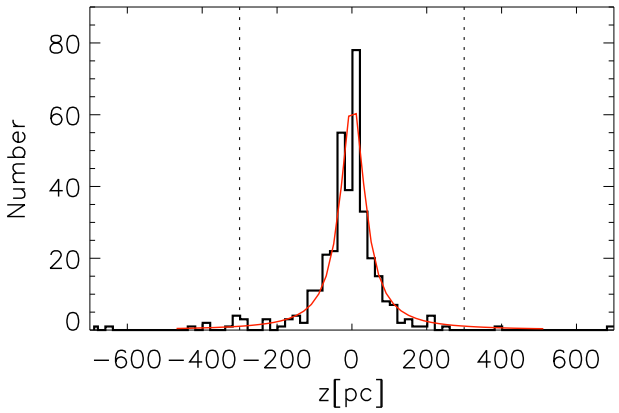

Figure 6. z distribution of 354 Galactic WR stars shown in 20 pc bins (thick black line) with a fitted three-parameter Lorentzian function (thin red line, Equation 8). Stars at $|z|>300$pc (outside dotted lines) are listed in Table 10.

no evidence for flaring of the WR star disk with increasing R_G, although this is likely due to the small number of WR stars identified beyond the solar circle. Paladini, Davies & De Zotti (2004) perform a Gaussian fit to the z-distribution of 456 Galactic H II regions interior to the solar circle, finding $\sigma \simeq 52$ pc (full width half maximum, FWHM ~ 125 pc). Although not identical to the form of our fit, this distribution is broader than what we observe for WR stars. The thickness of the OB star forming disk interior to the solar circle is measured by Bronfman et al. (2000), who find a FWHM of 30–50 pc - slightly narrower than the WR star disk - flaring to >200 pc beyond $R_G = 12$ kpc.

3.2.3 WR stars at large distances from the Galactic disk

A small fraction of WR stars are found at high vertical distances from the Galactic disk. Additional details of the 12 WR stars at $|z|>300$ pc ($\gtrsim 7\gamma$) are shown in Table 10, all of which are presumably runaways from star formation sites in the thin disk. We include WR 124 in Table 10 since it has previously been identified as an extreme runaway by its high peculiar radial velocity (156 kms^{-1}; Moffat, Lamontagne & Seggewiss 1982). Here we briefly discuss the possible events leading to their runaway status, and summarise the evidence for each.

First, we address the possibility that some of these objects are much fainter (thus less distant) WR-like central stars of planetary nebulae (CSPN). Both WC-like ([WC], e.g., Depew et al. 2011) and WN-like ([WN], e.g., Miszalski et al. 2012 and Todt et al. 2013) CSPN have been observed in the field, although [WC]-type are far more common. These objects are almost identical in spectral appearance to their high-mass analogues (Crowther et al. 2006a), yet are intrinsically fainter by several magnitudes.

We conduct a search for nebulosity around each $|z|>300$ pc WR star by inspection of SuperCOSMOS Hα images (Parker et al. 2005) and any other published Hα imaging. Identification of a surrounding nebula cannot alone prove any of these objects to be CSPN, as some WR stars are seen to posess ejecta nebulae (Stock & Barlow 2010), yet it would provide a strong indication. Nebulosity is only observed around WR 71, which are known to be a genuinely massive, potential WR+compact object binary system (Isserstedt et al. 1983). We therefore conclude that none of these 12 high-z WR stars are incorrectly classified CSPN.

There are two leading mechanisms by which massive stars can be ejected from their birthplaces; the binary supernova scenario where a massive binary system becomes unbound after a SN explosion (Blaauw 1961), and the dynamical ejection scenario where close encounters in a dense cluster can eject massive single or binary stars (Poveda, Ruiz & Allen 1967).

A WR star at $|z| = 700$ pc (similar to the highest observed), assuming $z = 0$ at birth and a time since ejection of 5 Myr (typical WR star age), would require an average velocity in the z direction of 140 kms^{-1}. In the case of dynamical interaction between massive single and binary stars, a typical ejection velocity is given by $v_{ej}^2 = GM_b/a$ (M_b = total mass of binary with semi-major axis a) according to Fujii & Portegies Zwart (2011), and the ejected star usually has the lowest mass of the three. By this reasoning, assuming a $M \gtrsim 25$ M$_\odot$ WR progenitor limit, a M_b=50 M$_\odot$ (160 M$_\odot$) binary with a period up to 170d (550d) would be capable of ejecting a WR progenitor star with at least $v_{ej} = 140$ kms^{-1}. Ejection of the binary system is also possible in such an interaction, which one might expect thereafter to be associated with considerable hard X-ray flux from the collision of stellar winds. In Table 10 we include available X-ray observations for these 12 stars, showing that only WR 3 is conspicuous, lying on the L_X/L_{bol} relation for spectroscopic O-star binaries (Oskinova 2005). However, Marchenko et al. (2004) find no evidence for short period (<2yr) radial velocity changes, concluding that WR 3 is likely a single star.

Alternatively, the locations of these stars may be explained by momentum gained from the supernova explosion of a companion. Dray et al. (2005) estimate that $^2/_3$ of massive runaways are produced this way. Isserstedt, Moffat & Niemela (1983) show that kick velocities of ~ 150 kms^{-1} may be imparted on a surviving star, and that this star and the resulting supernova remnant may remain bound if less than half the total system mass is lost during the supernova. Therefore, one would expect a fraction of massive runaway stars to have compact companions. Indeed, WR 148 is an SB1 (Drissen et al. 1986)

Table 10. Properties of 12 WR stars observed at $|z|>300$ pc, plus WR 124 which is known to be an extreme runaway.

WR#	Sp. type	z(pc)	Binary status	L_X (ergs s^{-1})	Hα Nebula?	Natal Cluster
17	WC5	-303 ± 59	single	not detected[d]	...	...
3	WN3ha	-308 ± 83	single	2.5×10^{32} [c]	...	...
56	WC7	-323 ± 58	single	not detected[d]	No	...
54	WN5	-378 ± 61	single	not detected[d]	No	...
49	WN5(h)	-386 ± 63	single	not detected[d]	No	...
75c	WC9	406 ± 78	single	...	No	...
61	WN5	-411 ± 66	single	$< 5.0 \times 10^{30}$ [c]	No	G305?
71	WN6	-689 ± 139	Binary? (SB1)[a]	not detected[d]	Yes[e]	...
93a	WN3	694 ± 214	single	...	No	GC?
123	WN8	-711 ± 120	single	not detected[d]	No	...
64	WC7	775 ± 127	single	not detected[d]	No	...
148	WN8h	814 ± 131	Binary (SB1)[b]	$< 1.6 \times 10^{32}$ [c]	...	...
124	WN8h	213 ± 39	single	$< 2.0 \times 10^{32}$ [c]	Yes[e]	...

[a]Isserstedt et al. (1983), [b]Drissen et al. (1986), [c]Oskinova (2005), [d](ROSAT, Pollock, Haberl & Corcoran 1995), [e]Stock & Barlow (2010).

and the strongest Galactic candidate after Cyg-X3 for a WR+compact object binary. Low amplitude photometric and spectroscopic variations have been observed in WR 71 and WR 124 (Isserstedt et al. 1983; Moffat et al. 1982), suggesting they may also be SB1 systems with small mass functions. However, the absence of X-ray emission from accretion onto a compact object remains unexplained in all 3 cases. We note that the WR+OB binary fraction amongst this sample is very low, and quite possibly zero.

It has been suggested that WN8–9 subtypes are more frequently observed as WR runaways (Moffat 1989). If we consider only the most extreme examples, i.e., $|z|>500$ pc plus WR 124, it can be seen from table 10 that 3/6 are of the WN8 subtype. Although numbers are small, a preference seems to exist for WN8 runaways. Moffat (1989) argue that a WN8 spectral appearance may arise from mass accretion from a binary companion. Combined with the unusually low WR+OB binary fraction and the low-mass companion of WR 148, this evidence favours a binary supernova origin for the extreme runaway WR population.

Two of the runaway stars listed in Table 10, WR 61 and WR 93a, are observed at similar Galactic longitudes to the G 305 complex and GC clusters, respectively. Considering our typical distance uncertainties (Figure 4), ejection from these massive star forming regions is a possible explanation for their large distance from the Galactic plane.

3.3 Subtype distributions across the Galactic metallicity gradient

Here we assess how WR subtypes vary across the Milky Way disk and compare this to the predictions of metallicity (Z)-dependent evolutionary models. By including WR stars in the Large and Small Magellanic Clouds (LMC and SMC), we may probe massive star evolution over a metallicity range $Z = 0.002$–0.04. A constant star formation rate is implicitly assumed in all regions considered, allowing us to relate the relative numbers of WR subtypes observed with the relative duration of associated phases.

We proceed by dividing the Galaxy into three broad zones of super-solar ($R_G < 6$ kpc), solar ($6 < R_G < 9$ kpc), and sub-solar ($R_G > 9$ kpc) metallicity. Based on the HII-region metallicity analysis of Balser et al. (2011), we assign approximate Oxygen abundances ($\log[^O/_H]+12$) of 8.85, 8.7 and 8.55 (± 0.1dex) to each zone respectively; each value is arrived at by inspection of their figure 8 and a derived (azimuthally averaged) $\log[^O/_H]$ gradient of -0.05 ± 0.02 dex kpc^{-1}. According to our distribution analysis of 354 WR stars, we find 187, 132 and 35 to inhabit the super-solar, solar, and sub-solar metallicity zones respectively. Additionally, there are 148 known WR stars in the LMC (Breysacher et al. 1999; Neugent et al. 2012 and references therein; Massey et al. 2014) for which the Oxygen abundance is $(\log[^O/_H]+12) = 8.38$ (Rolleston, Trundle & Dufton 2002), and 12 WR stars in the SMC (Massey & Duffy 2001b; Massey et al. 2003) for which $(\log[^O/_H]+12) = 8.13$ (Rolleston et al. 2003).

As recently highlighted by Groh et al. (2014), there is not a straightforward correspondence between spectroscopic and evolutionary phases in massive stars, particularly post-main sequence. Spectroscopically, any WN showing surface Hydrogen (WN#h or (h)) or with ionisation type $\geqslant 7$ is identified as late-type (WNL), while H-free WN of ionisation type $\leqslant 6$ or those displaying broad emission lines (WN#b) are early-type (WNE). We follow these definitions here, noting that the lack of near-IR hydrogen diagnostics is unlikely to significantly affect our measured N_{WNE}/N_{WNL}, as Galactic WN $\leqslant 7$ stars are generally H-free (Hamann, Gräfener & Liermann 2006), so division by ionisation type alone is sufficient. This assumption is less applicable in the lower metallicity regions of the outer Galaxy, however, low extinction in these directions means optical (hydrogen) diagnostics are commonly available. We include the WNha stars as WNL when evaluating subtype number ratios; their definition as such has minimal effect as only 18/235 WN considered belong to this class. The division in WC stars is more straightforward, with WC4–6 defined as early (WCE) and WC7–9 as late-type (WCL). In Table 11 we show the subtype breakdown of WR stars observed in each Galactic metallicity region.

In stellar models, stars have historically been matched with the aforementioned spectroscopic WR types using basic

surface abundance and effective temperature (T_{eff}) criteria. For example, Meynet & Maeder (2005) employ $T_{eff} > 10^4$ K and $X_H < 0.4$ as the definition of a WR star in their models, while Eldridge, Izzard & Tout (2008) add a further constraint of $\log(L/L_\odot) > 4.9$. This T_{eff} boundary is too low, since even the coolest WR stars (WN8–9) are found to have $\log(T_{eff}) \simeq 4.6$ (Hamann et al. 2006). A surface temperature of 10^4 K is more typical of late-B/early-A supergiants (Przybilla et al. 2006). Also, recent spectroscopic analysis of WC stars by Sander, Hamann & Todt (2012) indicate that some WC9 stars are very close to this lower luminosity limit. The transition between eWNE and eWNL phases (where 'e' denotes the definition in evolutionary models) is regarded to occur when $X_H < 10^{-5}$, and the eWC phase begins when carbon dominates nitrogen by mass (Meynet & Maeder 2005). By computing model spectra from evolutionary models, Groh et al. (2014) have shown that spectroscopic WNE and WNL lifetimes can differ radically from eWNE and eWNL lifetimes, as a star may have a WNE spectrum while retaining some surface hydrogen, hence this is a poor indicator. The problem is not so severe regarding the transition from WN to WC stars, as the change in surface carbon abundance is a rapid process, meaning the eWC phase corresponds well to the spectroscopic WC phase.

3.3.1 Incompleteness of the sample

Before comparing observed numbers with evolutionary model predictions, it is necessary to comment on two selection effects - one in our distribution analysis and one inherent to WR star surveys - that affect the star counts we present.

Firstly, as we cannot assume reliable near-IR absolute magnitudes for dusty WC stars they have been excluded from our distribution analysis. Thus, in Table 11 we count only those WC stars showing no evidence for circumstellar dust. However, by inspection of a local volume-limited (< 3 kpc) sample of WR stars (see Section 4.3.2 for full details), we estimate that 27($\pm$ 9)% of WC stars shown evidence of circumstellar dust. To account for the effect of these neglected stars, we plot in Figure 7 a set of enhanced WC/WN number ratios along with the values shown in Table 11. As this information is only available in the solar neighbourhood, we are forced to assume an unvarying fraction of dust-forming WC stars across the whole Galaxy. Late-type WC stars are known to dominate at higher metallicity, and it is predominantly these that are seen forming dust, hence we expect this fraction in reality to be higher towards the Galactic Centre. The slight downturn in N_{WC}/N_{WN} at $R_G < 6$ kpc could be due to a higher number of late WC stars omitted from our analysis in this region.

Secondly, the two most widely employed WR star survey techniques are both least effective at identifying weak-lined WNE stars. Narrow-band IR imaging surveys are biased against WNEs due to low photometric excesses from their weak emission lines. The IR excess emission from free-free scattering - exploited by broad-band selection techniques - is also weaker in WNE stars as their wind densities are lower than other WR subtypes. For these reasons, and considering their modest IR luminosities, we expect WNE stars to be slightly under-represented in our total sample, especially beyond the solar neighbourhood. Therefore, future observations will likely refine the numbers presented here by marginally decreasing N_{WC}/N_{WN} and increasing N_{WNE}/N_{WNL}.

3.3.2 Comparison to evolutionary predictions

In Figure 7 we plot observed N_{WC}/N_{WN} in different regions of the Galaxy, and the Magellanic Clouds, alongside the predictions of various evolutionary models for massive stars. Rotating single-star models are taken from Meynet & Maeder (2005), non-rotating single-star models with various $\dot{M}(Z)$ dependencies are taken from Eldridge & Vink (2006), and finally predictions for a population of non-rotating massive binaries exhibiting metallicity dependent mass-loss are taken from Eldridge et al. (2008) (BPASS[2]).

All models predict an increasing number of WC compared to WN stars with metallicity, due to increasingly rapid exposure of nuclear burning products caused by stronger stellar winds in more metal-rich environments. Our analysis shows only a modest variation of N_{WC}/N_{WN} (0.4–0.55) across the Galactic disk, whereas the ratio drops considerably to 0.2–0.1 at LMC and SMC metallicities. At all metallicities the observed N_{WC}/N_{WN} lies between the predictions from a population of binary stars (Eldridge et al. 2008) and single non-rotating stars. The addition of an estimated 28% of neglected (dusty) WC stars at Galactic metallicities does not significantly alter this. However, the predictions of evolutionary models including rotation lie ubiquitously lower than our observations at Galactic metallicities. Fast rotation has the effect of lengthening WR lifetimes, manifest predominantly in the eWNL phase, thus reducing N_{WC}/N_{WN} (Meynet & Maeder 2005). However, it is not expected that all massive stars are formed rotating as quickly ($v_i^{rot} = 300\,\mathrm{km\,s^{-1}}$) as those generated in these models (Penny & Gies 2009).

Figure 8 shows the number ratio of early to late WN stars in each Galactic metallicity zone, as well as in the LMC and SMC. An increase in the proportion of WNE can be seen with decreasing metallicity, and no WNL stars are known in the SMC. Contrary to this, the rotating models of Meynet & Maeder (2005) produce a *shorter* relative eWNE phase at lower metallicity, due to less efficient removal of the H-rich stellar envelope during prior evolutionary phases. Furthermore, rotationally induced mixing allows stars to become WR earlier in their evolution and experience an extended eWNL phase. The extreme sensitivity of the eWNE/eWNL transition to the chosen hydrogen surface abundance criterion clearly has a major influence on predictions (Groh et al. 2014). Therefore we interpret the disparity shown in figure 8 largely as a symptom of these definitions rather than a serious conflict with evolutionary theory.

Our results show that the WN phase of WR stars at sub-solar metallicities is almost entirely spent with a WNE spectral appearance, whereas the WNL spectral type endures longer on average at super-solar metallicities.

[2] http://www.bpass.org.uk/

Table 11. Observed Wolf-Rayet number ratios in the Galaxy, LMC and SMC. Galactic WC stars counted here show no evidence of circumstellar dust, results incorporating an estimated 28% of neglected (dusty) WC stars are parenthesised. The 4 WO stars are counted as WCE. An indication of uncertainty is given assuming $\sqrt{N}$ errors on each count.

Region ($\log[^O/_H]+12$)	N_{WR}	N_{WC} (N_{WCd})	N_{WN}	N_{WC}/N_{WN} ($N_{(WC+WCd)}/N_{WN}$)	N_{eWNE}/N_{eWNL}	$N_{(WCE+WO)}/N_{WCL}$
Inner Galaxy (8.85 ± 0.1)	187	63 (~ 22)	124	0.51 ± 0.08 (0.69)	0.23 ± 0.05	0.05 ± 0.03
Mid Galaxy (8.7 ± 0.1)	132	46 (~ 16)	86	0.53 ± 0.10 (0.73)	0.79 ± 0.17	1.00 ± 0.28
Outer Galaxy (8.55 ± 0.1)	35	10 (~ 4)	25	0.40 ± 0.16 (0.57)	1.27 ± 0.58	1.5 ± 0.97
LMC (8.38 ± 0.05)	148	26	122	0.21 ± 0.05	1.93 ± 0.37	26/0
SMC (8.13 ± 0.05)	12	1	11	0.10 ± 0.09	11/0	1/0

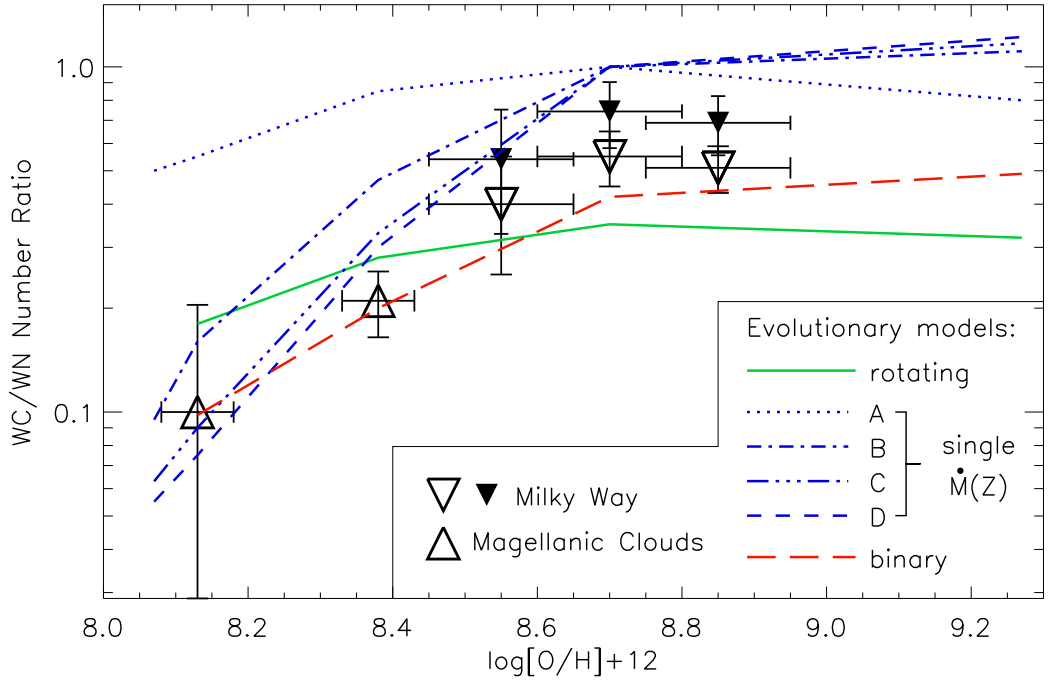

Figure 7. Number ratio of WC/WN stars in the LMC and SMC (triangles), and across three Milky Way regions (upsidedown triangles) where results omitting dusty WC stars (as in Table 11) are plotted as larger open symbols and smaller filled symbols represent the case where 28% of all WC stars posses hot circumstellar dust (Section 4.3.2). Solid (green) line shows the predictions of Meynet & Maeder (2005) for rotating single stars. Long-dashed (red) line shows the predictions of Eldridge et al. (2008) for a population of massive binaries. All other lines (blue) represent non-rotating single-star evolutionary predictions of Eldridge & Vink (2006) for four different $\dot{M}-Z$ dependencies. Errors on the number ratios shown are estimated assuming $\sqrt{N}$ counting errors in N_{WC} and N_{WN}. An uncertainty of 0.1 dex is assigned to each Galactic O/H value.

4 MODELLING THE TOTAL WR STAR POPULATION OF THE MILKY WAY

With knowledge of how WR subtypes vary with Galactocentric radius, and the intrinsic near-IR brightness of each subtype, we are in a position to model the observational properties of the whole Galactic WR population. To this end we develop a 3D, azimuthally symmetric "toy" model of the WR population - described in the following section - that is scalable to different total numbers of WR stars. For varying numbers of WR stars, we apply a simple Galactic dust distribution to redden the population, and derive magnitude distributions in various bands for comparison with the observed population, allowing us to estimate the total number of Galactic WR stars.

4.1 Populating the model

We do not attempt to incorporate complex structural features such as spiral arms or the Galactic bar into this model WR population, as our aim is to derive basic observational

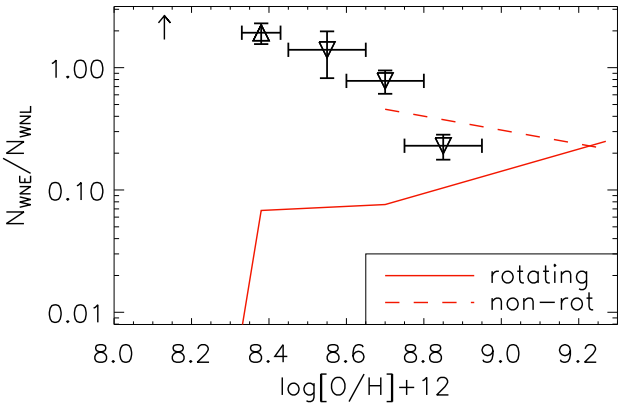

Figure 8. Number ratio of WNE/WNL stars across three metallicity zones in the Milky Way, LMC and SMC. Red lines show eWNE/eWNL predictions from rotating (solid) and non-rotating (dashed) evolutionary models (Meynet & Maeder 2005).

characteristics of the whole population, smoothing over any local enhancements. We therefore distribute model WR stars in an azimuthally symmetric disk, with the same thickness the observed population. We generate the z-coordinate of each star so they are Cauchy distributed, by computing

$$z_i = \gamma \tan(\pi r_{01} - \frac{1}{2}), \quad (9)$$

where r_{01} is a randomly generated number between 0 and 1 and γ is the observed HWHM (39.2 pc, Section 3.2.2). The z-distribution is truncated at $z = \pm 1$ kpc in accordance with the most extreme runaway stars observed.

We construct a model WR disk composed of 24 annuli of 0.5 kpc in width spanning radii $R_G = 3$–15 kpc. Rather than using our observed radial distribution of WR stars to dictate the relative number in each annulus, we utilise a normalised version of the radial HII-region distribution presented by Paladini et al. (2004), since we consider HII-regions to be a more complete tracer of hot young stars over a larger Galactic extent. Within each annulus, the model stars are randomly placed between the lower and upper radii at a random angle (θ) between 0 and $2\,\pi$ around the model disk. In these coordinates the Sun is located at $z = 20$ pc, $\theta = 0°$, and $R_G = 8000$ pc.

Interior to $R_G = 3$ kpc, where star formation is suppressed (aside from the CMZ) we include a fixed number of WR stars in every model. Dong et al. (2012) report on a Pa-α survey covering the central $\sim 0.6°$ (~ 80 pc) of the Galaxy, including the three massive clusters (Arches, Quintuplet and GC). Within this region they identify as many emission line sources (evolved massive star candidates) outside of these clusters as within them; given that ~ 80 WR stars are known to reside in these clusters, we estimate 160 WR stars present in the Dong et al. survey area. The CMZ is approximately 3° (400 pc) across, and the density of gas in this extreme environment is strongly centrally peaked, so that approximately 40% of the CMZ gas lies within the Dong et al. survey area (Ferrière 2008). Assuming the non-cluster population of WR stars roughly follows the amount of molecular gas, this would imply a further ~ 100 WR stars in the CMZ. The inner Galaxy ($R_G < 3$ kpc) contains little star formation outside the CMZ, we therefore populate this

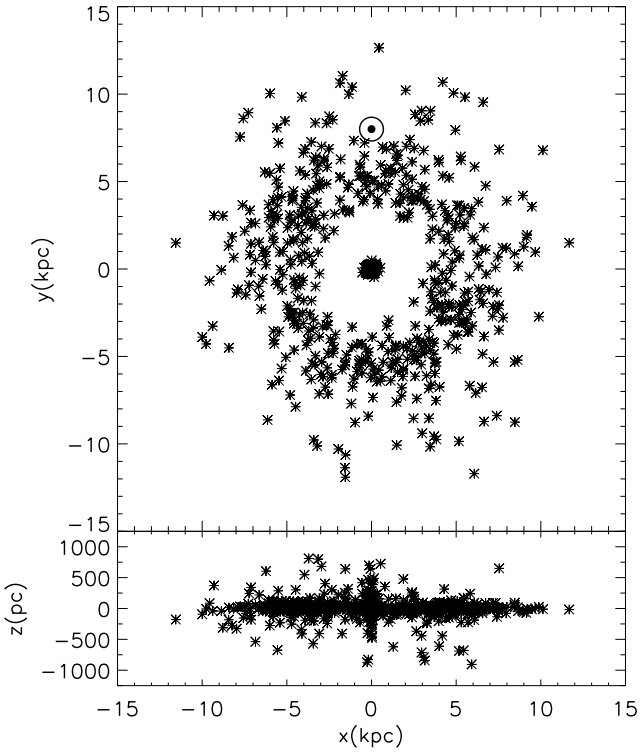

Figure 9. An example model WR population mimicking that of the Galaxy, containing 550 stars at $R_G = 3$–15 kpc and 250 at $R_G < 3$ kpc, shown in Cartesian coordinates. The location of the Sun is indicated by the standard symbol at (0,8 kpc) in the top panel.

area in our models with 250 WR stars, following a Gaussian distribution centred on $R_G = 0$ with $\sigma = 200$ pc. An example model is displayed in Figure 9.

The number of WR stars in each radial bin of our model population is divided into four components representing WNE, WNL, WCE and WCL. The relative numbers of each WR type match those observed (Table 11), varying from the model GC where late-types dominate to $R_G = 15$ kpc where early-types are in the majority. We assign absolute magnitudes of $M_{K_S} = -4.31$, -6.01, -4.45 and -4.89 to WNE, WNL, WCE, and WCL types respectively, based on averaging our calibration results (Section 2.5). We do not include WO or WN/C stars as they constitute a negligible fraction of the population.

4.2 A dust model for the Milky Way

We include two dust components in our model WR star disk; one associated with molecular (H_2) gas, the other with atomic H gas. We apply the same dust-to-gas mass ratio for each component. This assumption follows Bohlin et al. (1978) who derive a *total* neutral hydrogen to colour excess ratio, implying the each atom of H is responsible for a set amount of extinction, whether in molecular or atomic form. Both dust components are included as two dimensional functions in R_G and z, motivated by the spatial distribution measured for their respective gas species. These gas measurements are taken from Nakanishi & Sofue (2006)

and Nakanishi & Sofue (2003) for molecular (traced using CO) and atomic gas respectively.

Functions describing each dust component have the form $D_m(R_G) \times D_h(R_G, z)$, where $D_m(R_G)$ describes the dependence of midplane density on Galactocentric radius, and $D_h(R_G, z)$ describes how the density drops with vertical distance from the midplane.

Both dust components are included with a vertical dependence of the form $D_h(R_G, z) = \mathrm{sech}^2(\zeta)$, where

$$\zeta(R_G, z) = \log(1+\sqrt{2})\frac{z}{z_{1/2}(R_G)}. \quad (10)$$

and $z_{1/2}(R_G)$ is the height at which the density falls to half of the midplane value, which increases linearly with galactocentric radius for both gas species. For molecular gas, $z_{1/2}(R_G{=}0) = 25$ pc increasing to 90 pc at $R_G{=}10$ kpc (Nakanishi & Sofue 2006). For atomic gas, $z_{1/2}(R_G{=}0) = 100$ pc increasing to 500 pc at $R_G{=}15$ kpc (Nakanishi & Sofue 2003).

To represent the midplane density of molecular gas, we construct the following function:

$$D_m^{mol}(R_G) = N_0^{mol}\,\mathrm{sech}^2\left(\frac{R_G}{800pc}\right)... \\ ... + \exp\left[\frac{-(R_G-4300pc)^2}{2(2500pc)^2}\right][\mathrm{cm}^{-3}], \quad (11)$$

which is shown in Figure 10. The scaling values in Equation 11 and $N_0^{mol} = 10\,\mathrm{cm}^{-3}$ are chosen to reproduce the maps of Nakanishi & Sofue (2006).

To represent the midplane density of atomic gas, we employ a summation of two step functions:

$$D_m^{atom}(R_G) = N_0^{atom}\Big[1 + \frac{1.3}{1+\exp(\frac{-(R_G-6500pc)}{200pc})}... \\ ... - \frac{1.3}{1+\exp(\frac{-(R_G-13200pc)}{550pc})}\Big][\mathrm{cm}^{-3}] \quad (12)$$

as shown in Figure 10. Once again, we choose the scaling values and $N_0^{atom}{=}0.08\,\mathrm{cm}^{-3}$ to reproduce the maps of Nakanishi & Sofue (2003).

Finally, we integrate the total dust function,

$$D(R_G, z) = (D_m^{mol} \times D_h^{mol}) + (D_m^{atom} \times D_h^{atom}), \quad (13)$$

along the line of sight from the Sun to each model WR star to provide a total amount of obscuring dust. Hence we obtain an extinction to each model star, assuming A_{K_S} is proportional to the amount of dust along the line of sight, normalised to give $A_{K_S}{=}2.42$ mag towards the GC ($R_G = 0$, $z = 0$; Fritz et al. 2011).

4.3 Quantifying the total population

By combining our model WR star population (Section 4.1) with the dust function described in the previous section, we are able to generate a global magnitude distribution for a WR population containing any number of stars. The total WR star population follows an assessment of which predicted magnitude distribution most closely reproduces that observed.

Before deducing this number, it is worth reconsidering what the WR stars in our model represent. As their absolute magnitudes are based on our calibrated values for WR stars (Section 2), they represent what we will refer to as 'WR-dominated' systems, i.e., where any companion star(s) do not affect the systemic magnitude by more that 0.4 mag (typical error on our absolute magnitude calibrations), i.e., $(m_K^{\mathrm{WR}} - m_K^{sys}) > 0.4$, corresponding to a WR/system flux ratio of $\mathrm{F}_K^{\mathrm{WR}}/\mathrm{F}_K^{sys} > 0.7$. Also, these model stars do not represent WO, WN/C or dust-producing WC stars. Therefore, to achieve a like-for-like comparison to observations, we initially only consider observed 'WR-dominated' systems, and in Section 4.3.2 estimate the contribution of neglected WR types.

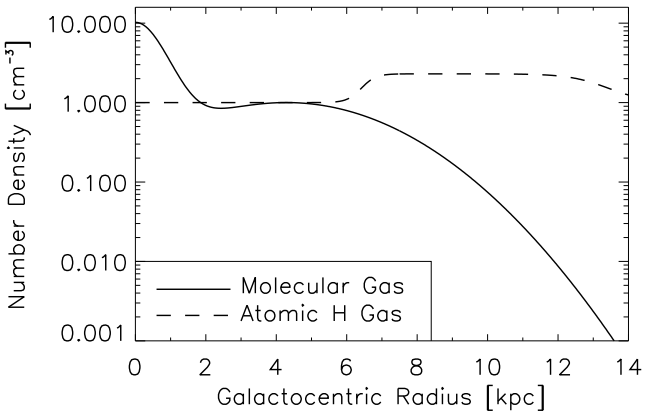

Figure 10. Midplane number density of molecular H_2 (solid) and atomic H (dashed) gas, used to govern our model dust distribution, as a function of Galactocentric radius (Equations 11 and 12, respectively).

4.3.1 Comparison to a magnitude-limited sample

For comparison to our model K_S-band magnitude distributions, we assemble a magnitude-limited sample of real WR-dominated systems. We note that $<5\%$ of WR stars discovered since the year 2011 are brighter than $K_S{=}8$ mag (Mauerhan et al. 2011; Shara et al. 2012; Smith et al. 2012; Chené et al. 2013). Therefore, we adopt this as the current completeness limit in *systemic* magnitude..

Figure 11 presents predicted magnitude distributions for WR populations containing 450, 550 and 650 stars between $R_G = 3$–15 kpc plus 250 central stars ($R_G < 3$ kpc). Also shown is the number of observed WR-dominated systems with systemic $K_S < 8$ mag. In spite of providing too few systems with $7.5 < K_S < 8.0$, the best agreement is found with the $550 + 250$ WR star model. Thus we take forward $800{\pm}100$ as the number of Galactic WR-dominated systems, with an approximate uncertainty based on the comparison shown in Figure 11.

Assuming a shallower extinction law along lines of sight towards the GC has the effect of brightening our calibrated M_{JHK_S} values for late-type WN and WC stars by up to 0.3 mag (Section 2.5.1). Upon altering the magnitudes of the late-type WR stars in our model population by this amount, we find more consistency with magnitude distributions drawn from models containing $\sim$100 fewer WR stars. Hence, the effect of a shallower GC extinction law is within the uncertainties.

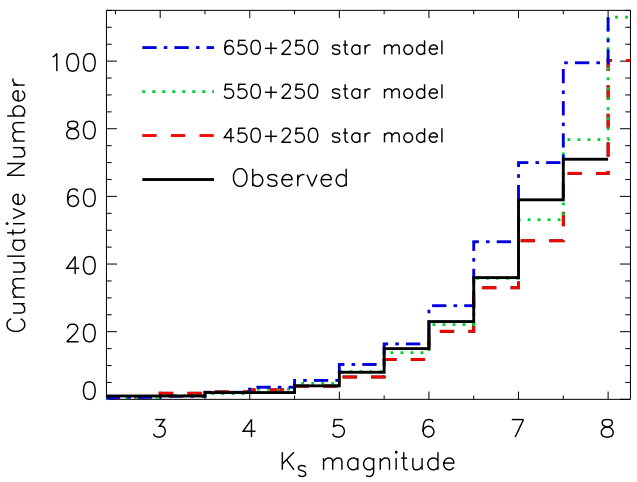

Figure 11. The cumulative number of observed WR-dominated systems (black solid line) in bins of 0.5 K_S mag, compared with that of three different model WR populations.

4.3.2 Fractions of dusty and companion-dominated WR systems in a volume-limited sample

Each point in our model WR star population represents a stellar system where a WR star is the dominant or sole near-IR source. To gain an insight into how many dusty and companion-dominated WR systems are overlooked by these models - and hence our initially deduced population of 800 - we construct a volume limited sample of nearby WR systems. In Appendix D we list all known WR stars within 3kpc of the Sun, where distances are taken from this work where possible (non-dusty WR stars), or by implementing $\bar{M}_v$-subtype calibrations of van der Hucht (2001). A v-band approach can be used to determine distances to dusty WC stars as hot dust emission does not contribute to the continuum flux at these wavelengths. We inspect the near-IR properties of these nearby WR stars, categorising each as either WR-dominated ($F_K^{WR}/F_K^{sys} > 0.7$), having a significant companion ($F_K^{WR}/F_K^{sys} < 0.7$), or dusty WC.

Of the 72 WR stars in this volume-limited sample, 41 are WC type of which 11 show evidence of circumstellar dust, indicating that $15 \pm 5\%$ of WR stars and $28 \pm 9\%$ of WC stars display circumstellar dust. A companion star dominates the near-IR continuum in 11 of the remaining 61 non-dusty WR systems ($18 \pm 6\%$). Uncertainties on these fractions are calculated assuming a $\sqrt{N}$ uncertainty on each number count.

The fractions derived from this volume-limited sample imply the previously derived population of 800 represents only 82% of the non-dusty population, as ∼18% (150) will have an IR bright companion. Furthermore, this non-dusty population of 1050 (=800+150) represents only 85% of the total population, as a further ∼15% (150) will be dusty WC stars. Two key assumptions underpin this estimate; constant fractions of companion-dominated and dust-producing WR stars at all Galactocentric radii. We can have confidence in the former, as metallicity is not expected to effect the binary fraction. The latter however is almost certainly invalid. The inner Galaxy is a preferential environment for WC stars, particularly late-type (WCL) which constitute 95% of WC stars (Table 11). If 100% of these WCL were dust-producing, this would equate to 31% of the total WR population. Mindful of this potential underestimate in the number of neglected systems in the model population, we estimate a total of 1200^{+300}_{-100} Galactic WR stars.

4.4 Expectations from star formation arguments

By combining the measured Milky Way star formation rate (SFR) with an initial mass function (IMF), it is possible to derive the average lifetime of the Wolf-Rayet phase ($\tau_{\rm WR}$) necessary to sustain a population of ∼1200 WR stars. Taking the Milky Way SFR to be $1.9\,{\rm M}_\odot{\rm yr}^{-1}$ (Chomiuk & Povich 2011), adopting a three-part Kroupa IMF (Kroupa & Weidner 2003), and assuming only stars with an initial mass $> 25\,{\rm M}_\odot$ experience a WR phase, our derived population can be reproduced with $\tau_{\rm WR} \simeq 0.25$ Myr.

This result is broadly consistent with rotating (non-rotating) Geneva models at solar metallicity (Georgy et al. 2012), which display $\tau_{\rm WR} = 0.45$ Myr (0.006 Myr) at $M_i = 32\,{\rm M}_\odot$ increasing with mass to 0.9 Myr (0.4 Myr) at $M_i = 120\,{\rm M}_\odot$. WR lifetimes as a result of binary evolution at solar metallicity are predicted to span $\tau_{\rm WR} = 0.5$ Myr at $M_i = 30\,{\rm M}_\odot$ to 1.0 Myr at $120\,{\rm M}_\odot$ (Eldridge et al. 2008). Although, binary evolution favours lower WR progenitor masses, so the assumed progenitor mass limit of $> 25\,M_\odot$ used to calculate of $\tau_{\rm WR}$ based on our population estimate may be inappropriate. Previously claimed population sizes exceeding 6000 (van der Hucht 2001; Shara et al. 2009) are difficult to reconcile with the measured Galactic SFR and a progenitor mass limit $M > 25\,{\rm M}_\odot$, as WR lifetimes in excess of 1 Myr would be required.

The CMZ accounts for an estimated ∼4–5% of Galactic star formation (Longmore et al. 2013), yet we estimate it contains ∼250 (13%) of the Galactic WR star population. The discrepancy between these fractions would suggest either we have underestimated WR numbers in the Galactic disk, or this CMZ star formation rate is insensitive to the most recent episodes of massive star formation.

4.5 Implications for future spectroscopic surveys

Near-IR surveys, both broad and narrow-band, continue to add to our knowledge of the obscured Galactic Wolf-Rayet population. A crucial question of to spectroscopic follow-up campaigns is how deep do spectroscopic surveys need to go? Figure 12 shows multi-band magnitude distributions derived from our favoured model WR star population. We estimate that to achieve 95% completeness, spectra of candidate WR stars need to be taken to a depth of $K_S \simeq 13$ mag - shallower by ∼2.5 mag than the 95% limit estimated by Shara et al. (2009).

The ESA *Gaia* mission will perform precision astrometry for a billion stars down to visual magnitudes of 20, and acquire low-resolution spectra of objects brighter that magnitude 16. To investigate the potential of *Gaia* in the search for and characterisation of WR stars, we derive the observed G-band distribution of our favoured model population (Figure 12). To do this we utilise magnitude transformations provided by Jordi et al. (2010), M_v for WR stars from van der Hucht (2001), and $(b-v)_o$ colours from Morris et al.

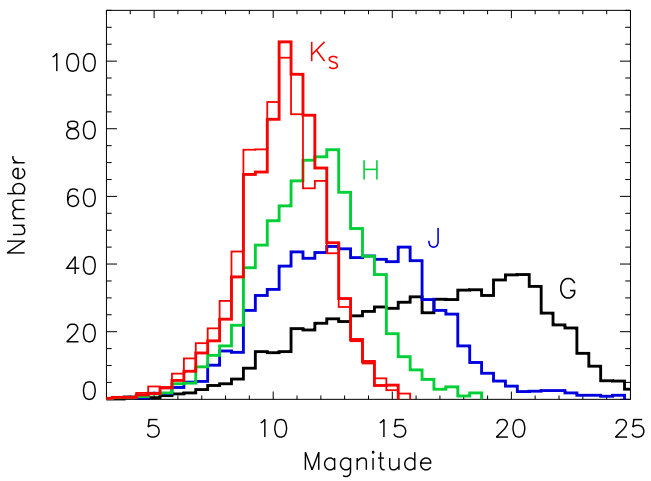

Figure 12. Histogram of 2MASS JHK_S and G-band (*Gaia*) magnitudes predicted for our preferred model Galactic WR star population. Each distribution shown is an average over 10 model repetitions. Two K_S-band distributions are plotted, the thin (red) line represents a model population where 28% of WC stars are dust forming (WC8d/9d, $M_{K_S} = -6.95$, Table 5). All thick lines represent populations consisting of WN and non-dusty WC stars.

(1993). We predict that approximately 600 ($\sim 1/3$ of total) WR stars will appear within *Gaia*'s $6 < G < 20$ observing range, with $\sim$300 brighter than the magnitude limit for spectroscopy. With the known population currently totalling $\sim$635, *Gaia* is unlikely to discover significant WR populations via spectroscopy, but the majority of those known will have distances measured to a significantly higher level of accuracy than is currently possible.

5 CONCLUSIONS

We have presented near-IR absolute magnitude-spectral type calibrations for WN, WC and WO type Wolf-Rayet stars, based on 126 examples with known distances (mostly by cluster or OB association membership). Applying these calibrations to the rapidly growing known Galactic population, we derive distances to a further 246 WR stars and present a 3D map of their locations. We note that approximately half as many WC stars are available for calibration as cluster/association members than WN, consistent with the findings of Smith & Tombleson (2014) than WC stars are generally more isolated. This challenges the idea that WC stars descend directly from WN, which in turn descend from the most massive O-stars. We have shown the heights of WR stars from the Galactic midplane to be Cauchy distributed with HWHM = 39.2 pc, where 12 stars reside at $|z| > 300$ pc. The low binary fraction and a preference for WN8 subtypes in this small sample of runaway stars indicates a binary supernova origin for the most extreme examples.

Exploiting the variation of metallicity across the Galactic disk, we have compared subtype number ratios measured in the inner Galaxy, solar neighbourhood, and outer Galaxy to the predictions of various metallicity-dependent evolutionary models. We measure N_{WC}/N_{WN} to be significantly higher than predicted by evolutionary models including fast rotation (Meynet & Maeder 2005), suggesting that lengthened WNL and shortened WC phases resulting from stellar rotation are not widely observed at ($Z \gtrsim Z_\odot$). Similarly, a shortened eWNE phase in such models - particularly at lower metallicity - is not manifest in our observations, as we observe approximately equal numbers of WNE and WNL stars in regions of $Z \lesssim Z_\odot$. Single-star models without rotation (Eldridge & Vink 2006) and models that account for the various effects of binary interaction (Eldridge et al. 2008) reproduce our measurements of N_{WC}/N_{WN} more appropriately. Hence, to a first approximation a population consisting of non-rotating single stars and interacting binaries would be consistent with the N_{WC}/N_{WN} we observe. However, we caution that all comparisons of this nature are subject to how the physics contained in stellar models is expected to translate into observable properties, which currently rests on estimations of surface abundances and temperatures that may not be appropriate (Groh et al. 2014), particularly for the transition between eWNE and eWNL subtypes.

Consolidating information gained about the spatial distribution, subtype variation, and intrinsic IR brightness of WR stars, we have created a scalable toy model of the Galactic WR population. By applying a 3D dust distribution to this model - spatially congruous with the gas content of the Galaxy - we derive observable properties for populations of various sizes at multiple wavelengths. Comparison of these model-derived observables to the observed population of non-dusty, WR-dominated ($m_K^{\rm WR} - m_K^{sys} > 0.4$) systems to a completeness limit of $m_K^{sys} < 8$ indicates a total of $\simeq$800 in the Galaxy. Using a volume-limited sample ($d < 3$kpc) we estimate such systems represent $\sim$69% of the whole WR population, hence we claim a Galactic WR population totalling 1200^{+300}_{-100}.

We deduce that an average WR phase duration of 0.25 Myr is necessary to sustain our estimated population, assuming a Kroupa IMF and a constant Milky Way star formation rate of $1.9\,{\rm M}_\odot{\rm yr}^{-1}$. This is compatible with the WR phase duration in rotating stellar models at solar metallicity (Georgy et al. 2012).

Looking to the future, we have used our favoured model WR population to estimate a required depth of $K_S < 13$ for spectroscopic surveys to achieve 95% completeness in Galactic WR stars. We have also predicted that the ESA *Gaia* mission will not deliver a significant number of WR star discoveries via low-resolution spectroscopy, but should provide improved distance measurements for the majority of the currently recognised population.

ACKNOWLEDGMENTS

The authors would like to thank he referee (A. F. J. Moffat) for a careful reading and useful comments that improved the paper. We also thank William. D. Vacca for making available high-quality spectra of selected WR stars, useful for refining near-IR classification diagnostics. We are also grateful to MPhys students Adrian Kus and Katie Baker for constructing and originally populating the Wolf-Rayet catalogue database. This work was supported in part by a UK Science and Technology Facilities Council studentship (CKR).

REFERENCES

Anderson G. E. et al., 2011, ApJ 727, 105
Arnal E. M., Cappa C. E., Rizzo J. R., Cichowolski S., 1999, AJ, 118, 1798
Balser D. S., Rood R. T., Bania T. M., Anderson L. D., 2011, ApJ, 738, 27
Baume G., Vázquez R. A., Carraro G., 2004, MNRAS, 355, 475
Benjamin R. A. et al., 2003, PASP, 115, 953
Bibby J. L., Crowther P. A., Furness J. P., Clark J. S., 2008, MNRAS, 386, L23
Blaauw A., 1961, Bull. Astron. Inst. Netherlands, 15, 265
Bohannan B., Crowther P. A., 1999, ApJ, 511, 374
Bohlin, R. C., Savage, B. D., & Drake, J. F., 1978, ApJ, 224, 132
Borissova, J. Georgiev, L. Hanson, M. M. et al. 2012, A&A 546, A110
Bressert, E., Bastian, N., Gutermuth, R. et al. 2010, MNRAS 409, L54
Breysacher J., Azzopardi M., Testor G., 1999, A&As, 137, 117
Bronfman L., Casassus S., May J., Nyman L.-Å., 2000, A&A, 358, 521
Burgemeister, S. Gvaramadze, V. V., Stringfellow, G. S., Kniazev, A. Y. Todt, H., Hamann, W.-R., 2013, MNRAS, 429, 3305
Cappa C. E., Goss W. M., Niemela V. S., Ostrov P. G., 1999, AJ, 118, 948
Cappa C. E., Vasquez J., Pineault S., Cichowolski S., 2010, MNRAS, 403, 387
Carraro G., Turner D., Majaess D., Baume G., 2012, in Proc. IAU Symp. 289, Beijing, arXiv:1209.2080
Chené A.-N., Borissova J., Bonatto C., Majaess D. J., Baume G., Clarke J. R. A., Kurtev R., Schnurr O., 2013, A&A, 549, A98
Chené A-N., Moffat A. F. J., St-Louis N., Schnurr O., Crowther P. A., Artiguau E., Alecian E., Wade G. A., 2014, MNRAS submitted
Chomiuk L., Povich M. S., 2011, AJ, 142, 197
Clark J. S., Negueruela I., Crowther P. A., Goodwin S. P., 2005, A&A, 434, 949
Cohen M., Parker Q. A., Green A. J., 2005, MNRAS, 360, 1439
Conti P. S., Massey P., Vreux J.-M., 1990, ApJ, 354, 359
Corradi, R. L. M., Valentini, M., Munari, U. et al., 2010, A&A 509, A41
Corti M., Bosch G., Niemela V., 2007, A&A, 467, 137
Cotera A. S., Simpson J. P., Erickson E. F., Colgan S. W. J., Burton M. G., Allen D. A., 1999, ApJ, 510, 747
Crowther P. A., 2003, Ap&SS, 285, 677
Crowther P. A., 2007, ARA&A, 45, 177
Crowther P. A., Smith L. J., 1996, A&A, 305, 541
Crowther P. A., Walborn N. R., 2011, MNRAS, 416, 1311
Crowther P. A., Smith L. J., Hillier D. J., 1995b, A&A, 302, 457
Crowther P. A., De Marco O., Barlow M. J., 1998, MNRAS, 296, 367
Crowther P. A., Morris P. W., Smith J. D., 2006a, ApJ, 636, 1033
Crowther, P. A., Smith, L. J., Hillier, D. J., & Schmutz, W., 1995a, A&A, 293, 427
Crowther P. A., Dessart L., Hillier D. J., Abbott J. B., Fullerton A. W., 2002, A&A, 392, 653
Crowther P. A., Hadfield L. J., Clark J. S., Negueruela I., Vacca W. D., 2006b, MNRAS, 372, 1407
Davies B., et al., 2012a, MNRAS, 419, 1871
Davies, B., de La Fuente, D., Najarro, F., Hinton, J. A., Trombley, C., Figer, D. F., Puga, E. 2012, MNRAS 419, 1860
Davis, A. B., Moffat, A. F. J., & Niemela, V. S., 1981, ApJ, 244, 528
de La Chevrotière A., Moffat A. F. J., Chené A.-N., 2011, MNRAS, 411, 635
de la Fuente, D., Najarro, F., Davies, B., Figer, D. F. 2013, in: Highlights of Spanish Astrophysics VII, p.534, Sociedad Española de Astronomía, arXiv:1210.1781
De Marco O., Schmutz W., 1999, A&A, 345, 163
Depew K., Parker Q. A., Miszalski B., De Marco O., Frew D. J., Acker A., Kovacevic A. V., Sharp R. G., 2011, MNRAS, 414, 2812
Djurašević G., Zakirov M., Eshankulova M., Erkapić S., 2001, A&A, 374, 638
Dong H., Wang Q. D., Morris M. R., 2012, MNRAS, 425, 884
Dray L. M., Dale J. E., Beer M. E., Napiwotzki R., King A. R., 2005, MNRAS, 364, 59
Dray L. M., Tout C. A., Karakas A. I., Lattanzio J. C., 2003, MNRAS, 338, 973
Drew, J. E., Barlow, M. J., Unruh, Y. C., Parker, Q. A., Wesson R., Pierce, M. J., Masheder, M. R. W., Phillipps, S., 2004, MNRAS, 351, 206
Drissen L., Lamontagne R., Moffat A. F. J., Bastien P., Seguin M., 1986, ApJ, 304, 188
Eikenberry S. S. et al., 2004, ApJ, 616, 506
Eldridge J. J., Izzard R. G., Tout C. A., 2008, MNRAS, 384, 1109
Eldridge J. J., Vink J. S., 2006, A&A, 452, 295
Eldridge, J. J., Fraser, M., Smartt, S. J., Maund, J. R., & Crockett, R. M., 2013, MNRAS, 436, 774
Espinoza P., Selman F. J., Melnick J., 2009, A&A, 501, 563
Esteban C., Peimbert M., 1995, A&A, 300, 78
Esteban C., Rosado M., 1995, A&A, 304, 491
Fahed, R., Moffat, A. F. J., 2012, MNRAS 424, 1601
Fahed, R., Moffat, A. F. J., Zorec, J., et al., 2011, MNRAS, 418, 2
Faherty, J. K., Shara, M. M., Zurek, D., Kanarek, G., Moffat, A. F. J. 2014, AJ 147, 115
Fang M., et al., 2012, A&A, 539, A119
Ferrière K., 2008, Astronomische Nachrichten, 329, 992
Figer D. F., McLean I. S., Morris M., 1999, ApJ, 514, 202
Figer D. F., McLean I. S., Najarro F., 1997, ApJ, 486, 420
Fritz T. K. et al., 2011, ApJ, 737, 73
Fujii M. S., Portegies Zwart S., 2011, Science, 334, 1380
Gamen R., et al. 2006, A&A, 460, 777
Gamen, R. C., Fernández-Lajús, E., Niemela, V. S., & Barbá, R. H., 2009, A&A, 506, 1269
Gamen, R. C, Collado, A., Barbá, R., Chené, A.-N., & St-Louis, N., 2014, A&A, 562, AA13
Garmany C. D., Stencel R. E., 1992, A&AS, 94, 211
Georgy C., Ekström S., Meynet G., Massey P., Levesque E. M., Hirschi R., Eggenberger P., Maeder A., 2012, A&A, 542, A29

Gillessen S., Eisenhauer F., Fritz T. K., Pfuhl O., Ott T., Genzel R., 2013, in de Grijs R., ed., IAU Symposium Vol. 289, pp 29–35
Gosset, E., Royer, P., Rauw, G., Manfroid, J., & Vreux, J.-M., 2001, MNRAS, 327, 435
Groh J. H., Meynet G., Ekström S, Georgy C., 2014, A&A, 564, A30
Gvaramadze, V. V., et al., 2009, MNRAS 400, 524
Gvaramadze V. V., Kniazev A. Y., Hamann W.-R., Berdnikov L. N., Fabrika S., Valeev A. F., 2010, MNRAS, 403, 760
Hadfield L. J., van Dyk S. D., Morris P. W., Smith J. D., Marston A. P., Peterson D. E., 2007, MNRAS, 376, 248
Hamann W.-R., Gräfener G., Liermann A., 2006, A&A, 457, 1015
Hanson M. M., Kurtev R., Borissova J., Georgiev L., Ivanov V. D., Hillier D. J., Minniti D., 2010, A&A, 516, A35
Harayama Y., Eisenhauer F., Martins F., 2008, ApJ, 675, 1319
Hill, G. M., Moffat, A. F. J., & St-Louis, N., 2002, MNRAS, 335, 1069
Hillenbrand L. A., Massey P., Strom S. E., Merrill K. M., 1993, AJ, 106, 1906
Homeier N. L., Blum R. D., Pasquali A., Conti P. S., Damineli A., 2003, A&A, 408, 153
Hopewell, E. C., Barlow, M. J., Drew, J. E., et al., 2005, MNRAS, 363, 857
Hopkins P. F., Quataert E., Murray N., 2011, MNRAS, 417, 950
Howarth I. D., Schmutz W., 1992, A&A, 261, 503
Howarth I. D., Schmutz W., 1995, A&A, 294, 529
Humphreys R. M., Larsen J. A., 1995, AJ, 110, 2183
Hur H., Sung H., Bessell M. S., 2012, AJ, 143, 41
Hyodo, Y. Tsujimoto, M. Koyama, K. Nishiyama, S. Nagata, T. Sakon, I. Murakami, H. Matsumoto, H. 2008, PASJ 60, 173
Indebetouw R., Mathis J. S., Babler B. L., Meade M. R., Watson C., Whitney B. A., Wolff M. J., Wolfire M. G., Cohen M., 2005, ApJ, 619, 931
Isserstedt J., Moffat A. F. J., Niemela V. S., 1983, A&A, 126, 183
Jordi C., et al., 2010, A&A, 523, A48
Kanarek, G. C., Shara, M. M., Faherty, J. K., Zurek, D., Moffat, A. F. J. 2014, AJ, submitted, arXiv:1403.0975
Kendrew S., et al., 2012, ApJ, 755, 71
Kothes R., Dougherty S. M., 2007, A&A, 468, 993
Koumpia E., Bonanos A. Z., 2012, A&A, 547, A30
Kroupa P., Weidner C., 2003, ApJ, 598, 1076
Kurtev R., Borissova J., Georgiev L., Ortolani S., Ivanov V. D., 2007, A&A, 475, 209
Lada C. J., Lada, E. A. 2003, ARA&A 41, 57
Lejeune T., Schaerer D., 2001, A&A, 366, 538
Lépine, S., Wallace, D., Shara, M. M., Moffat, A. F. J., & Niemela, V. S., 2001, AJ, 122, 3407
Liermann A., Hamann W.-R., Oskinova L. M., 2009, A&A, 494, 1137
Littlefield C., Garnavich P., "Howie" Marion G. H., Vinkó J., McClelland C., Rettig T., Wheeler J. C., 2012, AJ, 143, 136
Longmore S. N., et al., 2013, MNRAS, 429, 987
Lortet M. C., Testor G., Niemela V., 1984, A&A, 140, 24
Lundström I., Stenholm B., 1984, A&As, 58, 163
Neugent, K. F., Massey, P., & Morrell, N., 2012, AJ, 144, 162
Maeder A., Lequeux J., 1982, A&A, 114, 409
Maeder A., Meynet G., 2000, ARA&A, 38, 143
Maíz Apellániz J., Walborn N. R., Morrell N. I., Niemela V. S., Nelan E. P., 2007, ApJ, 660, 1480
Malchenko S. L., Tarasov A. E., 2009, Astrophysics, 52, 235
Marchenko S. V., Moffat A. F. J., Crowther P. A., 2010, ApJL, 724, L90
Marchenko S. V. et al., 2004, MNRAS, 353, 153
Marchenko S. V., Moffat A. F. J., Eenens P. R. J., 1998, PASP, 110, 1416
Marchenko S. V., Moffat A. F. J., Koenigsberger G., 1994, ApJ, 422, 810
Marston, A., Mauerhan, J. C.m Van Dyk, S., Cohen, M., Morris, P. 2013, in: *Massive Stars: From Alpha to Omega*, Rhodes, Greece, arXiv:1309.1584
Martín M. C., Cappa C. E., Testori J. C., 2007, Rev. Mex. Astron. Astrofis., 43, 243
Martins F., Hillier D. J., Paumard T., Eisenhauer F., Ott T., Genzel R., 2008, A&A, 478, 219
Martins F., Plez B., 2006, A&A, 457, 637
Martins F., Schaerer D., Hillier D. J., 2005, A&A, 436, 1049
Massey P., Conti P. S., 1983, ApJ, 273, 576
Massey P., Duffy A. S., 2001b, ApJ, 550, 713
Massey P., DeGioia-Eastwood K., Waterhouse E., 2001a, AJ, 121, 1050
Massey P., Olsen K. A. G., Parker J. W., 2003, PASP, 115, 1265
Massey, P., Neugent, K. F., Morrell, N., & Hillier, D. J., 2014, ApJ, 788, 83
Mauerhan J. C., van Dyk S. D., Morris P. W., 2009, PASP, 121, 591
Mauerhan J. C., Muno M. P., Morris M. R., Stolovy S. R., Cotera A., 2010, ApJ, 710, 706
Mauerhan J. C., Wachter S., Morris P. W., Van Dyk S. D., Hoard D. W., 2010b, ApJL, 724, L78
Mauerhan J. C., Cotera A., Dong H., Morris M. R., Wang Q. D., Stolovy S. R., Lang C., 2010c, ApJ, 725, 188
Mauerhan J. C., Van Dyk S. D., Morris P. W., 2011, AJ, 142, 40
Melena N. W., Massey P., Morrell N. I., Zangari A. M., 2008, AJ, 135, 878
Mel'Nik A. M., Dambis A. K., 2009, MNRAS, 400, 518
Messineo M., Davies B., Figer D. F., Kudritzki R. P., Valenti E., Trombley C., Najarro F., Rich R. M., 2011, ApJ, 733, 41
Messineo M., Davies B., Ivanov V. D., Figer D. F., Schuller F., Habing H. J., Menten K. M., Petr-Gotzens M. G., 2009, ApJ, 697, 701
Meynet G., Maeder A., 2005, A&A, 429, 581
Mikles, V. J., Eikenberry, S. S., Muno, M. P., Bandyopadhyay, R. M., Patel, S. 2006, ApJ 651, 408
Miszalski B., Crowther P. A., De Marco O., Köppen J., Moffat A. F. J., Acker A., Hillwig T. C., 2012, MNRAS, 423, 934
Moffat, A. F. J., 1989, ApJ, 347, 373
Moffat, A. F. J. Shara, M. M., 1983, ApJ 273, 544
Moffat, A. F. J., Lamontagne, R., & Seggewiss, W., 1982, A&A, 114, 135
Moffat A. F. J., Shara M. M., Potter M., 1991, AJ, 102,

642
Monnier J. D., Zhao M., Pedretti E. et al. 2011, ApJ, 742, 1
Morris P. W., Brownsberger K. R., Conti P. S., Massey P., Vacca W. D., 1993, ApJ, 412, 324
Motch, C., Warwick, R., Cropper, M. S. et al. 2010, A&A 523, A92
Nakanishi H., Sofue Y., 2003, PASJ, 55, 191
Nakanishi H., Sofue Y., 2006, PASJ, 58, 847
Nishiyama S., Tamura M., Hatano H., Kato D., Tanabé T., Sugitani K., Nagata T., 2009, ApJ, 696, 1407
Oskinova L. M., 2005, MNRAS, 361, 679
Paladini R., Davies R. D., De Zotti G., 2004, MNRAS, 347, 237
Parker Q. A., et al., 2005, MNRAS, 362, 689
Pasquali, A., Comerón, F., Gredel, R., Torra, J., & Figueras, F., 2002, A&A, 396, 533
Penny L. R., Gies D. R., 2009, ApJ, 700, 844
Pollock A. M. T., Haberl F., Corcoran M. F., 1995, in van der Hucht K. A., Williams P. M., eds, Wolf-Rayet Stars: Binaries; Colliding Winds; Evolution Vol. 163 of IAU Symposium, The ROSAT PSPC survey of the Wolf-Rayet stars. p. 512
Poveda A., Ruiz J., Allen C., 1967, Bol. Obs. Tonantzintla Tacubaya, 4, 86
Przybilla N., Butler K., Becker S. R., Kudritzki R. P., 2006, A&A, 445, 1099
Puls J., Vink J. S., Najarro F., 2008, A&ARv, 16, 209
Rahman, M., Moon, D.-S., Matzner, C. D. 2011, ApJ 743, L28
Rauw G., et al., 2005, A&A, 432, 985
Rauw G., Manfroid J., Gosset E., Nazé Y., Sana H., De Becker M., Foellmi C., Moffat A. F. J., 2007, A&A, 463, 981
Rauw G., Sana H., Nazé Y., 2011, A&A, 535, A40
Reid M. J., Menten K. M., Zheng X. W., Brunthaler A., Xu Y., 2009, ApJ, 705, 1548
Reid M. J., McClintock J. E., Narayan R., Gou L., Remillard R. A., Orosz J. A., 2011, ApJ, 742, 83
Rieke G. H., Lebofsky M. J., 1985, ApJ, 288, 618
Rolleston W. R. J., Trundle C., Dufton P. L., 2002, A&A, 396, 53
Rolleston W. R. J., Venn K., Tolstoy E., Dufton P. L., 2003, A&A, 400, 21
Roman-Lopes A., 2011b, ISRNA&A, 2011E, 8
Roman-Lopes A., 2011c, MNRAS, 410, 161
Roman-Lopes A., 2012, MNRAS, 427, L65
Roman-Lopes A., 2013, MNRAS, 433, 712
Roman-Lopes A., Barba, R. H., Morrell, N. I., 2011a, MNRAS 416, 501
Rygl K. L. J., et al., 2012, A&A, 539, A79
Sana H., Gosset E., Rauw G., Sung H., Vreux J.-M., 2006, A&A, 454, 1047
Sander A., Hamann W.-R., Todt H., 2012, A&A, 540, A144
Schaerer D., Vacca W. D., 1998, ApJ, 497, 618
Schnurr O., Casoli J., Chené A.-N., Moffat A. F. J., St-Louis N., 2008, MNRAS, 389, L38
Schweickhardt J., Schmutz W., Stahl O., Szeifert Th., Wolf B., 1999, A&A, 347, 127
Shara M. M., Smith L. F., Potter M., Moffat A. F. J., 1991, AJ, 102, 716
Shara M. M., Moffat A. F. J., Smith L. F., Niemela V. S., Potter M., Lamontagne R., 1999, AJ, 118, 390
Shara M. M., et al., 2009, AJ, 138, 402
Shara M. M., Faherty J. K., Zurek D., Moffat A. F. J., Gerke J., Doyon R., Artigau E., Drissen L., 2012, AJ, 143, 149
Shetty R., Ostriker E. C., 2008, ApJ, 684, 978
Skrutskie M. F., Cutri R. M., Stiening R., Weinberg M. D., Schneider S., Carpenter J. M., Beichman C., Capps R., et al., 2006, AJ, 131, 1163
Smith J. D. T., Cushing M., Barletta A., McCarthy D., Kulesa C., Van Dyk S. D., 2012, AJ, 144, 166
Smith L. F., 1968, MNRAS, 141, 317
Smith L. F., Shara M. M., Moffat A. F. J., 1990, ApJ, 358, 229
Smith L. F., Shara M. M., Moffat A. F. J., 1996, MNRAS, 281, 163
Smith N., 2006, ApJ, 644, 1151
Smith N., Tombleson R., 2014, MNRAS, accepted, arXiv:1406.7431
Stead J. J., Hoare M. G., 2009, MNRAS, 400, 731
Stock D. J., Barlow M. J., 2010, MNRAS, 409, 1429
Todt H., et al., 2013, MNRAS, 430, 2302
Tovmassian H. M., Navarro S. G., Cardona O., 1996, AJ, 111, 306
Turner D. G., 1980, ApJ, 235, 146
Turner D. G., Rohanizadegan M., Berdnikov L. N., Pastukhova E. N., 2006, PASP, 118, 1533
Tuthill P. G., Monnier J. D., Lawrance N., Danchi W. C., Owocki S. P., Gayley K. G., 2008, ApJ, 675, 698
Underhill A. B., Hill G. M., 1994, ApJ, 432, 770
van der Hucht K. A., 2001, New.Astron.Rev, 45, 135
van der Hucht K. A., 2006, A&A, 458, 453
van Leeuwen F., 2007, A&A, 474, 653
Varricatt, W. P., & Ashok, N. M., 2006, MNRAS, 365, 127
Vázquez R. A., Baume G., 2001, A&A, 371, 908
Vázquez R. A., Baume G. L., Feinstein C., Nuñez J. A., Vergne M. M., 2005, A&A, 430, 471
Vazquez R. A., Will J.-M., Prado P., Feinstein A., 1995, A&AS, 111, 85
Wachter S., Mauerhan J. C., Van Dyk S. D., Hoard D. W., Kafka S., Morris P. W., 2010, AJ, 139, 2330
Wegner W., 2006, MNRAS, 371, 185
Williams, P. M., van der Hucht, K. A., Pollock, A. M. T., Florkowski, D. R., van der Woerd, H., Wamsteker, W. M., 1990a, MNRAS, 243, 662
Williams P. M., van der Hucht K. A., Sandell G., The P. S., 1990b, MNRAS, 244, 101
Williams, P. M., van der Hucht, K. A., Bouchet, P., et al., 1992, MNRAS, 258, 461
Williams P. M., et al., 2001, MNRAS, 324, 156
Williams, P. M., Rauw, G., & van der Hucht, K. A., 2009b, MNRAS, 395, 2221
Wright E. L., et al., 2010, AJ, 140, 1868
Yusof N., et al., 2013, MNRAS, 433, 1114

Table 8. Full version.

WR#	Sp. Type	ref	J	H	K_S	$\bar{A}_{K_S}$	d(kpc)	R_G(kpc)	z(pc)
3	WN3ha	1	10.24	10.13	10.01	0.18 ± 0.02	4.53 ± 1.15	11.41 ± 1.18	-308 ± 83
4	WC5	2	8.75	8.57	7.88	0.13 ± 0.01	2.69 ± 0.49	10.15 ± 0.55	-121 ± 25
5	WC6	2	8.63	8.34	7.65	0.16 ± 0.02	2.69 ± 0.84	10.18 ± 0.88	-82 ± 32
13	WC6	2	10.14	9.64	8.86	0.29 ± 0.02	4.42 ± 1.38	9.46 ± 1.40	-40 ± 19
15	WC6	2	7.85	7.34	6.60	0.28 ± 0.02	1.57 ± 0.49	8.11 ± 0.55	-10 ± 9
16	WN8h	2	6.97	6.71	6.38	0.24 ± 0.02	2.77 ± 0.46	7.95 ± 0.52	-104 ± 20
17	WC5	2	9.93	9.74	9.17	0.07 ± 0.02	5.02 ± 0.91	8.31 ± 0.95	-303 ± 59
17-1	WN5b	3	11.73	10.38	9.53	0.85 ± 0.05	5.43 ± 0.86	8.58 ± 0.89	-41 ± 10
19	WC5+O9	4,5	9.75	9.13	8.53	0.20 ± 0.02	3.52 ± 0.64	7.93 ± 0.69	-54 ± 13
19a	WN7(h)	2	9.07	8.13	7.50	0.71 ± 0.04	2.41 ± 0.47	7.78 ± 0.53	-23 ± 8
20	WN5	2	11.00	10.43	9.93	0.45 ± 0.03	4.65 ± 0.72	8.18 ± 0.76	-130 ± 23
20b	WN6ha	2	8.65	7.80	7.18	0.75 ± 0.04	4.84 ± 0.79	8.26 ± 0.83	-10 ± 5
27	WC6	2	9.88	9.17	8.30	0.44 ± 0.03	3.18 ± 0.99	7.69 ± 1.02	26 ± 2
31c	WC6	2	11.04	10.34	9.49	0.42 ± 0.03	5.56 ± 1.74	8.09 ± 1.76	-50 ± 22
33	WC6	4	10.62	10.35	9.69	0.13 ± 0.01	6.98 ± 2.18	8.79 ± 2.19	251 ± 72
34	WN5	2	11.20	10.59	10.04	0.50 ± 0.03	4.78 ± 0.74	7.79 ± 0.78	-96 ± 18
37	WN4b	2	11.03	10.34	9.67	0.50 ± 0.03	6.36 ± 1.11	8.29 ± 1.14	-97 ± 20
38	WC4	2	11.99	11.50	10.79	0.25 ± 0.03	6.43 ± 0.98	8.32 ± 1.01	-84 ± 16
38a	WN5	2	11.53	11.21	10.70	0.40 ± 0.05	6.81 ± 1.07	8.49 ± 1.10	-90 ± 17
40	WN8h	2	6.62	6.41	6.11	0.20 ± 0.02	2.48 ± 0.41	7.42 ± 0.48	-190 ± 34
42a	WN5b	2	12.08	11.31	10.81	0.38 ± 0.03	12.20 ± 1.91	11.93 ± 1.93	-84 ± 16
42b	WN4b	2	11.35	10.52	9.90	0.51 ± 0.03	7.05 ± 1.23	8.48 ± 1.25	-168 ± 33
42c	WN5	2	11.15	10.47	9.90	0.53 ± 0.03	4.41 ± 0.68	7.59 ± 0.73	-10 ± 5
42d	WN5b	2	10.20	9.52	8.91	0.45 ± 0.03	4.92 ± 0.77	7.70 ± 0.81	-21 ± 6
43-1	WN4b	6	13.16	11.57	10.47	1.13 ± 0.06	6.88 ± 1.21	8.39 ± 1.24	-59 ± 14
44	WN4	2	11.16	10.89	10.48	0.45 ± 0.03	4.83 ± 0.98	7.71 ± 1.01	125 ± 22
44a	WN5b	2	12.07	11.34	10.82	0.39 ± 0.03	12.18 ± 1.91	11.79 ± 1.93	-95 ± 18
45	WC6	2	10.60	9.99	9.19	0.35 ± 0.02	5.03 ± 1.57	7.48 ± 1.59	-33 ± 16
45a	WN5	2	11.90	11.24	10.73	0.48 ± 0.03	6.66 ± 1.03	7.93 ± 1.06	75 ± 9
45b	WN4b	2	11.45	10.61	9.92	0.57 ± 0.03	6.91 ± 1.20	7.98 ± 1.23	-28 ± 8
45-3	WN5b	3	12.57	11.57	10.94	0.57 ± 0.04	11.89 ± 1.87	11.04 ± 1.89	-152 ± 27
45-4	WN6	6	11.65	10.76	10.14	0.64 ± 0.04	6.73 ± 1.33	7.81 ± 1.35	-47 ± 13
45c	WN5	2	11.35	10.79	10.32	0.42 ± 0.03	5.66 ± 0.88	7.45 ± 0.91	-34 ± 8
46a	WN4	2	12.08	11.42	10.92	0.65 ± 0.04	5.38 ± 1.09	7.18 ± 1.12	-89 ± 22
46-1	WN6	7	11.55	10.82	10.22	0.57 ± 0.03	7.24 ± 1.43	7.89 ± 1.45	-7 ± 5
46-8	WN6	8	12.02	10.70	9.85	0.96 ± 0.05	5.08 ± 1.01	7.16 ± 1.04	-20 ± 8
46-9*	WN5	3	12.07	10.72	9.88	0.96 ± 0.06	3.60 ± 0.56	7.04 ± 0.62	4 ± 2
46-2	WN7h	7	10.56	9.64	9.03	0.68 ± 0.04	4.93 ± 0.95	7.10 ± 0.98	-31 ± 10
46-5	WN6	9	-	-	10.92	1.18 ± 0.13[7]	8.63 ± 1.97	8.49 ± 1.99	-42 ± 14
46-6	WN7	9	-	-	10.48	1.18 ± 0.13[7]	9.10 ± 2.24	8.76 ± 2.25	-45 ± 16
46-15	WN8	10	13.13	11.03	9.84	1.51 ± 0.08	7.58 ± 1.28	7.94 ± 1.30	-7 ± 4
46-12	WN4b	3	13.56	12.55	11.84	0.64 ± 0.04	16.19 ± 2.82	13.97 ± 2.83	-128 ± 26
46-14	WN5b	6	12.93	11.76	10.96	0.75 ± 0.04	11.04 ± 1.74	9.68 ± 1.76	-91 ± 17
47a	WN8h	2	10.44	9.68	9.06	0.64 ± 0.04	7.90 ± 1.30	7.67 ± 1.33	-159 ± 29
47-1	WN6	7	12.18	11.22	10.56	0.70 ± 0.04	7.96 ± 1.57	7.70 ± 1.59	7 ± 3
47b	WN9h	2	10.29	9.44	8.84	0.65 ± 0.04	7.96 ± 1.23	7.67 ± 1.26	-88 ± 17
47c	WC5	2	11.24	10.48	9.89	0.20 ± 0.02	6.60 ± 1.20	7.06 ± 1.22	-85 ± 19
48-1	WC7	7	11.06	10.09	9.31	0.41 ± 0.03	5.59 ± 0.94	6.62 ± 0.97	33 ± 2
48-5	WN6b	3	13.06	11.34	10.26	1.15 ± 0.06	7.14 ± 1.24	6.99 ± 1.27	-21 ± 7
49	WN5(h)	2	11.89	11.57	11.21	0.25 ± 0.02	9.19 ± 1.42	7.96 ± 1.44	-386 ± 63
49-1	WN8	10	13.82	11.88	10.67	1.48 ± 0.08	11.29 ± 1.91	9.28 ± 1.93	88 ± 12
52	WC4	2	8.41	8.21	7.55	0.11 ± 0.02	1.54 ± 0.23	7.19 ± 0.34	142 ± 18
52-1	WN6	6	14.77	12.69	11.55	1.42 ± 0.08	9.02 ± 1.81	7.72 ± 1.83	42 ± 5
52-2	WN6	6	12.52	11.40	10.68	0.79 ± 0.05	8.10 ± 1.60	7.15 ± 1.62	84 ± 13
54	WN5	2	10.85	10.48	10.09	0.29 ± 0.02	5.40 ± 0.84	6.39 ± 0.87	-216 ± 37
55	WN7	2	8.77	8.49	8.01	0.36 ± 0.03	3.57 ± 0.69	6.46 ± 0.74	29 ± 2
56	WC7	2	11.84	11.48	10.77	0.21 ± 0.03	12.02 ± 2.03	9.55 ± 2.04	-323 ± 58
57	WC8	2	9.09	8.75	8.01	0.37 ± 0.02	2.98 ± 0.52	6.61 ± 0.57	-242 ± 45
57-1	WN7	10	15.01	12.77	11.46	1.65 ± 0.09	9.68 ± 1.92	7.77 ± 1.93	-64 ± 17
60	WC8	2	8.91	8.37	7.70	0.39 ± 0.03	2.56 ± 0.45	6.63 ± 0.51	53 ± 6
60-1	WC8	6	15.30	12.43	10.60	2.04 ± 0.11	4.56 ± 0.82	5.98 ± 0.86	34 ± 3
60-5	WC7	3	10.84	10.12	9.39	0.32 ± 0.03	6.02 ± 1.01	5.98 ± 1.04	134 ± 19

Table 8. (Continued)

WR#	Sp. Type	ref	J	H	K_S	$\bar{A}_{K_S}$	d(kpc)	R_G(kpc)	z(pc)
60-4	WC8	10	15.58	12.71	11.00	1.93 ± 0.11	5.75 ± 1.03	6.00 ± 1.06	35 ± 3
61	WN5	2	10.96	10.67	10.35	0.21 ± 0.02	6.32 ± 0.98	6.10 ± 1.01	-411 ± 67
61-2	WN5b	6	13.60	11.39	10.01	1.55 ± 0.09	4.92 ± 0.79	5.88 ± 0.83	11 ± 1
61-3	WC9	10	13.62	11.63	10.38	1.41 ± 0.08	4.79 ± 0.98	5.84 ± 1.02	37 ± 4
61-1	WN6	8	11.68	10.43	9.61	0.91 ± 0.05	4.68 ± 0.93	5.83 ± 0.96	72 ± 10
62	WN6b	2	9.11	8.35	7.75	0.46 ± 0.03	3.08 ± 0.53	6.24 ± 0.59	-21 ± 7
62b	WN5	2	12.01	11.44	10.97	0.42 ± 0.09	7.64 ± 1.41	5.82 ± 1.43	-153 ± 32
64	WC7	2	12.50	12.03	11.33	0.23 ± 0.02	15.35 ± 2.59	10.55 ± 2.61	775 ± 127
64-1	WN4b	6	13.84	11.83	10.64	1.32 ± 0.07	6.83 ± 1.21	5.32 ± 1.23	-38 ± 10
67-2	WC7	3	10.34	9.26	8.46	0.46 ± 0.03	3.68 ± 0.62	5.62 ± 0.67	-7 ± 5
68a	WN6	2	9.59	9.02	8.62	0.36 ± 0.02	3.80 ± 0.75	5.52 ± 0.79	-22 ± 8
68-1	WN4b	6	13.88	12.15	11.06	1.16 ± 0.07	8.88 ± 1.56	5.56 ± 1.58	-11 ± 5
70a	WN6	2	10.94	10.24	9.76	0.47 ± 0.03	6.13 ± 1.21	4.26 ± 1.24	-72 ± 18
70-1	WN7	8	13.84	12.39	11.46	1.10 ± 0.06	12.40 ± 2.42	7.51 ± 2.43	-23 ± 8
70-3	WC7	3	10.96	9.94	9.06	0.53 ± 0.03	4.68 ± 0.79	4.89 ± 0.83	9 ± 2
70-4	WN9h	11	14.58	12.22	10.87	1.72 ± 0.10	12.46 ± 1.99	7.20 ± 2.01	219 ± 32
70-5	WC9	11	11.19	9.71	8.49	1.24 ± 0.07	2.17 ± 0.44	6.31 ± 0.51	-2 ± 5
70-6	WN6b	3	15.16	12.51	10.97	1.80 ± 0.10	7.34 ± 1.30	4.29 ± 1.33	25 ± 1
70-7	WN6b	10	15.94	13.05	11.36	2.00 ± 0.11	7.99 ± 1.43	4.27 ± 1.45	52 ± 6
70-8	WN7	10	15.64	12.59	10.91	2.20 ± 0.12	5.84 ± 1.16	4.19 ± 1.19	105 ± 17
70-2	WN5b	3	10.88	9.52	8.66	0.86 ± 0.05	3.63 ± 0.57	5.20 ± 0.63	69 ± 8
70-9	WC8	10	15.56	12.87	11.31	1.75 ± 0.10	7.20 ± 1.28	4.10 ± 1.31	29 ± 2
70-11	WN7	3	12.02	10.65	9.88	0.94 ± 0.05	6.47 ± 1.25	4.05 ± 1.27	96 ± 15
71	WN6	2	9.48	9.31	9.09	0.10 ± 0.01	5.34 ± 1.05	4.93 ± 1.09	-689 ± 139
72-3	WC9	12	15.62	13.05	11.53	1.82 ± 0.10	6.74 ± 1.40	3.80 ± 1.42	92 ± 15
72-1	WC9	7	10.16	9.25	8.46	0.72 ± 0.04	2.73 ± 0.56	5.76 ± 0.61	-4 ± 5
73-1	WC7	3	15.05	12.79	11.54	1.18 ± 0.07	10.94 ± 1.88	5.42 ± 1.90	-45 ± 11
74	WN7	2	9.73	9.22	8.80	0.40 ± 0.03	5.04 ± 0.97	4.28 ± 1.00	-36 ± 11
74-1	WN9ha	10	15.50	12.28	10.59	2.37 ± 0.13	8.15 ± 1.24	3.71 ± 1.27	13 ± 1
74-2	WN7	10	15.64	12.90	11.43	1.94 ± 0.11	8.34 ± 1.66	3.64 ± 1.68	27 ± 2
75	WN6b	2	8.60	8.24	7.84	0.19 ± 0.02	3.64 ± 0.62	5.05 ± 0.67	-74 ± 16
75a	WC9	2	9.96	9.14	8.50	0.56 ± 0.03	2.98 ± 0.60	5.48 ± 0.65	-26 ± 9
75-1	WC8	6	13.28	11.76	10.73	0.97 ± 0.06	7.89 ± 1.40	3.48 ± 1.42	57 ± 7
75-14	WC9	3	14.50	12.37	11.22	1.37 ± 0.08	7.17 ± 1.50	3.34 ± 1.52	51 ± 7
75b	WC9	2	9.76	9.00	8.36	0.54 ± 0.04	2.82 ± 0.57	5.55 ± 0.63	36 ± 3
75-15	WC8	12	-	13.16	11.50	1.81 ± 0.25	7.66 ± 1.61	3.32 ± 1.63	57 ± 8
75-6	WN5b	10	14.65	12.80	11.76	1.15 ± 0.07	13.28 ± 2.12	6.86 ± 2.14	37 ± 3
75-16	WC8	12	-	13.49	11.83	1.81 ± 0.25	8.90 ± 1.86	3.66 ± 1.88	43 ± 5
75-2	WC8	6	15.56	12.86	11.32	1.73 ± 0.10	7.31 ± 1.31	3.23 ± 1.33	44 ± 4
75-3	WC8	6	15.11	12.86	11.47	1.49 ± 0.09	8.75 ± 1.57	3.52 ± 1.59	43 ± 4
75-4	WN5b	6	15.00	12.70	11.34	1.55 ± 0.09	9.08 ± 1.47	3.65 ± 1.49	46 ± 4
75-17	WC8	12	16.00	14.17	12.75	1.39 ± 0.09	16.51 ± 3.05	9.73 ± 3.06	48 ± 5
75-7	WC9	10	14.97	12.96	11.63	1.49 ± 0.08	8.21 ± 1.69	3.32 ± 1.71	46 ± 5
75-8	WN4b	3	15.00	12.44	10.90	1.78 ± 0.10	6.22 ± 1.12	3.42 ± 1.14	-11 ± 6
75c	WC9	13	11.62	11.12	10.52	0.44 ± 0.03	8.00 ± 1.62	2.83 ± 1.64	406 ± 78
75d	WC9	13	10.68	9.88	9.12	0.66 ± 0.04	3.78 ± 0.77	4.72 ± 0.81	90 ± 14
75-10	WN6b	3	13.75	11.70	10.46	1.38 ± 0.08	7.03 ± 1.23	3.11 ± 1.26	63 ± 8
75-5	WC8	6	14.90	12.77	11.43	1.41 ± 0.08	8.93 ± 1.60	3.57 ± 1.62	-48 ± 12
75-12	WN6	10	15.02	12.85	11.49	1.63 ± 0.09	7.98 ± 1.63	3.15 ± 1.65	49 ± 6
75-22	WC9	12	-	13.72	12.03	2.01 ± 0.30	7.80 ± 1.99	3.14 ± 2.00	30 ± 3
75-13	WC8	10	13.60	11.67	10.39	1.30 ± 0.07	5.80 ± 1.03	3.48 ± 1.06	26 ± 1
75-23	WC9	12	10.27	9.59	8.93	0.54 ± 0.03	3.67 ± 0.75	4.80 ± 0.79	49 ± 6
76-1	WN9	10	14.84	12.00	10.42	2.05 ± 0.11	8.69 ± 1.41	3.14 ± 1.43	82 ± 10
77-1	WN7b	3	10.06	9.00	8.29	0.65 ± 0.04	4.03 ± 0.63	4.45 ± 0.67	38 ± 3
77-2	WN7	8	10.75	9.52	8.73	0.93 ± 0.05	3.83 ± 0.74	4.60 ± 0.78	5 ± 3
77-5	WN6	12	10.56	9.71	9.14	0.58 ± 0.03	4.37 ± 0.86	4.22 ± 0.90	17 ± 1
77-3	WN6	10	11.12	9.84	9.10	0.85 ± 0.05	3.79 ± 0.75	4.64 ± 0.79	-19 ± 8
77-4	WN6	3	14.14	11.85	10.59	1.58 ± 0.09	5.38 ± 1.09	3.51 ± 1.12	-54 ± 15
77-6	WN6b	3	13.56	11.93	10.95	1.04 ± 0.06	10.27 ± 1.78	3.65 ± 1.80	120 ± 17
77-7	WC9	12	-	13.46	12.06	1.60 ± 0.22	9.51 ± 2.17	3.18 ± 2.19	61 ± 10
81	WC9	2	8.29	7.76	7.12	0.48 ± 0.03	1.64 ± 0.34	6.47 ± 0.42	-55 ± 15
82	WN7(h)	2	9.48	9.04	8.69	0.32 ± 0.02	4.98 ± 0.95	3.61 ± 0.99	-182 ± 39

Table 8. (Continued)

WR#	Sp. Type	ref	J	H	K_S	$\bar{A}_{K_S}$	d(kpc)	R_G(kpc)	z(pc)
83	WN5	2	10.26	9.89	9.53	0.27 ± 0.02	4.20 ± 0.65	4.24 ± 0.70	-281 ± 47
84	WN7	2	9.58	8.96	8.50	0.46 ± 0.10	4.28 ± 0.93	3.95 ± 0.96	4 ± 3
84-2	WC8	12	13.98	12.20	10.98	1.21 ± 0.07	7.95 ± 1.41	1.73 ± 1.43	43 ± 4
84-1	WN9	3	12.37	10.43	9.19	1.51 ± 0.08	6.31 ± 1.00	2.28 ± 1.03	40 ± 3
84-4	WN7ha	3	10.88	10.00	9.49	0.69 ± 0.04	16.50 ± 3.02	8.86 ± 3.03	35 ± 3
84-5	WC9	12	14.34	12.78	11.59	1.24 ± 0.07	9.03 ± 1.86	1.97 ± 1.87	75 ± 11
88	WC9	2	9.03	8.56	8.05	0.36 ± 0.03	2.66 ± 0.54	5.37 ± 0.60	114 ± 19
90	WC7	2	6.25	6.09	5.52	0.05 ± 0.02	1.14 ± 0.19	6.92 ± 0.32	-76 ± 16
91	WN7b	2	9.53	8.77	8.20	0.44 ± 0.03	4.25 ± 0.66	3.92 ± 0.70	-60 ± 12
91-1	WC7	3	15.11	12.05	10.33	1.80 ± 0.10	4.69 ± 0.82	3.41 ± 0.85	80 ± 11
92	WC9	2	9.50	9.22	8.82	0.21 ± 0.02	4.07 ± 0.82	4.20 ± 0.86	-294 ± 63
93a	WN3	2	13.88	13.22	12.72	0.65 ± 0.02	10.22 ± 3.25	2.20 ± 3.27	694 ± 214
93b	WO3	14	-	-	10.17	0.73 ± 0.04	2.18 ± 0.32	5.84 ± 0.40	-13 ± 5
94	WN5	2	7.09	6.19	5.91	0.32 ± 0.02	0.78 ± 0.12	7.23 ± 0.28	16 ± 1
94-1	WC9	12	15.99	12.59	10.76	2.31 ± 0.13	3.78 ± 0.81	4.24 ± 0.85	35 ± 3
98-1	WC8	12	13.52	11.70	10.56	1.17 ± 0.03	6.67 ± 1.18	1.34 ± 1.20	45 ± 5
100	WN7b	2	8.85	8.27	7.72	0.38 ± 0.03	3.50 ± 0.54	4.51 ± 0.60	-58 ± 12
100-3	WN8	12	13.90	11.52	10.17	1.71 ± 0.05	7.20 ± 1.21	0.82 ± 1.24	-17 ± 6
100-1	WN7b	3	15.12	12.61	11.08	1.75 ± 0.04	8.75 ± 1.37	0.75 ± 1.39	12 ± 1
101	WC8	2	9.62	8.78	7.89	0.66 ± 0.04	2.46 ± 0.43	5.54 ± 0.50	-42 ± 11
101-3	WN8	3	16.67	13.08	11.09	2.61 ± 0.05	7.49 ± 1.26	0.51 ± 1.28	25 ± 1
101-8	WC9	15	-	14.67	12.70	2.31 ± 0.11	9.23 ± 1.93	1.23 ± 1.94	5 ± 3
101-5	WN6b	3	-	15.21	12.22	3.68 ± 0.17	5.50 ± 1.04	2.50 ± 1.07	22 ± 1
101-9	WC9	15	-	14.62	12.02	3.17 ± 0.13	4.53 ± 0.96	3.47 ± 0.99	15 ± 1
101-1	WN9h	3	15.55	12.26	10.42	2.39 ± 0.05	7.40 ± 1.15	0.60 ± 1.18	19 ± 0
101p	WC8	3	16.32	13.05	11.20	2.16 ± 0.06	5.68 ± 1.02	2.32 ± 1.05	21 ± 1
102	WO2	2	-	-	10.62	0.50 ± 0.10	2.99 ± 0.45	5.02 ± 0.52	93 ± 11
102-12	WN9	3	-	13.61	11.14	3.20 ± 0.14	7.11 ± 1.18	0.89 ± 1.20	22 ± 1
102b	WN7b	3	15.44	12.48	10.85	1.95 ± 0.04	7.18 ± 1.11	0.82 ± 1.14	14 ± 1
102bd	WC9	3	16.26	13.47	11.49	2.26 ± 0.07	5.40 ± 1.14	2.60 ± 1.16	15 ± 1
102-17	WN6b	3	16.33	13.27	11.43	2.16 ± 0.04	7.69 ± 1.33	0.32 ± 1.35	9 ± 2
102-8	WN9	3	-	13.74	11.24	3.23 ± 0.15	7.34 ± 1.24	0.66 ± 1.26	14 ± 1
102-9	WN9	3	16.56	12.72	10.54	2.84 ± 0.05	6.37 ± 0.99	1.63 ± 1.02	12 ± 1
102-10	WN8	3	17.06	13.07	10.78	2.97 ± 0.06	5.48 ± 0.92	2.52 ± 0.95	12 ± 1
102-19	WN5	12	11.84	10.95	10.32	0.65 ± 0.04	5.08 ± 0.79	2.98 ± 0.83	73 ± 8
102-20	WC9	12	-	12.38	10.89	1.74 ± 0.26	5.22 ± 1.25	2.85 ± 1.27	-3 ± 5
102l	WN8	2	8.83	8.10	7.57	0.56 ± 0.04	4.15 ± 0.69	3.91 ± 0.73	36 ± 3
107	WN8	2	9.38	8.69	8.19	0.52 ± 0.04	5.62 ± 0.93	2.57 ± 0.96	4 ± 3
107a	WC6	2	11.17	10.31	9.38	0.53 ± 0.04	5.04 ± 1.58	3.09 ± 1.60	-17 ± 12
108	WN9ha	2	7.66	7.34	7.10	0.30 ± 0.02	4.25 ± 0.60	3.82 ± 0.65	-44 ± 9
110	WN5b	2	7.12	6.72	6.22	0.27 ± 0.02	1.55 ± 0.24	6.48 ± 0.35	30 ± 2
111-1	WN6	7	12.58	11.06	10.31	0.91 ± 0.05	6.45 ± 1.27	2.01 ± 1.30	-26 ± 9
111-5*	WN9	3	13.80	11.97	10.92	1.32 ± 0.07	15.29 ± 2.41	7.66 ± 2.43	-14 ± 5
111-6	WC9	12	14.24	13.35	10.75	2.05 ± 0.13	4.22 ± 0.92	3.99 ± 0.95	21 ± 1
111-3	WC8	6	11.21	9.70	8.57	1.05 ± 0.06	2.81 ± 0.49	5.30 ± 0.55	26 ± 1
113-1	WN7	7	9.09	8.30	7.76	0.58 ± 0.04	2.88 ± 0.56	5.27 ± 0.61	-0 ± 4
114-1	WN7b	7	12.21	11.24	10.61	0.55 ± 0.04	12.25 ± 1.91	5.52 ± 1.93	230 ± 33
114-2	WC8	12	14.45	12.90	11.69	1.13 ± 0.07	11.43 ± 2.07	4.66 ± 2.09	138 ± 22
115-1	WN6	7	10.32	9.52	8.96	0.56 ± 0.03	4.07 ± 0.80	4.32 ± 0.84	-21 ± 8
115-2	WN8	10	11.53	10.13	9.28	1.02 ± 0.06	7.36 ± 1.22	2.56 ± 1.25	-16 ± 6
115-3	WN7	10	9.59	8.82	8.30	0.56 ± 0.03	3.72 ± 0.71	4.63 ± 0.76	-8 ± 5
116	WN8h	2	8.21	7.57	6.95	0.60 ± 0.03	3.07 ± 0.50	5.20 ± 0.56	3 ± 3
116-2	WN5	6	14.07	12.75	11.93	0.94 ± 0.05	9.32 ± 1.46	3.65 ± 1.48	162 ± 22
116-3	WN6ha	3	10.68	9.91	9.43	0.61 ± 0.04	14.53 ± 2.36	7.66 ± 2.37	-29 ± 8
117-1	WN7	10	9.09	8.29	7.63	0.68 ± 0.04	2.59 ± 0.50	5.67 ± 0.56	11 ± 2
118-4	WC8	10	12.18	10.52	9.36	1.12 ± 0.06	3.92 ± 0.68	4.63 ± 0.73	-7 ± 5
118-7	WC9	12	15.91	12.89	11.01	2.25 ± 0.12	4.37 ± 0.92	4.42 ± 0.95	30 ± 2
118-8	WC9	12	15.63	13.02	11.29	2.00 ± 0.11	5.55 ± 1.16	3.84 ± 1.19	23 ± 1
118-6	WN7	10	13.64	11.73	10.59	1.42 ± 0.08	7.21 ± 1.40	3.39 ± 1.43	-31 ± 10
118-9	WC9	12	14.78	13.04	11.15	1.87 ± 0.12	5.54 ± 1.20	3.89 ± 1.22	29 ± 2
119-2	WC8	10	11.83	10.49	9.56	0.83 ± 0.05	4.90 ± 0.85	4.22 ± 0.89	21 ± 1
119-3	WN7	12	13.27	11.50	10.50	1.25 ± 0.07	7.46 ± 1.46	3.47 ± 1.48	-40 ± 12

Table 8. (Continued)

WR#	Sp. Type	ref	J	H	K_S	$\bar{A}_{K_S}$	d(kpc)	R_G(kpc)	z(pc)
120	WN7	2	8.90	8.41	8.01	0.38 ± 0.03	3.54 ± 0.68	5.14 ± 0.73	37 ± 3
120-1	WC9	7	11.05	10.17	9.44	0.65 ± 0.04	4.41 ± 0.90	4.56 ± 0.93	24 ± 1
120-11	WC8	12	12.35	11.15	10.25	0.77 ± 0.04	6.95 ± 1.21	3.60 ± 1.23	-25 ± 8
120-7	WN7	10	10.22	9.21	8.51	0.78 ± 0.04	3.71 ± 0.71	5.00 ± 0.76	12 ± 2
120-8	WN9	3	12.86	10.82	9.66	1.47 ± 0.08	7.97 ± 1.26	3.91 ± 1.29	60 ± 6
120-3	WN9	16	11.95	10.22	9.16	1.29 ± 0.07	6.89 ± 1.08	3.82 ± 1.11	60 ± 6
120-4	WN9	16	11.85	10.26	9.27	1.20 ± 0.07	7.55 ± 1.19	3.85 ± 1.21	60 ± 6
120-5	WC8	16	12.39	10.83	9.75	1.03 ± 0.06	4.89 ± 0.85	4.37 ± 0.89	47 ± 5
120-6	WN6	11	13.51	12.83	12.32	0.48 ± 0.03	19.85 ± 3.92	13.44 ± 3.92	177 ± 31
120-9	WN7ha	3	15.15	12.55	11.14	1.95 ± 0.11	19.74 ± 3.81	13.27 ± 3.82	-16 ± 7
120-10	WN7	10	10.00	9.16	8.53	0.67 ± 0.04	3.94 ± 0.76	4.97 ± 0.80	47 ± 5
121-2	WN7	10	14.22	12.23	11.13	1.40 ± 0.08	9.29 ± 1.84	4.53 ± 1.85	8 ± 2
121-3	WN7	10	13.81	11.87	10.73	1.43 ± 0.08	7.66 ± 1.49	3.95 ± 1.51	4 ± 3
121-1	WN7h	11	10.94	10.07	9.47	0.66 ± 0.04	6.12 ± 1.18	4.27 ± 1.21	14 ± 1
121-4	WC7	12	14.13	12.13	10.66	1.31 ± 0.07	6.89 ± 1.18	4.07 ± 1.21	-62 ± 14
122-2	WN9	3	12.49	10.68	9.61	1.33 ± 0.07	8.35 ± 1.32	4.68 ± 1.34	-13 ± 5
122-3	WN6	3	12.81	11.06	9.99	1.27 ± 0.07	4.72 ± 0.94	4.90 ± 0.97	25 ± 1
122-4	WC8	10	14.70	12.67	11.25	1.45 ± 0.08	8.07 ± 1.44	5.17 ± 1.46	-45 ± 12
122-5	WC8	10	14.25	12.27	10.99	1.31 ± 0.08	7.61 ± 1.35	5.03 ± 1.37	-42 ± 11
123	WN8	2	9.52	9.28	8.92	0.26 ± 0.02	8.81 ± 1.45	4.48 ± 1.48	-711 ± 120
123-1	WN6	7	10.59	9.47	8.71	0.83 ± 0.05	3.20 ± 0.63	6.04 ± 0.68	28 ± 2
123-4	WC8	12	16.31	14.38	13.68	0.80 ± 0.09	33.24 ± 6.41	27.58 ± 6.42	-56 ± 15
123-3	WN8	10	12.22	10.81	9.94	1.05 ± 0.06	9.83 ± 1.63	6.79 ± 1.65	110 ± 15
124-8	WN6	12	8.61	7.99	7.80	0.18 ± 0.02	2.84 ± 0.56	6.36 ± 0.61	46 ± 5
124-3	WC7	12	12.95	11.82	10.77	0.71 ± 0.04	9.47 ± 1.60	7.11 ± 1.61	85 ± 11
124-9	WC6	12	13.90	12.72	11.67	0.73 ± 0.04	13.17 ± 4.12	9.88 ± 4.13	195 ± 55
124-10	WC6	12	14.35	12.59	11.33	1.06 ± 0.06	9.66 ± 3.03	7.37 ± 3.04	79 ± 19
124-6	WC6	3	12.67	10.91	9.68	1.04 ± 0.06	4.57 ± 1.43	6.08 ± 1.45	-11 ± 9
124-7	WC8	12	12.83	11.02	9.58	1.40 ± 0.08	3.82 ± 0.67	6.21 ± 0.72	-5 ± 4
124-11	WN6b	3	12.65	11.19	10.25	0.95 ± 0.05	7.77 ± 1.35	6.92 ± 1.37	112 ± 16
125-1	WC8	7	10.20	9.61	9.07	0.28 ± 0.02	5.06 ± 0.87	6.56 ± 0.91	6 ± 2
125-4	WN7	10	12.71	11.07	10.12	1.18 ± 0.07	6.47 ± 1.26	6.61 ± 1.28	-1 ± 4
128	WN4(h)	2	9.97	9.84	9.62	0.25 ± 0.02	3.57 ± 0.72	6.67 ± 0.77	-216 ± 48
129	WN4	2	11.08	10.72	10.40	0.41 ± 0.03	4.75 ± 0.96	7.47 ± 0.99	222 ± 41
130	WN8h	2	8.45	7.87	7.45	0.42 ± 0.03	4.16 ± 0.69	7.52 ± 0.73	89 ± 11
132	WC6	2	10.18	9.76	9.05	0.22 ± 0.02	4.97 ± 1.55	7.80 ± 1.57	115 ± 30
142a	WC7	17	9.27	8.09	7.12	0.64 ± 0.04	1.83 ± 0.31	7.87 ± 0.40	91 ± 12
142-1	WN6	18	8.77	7.86	7.19	0.69 ± 0.04	1.70 ± 0.34	7.93 ± 0.42	106 ± 17
147	WN8(h)+OB	2	6.01	4.86	4.11	0.87 ± 0.05	0.73 ± 0.12	7.90 ± 0.28	15 ± 1
148	WN8h	2	8.76	8.53	8.32	0.15 ± 0.02	7.05 ± 1.16	10.64 ± 1.20	814 ± 131
149	WN5	2	10.62	10.06	9.61	0.40 ± 0.03	4.11 ± 0.64	8.96 ± 0.68	66 ± 7
150	WC5	2	10.72	10.31	9.60	0.22 ± 0.02	5.71 ± 1.03	10.31 ± 1.07	-228 ± 45

Spectral types: (1)Marchenko et al. (2004), (2)van der Hucht (2001), (3) this work, (4)Crowther et al. (1998), (5)Williams, Rauw & van der Hucht (2009b), (6)Shara et al. (2009), (7)Hadfield et al. (2007), (8)Mauerhan et al. (2009), (9)Kurtev et al. (2007), (10)Mauerhan et al. (2011), (11)Wachter et al. (2010), (12)Shara et al. (2012), (13)Hopewell et al. (2005), (14)Drew et al. (2004), (15)Mauerhan et al. (2010c), (16)Mauerhan et al. (2010b), (17)Pasquali et al (2002), (18)Littlefield et al. (2012),

APPENDIX A: RECENTLY DISCOVERED WR STARS

In Table A1 provide identifcations and coordinates of all 322 Wolf-Rayet stars discovered between publication of the Annex (van der Hucht 2006) to the VIIth catalogue of WR stars (van der Hucht 2001) and March 2014. Table A1 includes revised distances for stars for which high quality near-IR photometry and a well-determined spectral type (± 1) are available. Following a request to the IAU Working Group for Massive Stars, a panel comprising P.A. Crowther, W-R Hamann, I.D. Howarth, K.A. van der Hucht, G. Rauw came up with a set of proposals that was approved by the Working Group in December 2012. Consequently, a revised nomenclature scheme has been introduced for Galactic WR stars as follows:

(i) All WR identifications up to the VIIth Catalogue (van der Hucht 2001) and Annex (van der Hucht 2006) remain unchanged since many are in widespread usage in the literature (e.g. WR 20, WR 20a).

(ii) All subsequent discoveries are switched from alphabetical (WRXXa, b) to numerical (WRXX-1, -2) identification, sorted by year/month of discovery, in RA order if multiple discoveries arise from a single source. By way of example, three WR stars have been discovered since 2006 between the RA's of WR 20 and WR 21. The first, discovered by Mauerhan et al. (2011), is assigned WR 20-1, while two further discoveries from Roman-Lopes, Barba, & Morrell (2011a) are assigned WR 20-2 and -3 (RA ordered).

(iii) Multiple WR stars identified within a single source are indicated with CAPITAL letters (e.g. WR 43a, b, c replaced with WR 43A, B, C).

(iv) The current Galactic WR census is maintained at `http://pacrowther.staff.shef.ac.uk/WRcat/`

Table A1. WR stars discovered since the van der Hucht (2006) updated catalogue (up to March 2014). Distances are indicated for the stars that feature in this study.

WR	Alias	RA (hh:mm:ss)	Dec (±dd:mm:ss)	Ref	Sp Type	Ref	Distance kpc
17-1	SMG09 668_4	10:16:26.226	-57:28:05.70	1	WN5b	1	5.4±0.9
20-2	WR 20aa, SS215	10:23:23.49	-58:00:20.80	19	O2 If/WN6	19	—
20-1	MDM11 1	10:23:28.80	-57:46:29.4	5	WN7–8	5	—
20-3	WR 20c	10:25:02.60	-57:21:47.30	19	O2 If/WN6	19	—
42-1	WR 42e, SB04 #954	11:14:45.50	-61:15:00.1	21	O2 If/WN6	21	—
43-2	MTT 58	11:15:07.60	-61:16:54.8	22	O2 If/WN6	22	—
43-1	SMG09 740_21	11:16:03.536	-61:26:58.34	1	WN4b	1	6.9±1.2
44-1	SMG09 740_16	11:19:42.96	-61:27:12.40	1	WCE	1	–
45-1	HDM07 1	11:42:37.66	-62:41:19.30	2	WN9–10h	2	–
45-2	SMG09 768_6	11:46:06.66	-62:47:12.70	1	WN5	1	–
45-3	SMG09 772_17	11:50:04.242	-62:52:15.44	1	WN5b	0	11.9±1.9
45-4	SMG09 776_3	11:55:52.116	-62:45:02.28	1	WN6	1	6.7±1.3
45-5	VVV CL009-6	11:56:03.78	-63:18:54.44	23	Of/WN7	23	–
46-1	HDM07 2	12:06:56.480	-62:38:30.45	2	WN6o	2	7.2±1.4
46-7	J12100795-6244194	12:10:07.95	-62:44:19.40	3	WC5–7	3	–
46-8	J12110256-6257476	12:11:02.567	-62:57:47.61	3	WN6	3	5.1±1.0
46-16	RMM11 #5	12:11:54.1	-63:17:04.0	24	WN9	24	–
46-9	J12121681-6246145	12:12:16.814	-62:46:14.54	3	WN5	0	3.6±0.6
46-17	VVV CL011-2	12:12:41.13	-62:42:30.71	23	WN9/OIf+	23	–
46-10	SMG09 791_12c	12:13:28.29	-62:41:42.90	1	WCE	1	–
46-2	HDM07 3	12:13:38.790	-63:08:58.06	2	WN7h	2	4.9±0.9
46-3	KBG07 4	12:14:31.54	-62:58:54.30	4	WN7–8	4	–
46-4	KBG07 3	12:14:31.76	062:58:51.90	4	Ofp/WN	4	–
46-5	KBG07 2	12:14:33.090	-62:58:51.00	4	WN6	4	8.6±2.0
46-6	KBG07 1	12:14:33.910	-62:58:48.70	4	WN7	4	9.1±2.2
46-15	MDM11 2	12:15:12.492	-62:46:43.89	5	WN8	5	7.6±1.3
46-11	SMG09 808_14	12:28:41.91	-63:25:46.10	1	WCE	1	–
46-12	SMG09 808_23	12:28:50.995	-63:17:00.23	1	WN4b	0	16.2±2.8
46-13	SMG09 807_16	12:30:03.86	-62:50:17.10	1	WC7	1	–
46-14	SMG09 816_10	12:38:18.781	-63:24:19.74	1	WN5b	1	11.0±1.7
47-1	HDM07 4	12:46:16.140	-62:57:23.47	2	WN6o	2	8.0±1.6
47-2	SMG09 832_25	12:55:44.26	-63:35:50.0	1	WC5–6	1	–
47-3	SMG09 856_13c	13:03:11.08	-63:42:16.20	1	WC5–6	1	–
47-4	SMG09 839_12	13:04:50.08	-63:04:40.20	1	WC5–6	1	–
48-1	HDM07 5	13:10:12.073	-62:39:06.57	2	WC7	2	5.6±0.9
48-6	MDM11 3	13:12:09.059	-62:43:26.71	5	WN9	5, 0	4.2±0.6
48-3	SMG09 845_34	13:12:21.307	-62:40:12.58	1	WC8	1	4.2±0.6
48-10	DCT12 D1-2	13:12:24.980	-62:42:00.20	6	WN9h	0	4.2±0.6
48-7	MDM11 5	13:12:25.460	-62:44:41.70	5	WN8	0	4.2±0.6
48-4	SMG09 845_35, MDM11 6	13:12:27.670	-62:44:22.00	1	WC6	0	4.2±0.6
48-8	MDM11 7, DCT12 D1-5	13:12:28.50	-62:41:50.9	5, 6	WNLh	6	–
48-9	MDM11 8, DCT12 D1-1	13:12:28.550	-62:41:43.80	5, 6	WN9h	5	4.2±0.6
48-5	SMG09 847_8	13:12:45.354	-63:05:52.00	1	WN6b	0	7.1±1.2
48-2	DCT12 D2-3	13:12:57.700	-62:40:59.90	3	WC7–8	6	4.2±0.6
49-1	MDM11 9	13:14:57.048	-62:23:53.34	5	WN8	5	11.3±1.9
52-1	SMG09 853_9	13:22:16.082	-62:30:57.45	1	WN6	1	9.0±1.8
52-2	SMG09 858_26	13:28:15.876	-62:06:23.57	1	WN6	1	8.1±1.6
57-1	MDM11 10	13:44:06.952	-62:45:02.20	5	WN7	5	9.7±1.9
59-1	SMG09 883_18	13:52:02.36	-62:26:46.0	1	WCE	1	–
59-2	SMC09 885_11	13:54:13.45	-61:50:01.80	1	WC5–6	1	–
60-3	MDM11 11	14:01:15.49	-62:38:19.9	5	WC7	5	–
60-4	MDM11 12	14:04:36.672	-61:29:16.52	5	WC8	5	5.7±1.0
60-5	WR 60a	14:06:03.619	-60:27:29.58	7	WC7	0	6.0±1.0
60-6	VVV CL036-9	14:09:04.30	-61:15:53.78	23	WN6	23	–
60-1	SMG09 897_5	14:10:10.015	-61:15:25.59	1	WC8	1	4.6±0.8
60-2	SMG09 903_15c	14:12:36.54	-61:45:32.70	1	WC8	1	–
61-2	SMG09 907_18	14:16:27.372	-61:17:56.25	1	WN5b	1	4.9±0.8
61-3	MDM11 13	14:20:30.746	-60:48:22.12	5	WC9	5	4.8±1.0
61-1	J14212314-6018041	14:21:23.148	-60:18:04.12	3	WN6	3	4.7±0.9
62-1	AX J144701-5919	14:46:53.58	-59:19:38.3	25	WN7-8h	25	–

Table A1. (Continued)

WR	Alias	RA (hh:mm:ss)	Dec (±dd:mm:ss)	Ref	Sp Type	Ref	Distance kpc
64-1	SMG09 956_25	15:01:30.119	-59:16:12.06	1	WN4b	1	6.8±1.2
67-3	G321.0331-0.4274	15:15:39.44	-58:08:16.0	26	WN10	26	–
67-1	WR67a	15:16:36.96	-58:09:58.7	8	WN6h	8	–
67-2	WR67b	15:17:46.301	-57:56:59.29	8	WC7	0	3.7±0.6
68-1	SMG09 979_11	15:20:35.916	-57:27:11.95	1	WN4b	1	8.9±1.6
70-1	WMD10 9, J15352652-5604123	15:35:26.528	-56:04:12.33	3	WN7	3	12.4±2.4
70-3	SMG09 1011_24	15:43:04.681	-55:11:12.35	1	WC7	0	4.7±0.8
70-4	WMD10 10	15:45:59.143	-53:32:32.50	9	WN9h	9	12.5±2.0
70-5	WMD10 11b	15:48:42.105	-55:07:54.21	9	WC9	9	2.2±0.4
70-10	SFZ12 1023-63L	15:52:09.48	-54:17:14.5	10	WC7:	10	–
70-6	MDM11 14	15:53:31.854	-53:45:44.40	5	WN6b	0	7.3±1.3
70-7	MDM11 15	15:58:49.712	-52:51:32.46	5	WN6b	5	8.0±1.4
70-8	MDM11 16	15:58:54.933	-52:02:45.52	5	WN7	5	5.8±1.2
70-2	J15595671-5159299	15:59:56.715	-51:59:29.93	3	WN5b	0	3.6±0.6
70-9	MDM11 17	16:00:23.265	-52:51:42.32	5	WC8	5	7.2±1.3
70-11	SFZ12 1042-25L	16:00:25.264	-52:03:29.62	10	WN7	0	6.5±1.2
70-12	SFZ12 1038-22L	16:00:26.41	-52:11:10.1	10	WC7:	10	–
72-3	SFZ12 1054-43L, MDM11 18	16:10:06.251	-50:47:58.56	10	WC9	10	6.7±1.4
72-4	SFZ12 1051-67L	16:00:06.67	-51:47:24.5	10	WC7:	10	–
72-1	HDM07 6	16:11:39.271	-52:05:45.81	2	WC9	2	2.7±0.6
72-2	SMG09 1053_27	16:11:43.70	-51:10:16.6	1	WC8	1	–
73-1	SMG09 1059_34	16:14:37.237	-51:26:26.33	1	WC7	0	10.9±1.9
74-1	MDM11 19	16:20:51.436	-50:04:03.33	5	WN9ha	5	8.1±1.2
74-3	SFZ12 1077-55L	16:24:22.70	-49:00:42.3	10	WC6:	10	–
74-2	MDM11 20	16:24:23.294	-49:21:29.59	5	WN7	5	8.3±1.7
75-1	SMG09 1081_21	16:24:58.868	-48:56:52.45	1	WC8	1	7.9±1.4
75-14	SFZ12 1085-72L	16:27:42.390	-48:30:34.20	10	WC9	0	7.2±1.5
75-15	SFZ12 1085-69L	16:28:40.260	-48:18:12.95	10	WC8	10	7.7±1.6
75-6	MDM11 21	16:28:53.428	-48:33:39.41	5	WN5b	5	13.3±2.1
75-16	SFZ12 1085-83L	16:29:35.838	-48:19:34.20	10	WC8	10	8.9±1.9
75-25	VVV CL073-2	16:30:23.73	-48:13:05.48	23	WN9/O4–6If+	23	–
75-26	VVV CL073-4	16:30:23.98	-48:13:05.48	23	WN7	23	–
75-2	SMG09 1093_34	16:31:29.234	-47:56:16.40	1	WC8	1	7.3±1.3
75-30	KSF14 1089-1117	16:31:37.79	-48:14:55.3	27	WN9	27	–
75-3	SMG09 1093_33	16:31:49.062	-47:56:04.47	1	WC8	1	8.8±1.6
75-27	VVV CL074-2	16:32;05.27	-47:49:14.25	23	WC8	23	–
75-28	VVV CL074-3	16:32:05.46	-47:49:28.10	23	WN8	23	–
75-29	VVV CL1074-9	16:32:05.93	-47:49:30.92	23	WN7/O4–6If+	23	–
75-4	SMG09 1093_53, WMD10 16	16:32:12.986	-47:50:35.88	1	WN5b	1	9.1±1.5
75-17	SFZ12 1093-138L	16:32:15.223	-47:56:12.71	10	WC8:	10	16.5±3.0
75-7	MDM11 22	16:32:22.051	-47:47:42.60	5	WC9	5	8.2±1.7
75-31	KSF14 1093-1765	16:32:25.70	-47:50:46.1	27	WN6	27	–
75-18	SFZ12 1093-140LB	16:32:48.55	-47:45:06.2	25	WN9	10	–
75-19	SFZ12 1093-140L	16:32:49.78	-47:44:31.4	10	WC7:	10	–
75-8	MDM11 23	16:33:11.207	-48:19:41.26	5	WN4b	0	6.2±1.1
75-20	SFZ12 1091-46L	16:33:14.06	-48:17:37.2	10	WC8	10	–
75-9	MDM11 24, SFZ12 1093-59L	16:33:45.45	-47:51:29.1	5	WC8-9d?	5	–
75-21	SFZ12 1095-189L	16:33:48.13	-47:52:52.8	10	WC7:	10	–
75-10	MDM11 25, SFZ12 1097-156L	16:34:57.467	-47:04:12.95	5	WN5-6b	5	7.0±1.2
75-11	MDM11 26	16:35:05.55	-47:17:13.5	5	WC9d?	5	–
75-5	SMG09 1096_22, SFZ12 1095-98L	16:35:23.317	-48:09:18.09	1	WC8	1	8.9±1.6
75-12	MDM11 27	16:35:38.882	-47:09:13.09	5	WN6	5	8.0±1.6
75-22	SFZ12 1097-71L	16:35:44.347	-47:19:42.28	10	WC9	10	7.8±2.0
75-13	MDM11 28, SFZ12 1097-34L	16:35:51.169	-47:19:51.54	5	WC8	5	5.8±1.0

Table A1. (Continued)

WR	Alias	RA (hh:mm:ss)	Dec (±dd:mm:ss)	Ref	Sp Type	Ref	Distance kpc
75-23	SFZ12 1106-31L	16:37:23.991	-46:26:28.73	10	WC9	10	3.7±0.7
75-24	SFZ12 1105-76L	16:38:20.18	-46:23:43.8	10	WC8	10	–
76-10	SFZ12 1109-74L	16:40:17.12	-46:20:09.7	10	WC7:	10	–
76-2	Mercer 81-5	16:40:28.35	-46:23:25.6	28	WN7–8	29	–
76-3	Mercer 81-8	16:40:28.94	-46:23:27.1	28	WN8:	29, 0	–
76-4	Mercer 81-6	16:40:29.32	-46:23:11.6	28	WN9ha	29, 0	–
76-5	Mercer 81-9	16:40:29.32	-46:23:38.2	28	WN9ha	29, 0	–
76-6	Mercer 81-7	16:40:29.60	-46:23:25.6	28	WN7–8	29	–
76-7	Mercer 81-2	16:40:29.65	-46:23:29.1	28	WN7–8	29	–
76-8	Mercer 81-4	16:40:29.65	-46:23:28.7	28	(WN7–8)	0	–
76-9	Mercer 81-3	16:40:30.08	-46:23:11.4	28	WN7–8	28	–
76-1	MDM11 29	16:40:50.787	-45:51:23.11	5	WN9	5	8.7±1.4
77-5	SFZ12 1115-197L	16:43:40.369	-45:57:57.60	10	WN6	10	4.4±0.9
77-1	J16441069-4524246	16:44:10.695	-45:24:24.70	3	WN7b	0	4.0±0.6
77-2	J16465342-4535590	16:46:53.428	-45:35:59.02	3	WN7	3	3.8±0.7
77-3	MDM11 30	16:47:46.036	-45:59:04.93	5	WN6	5	3.8±0.8
77-4	MDM11 31	16:48:27.584	-46:09:27.20	5	WN6	0	5.4±1.1
77-6	SFZ12 1138-133L	16:51:19.330	-43:26:55.27	10	WN6b	0	10.3±1.8
77-7	SFZ12 1133-59L	16:51:29.702	-43:53:35.52	10	WC9	10	9.5±2.2
78-1	KSF14 1139-49EA	16:54:08.46	-43:49:25.3	27	WC6:	27	–
82-2	KSF14 1178-66B	17:07:23.95	-39:19:54.4	27	WC9	27	–
82-1	SFZ12 1168-91L	17:09:32.64	-41:29:47.3	10	WC7:	10	–
83-1	SFZ12 1179-129L	17:11:00.84	-39:49:31.2	10	WC6:	10	–
84-2	SFZ12 1181-82L	17:11:28.502	-39:13:16.8	10	WC8	10	7.9 ±1.4
84-6	DBS03 179 #15	17:11:31.80	-39:10:46.8	30	WN8–9	30	–
84-7	DBS03 179 #4	17:11:31.88	-39:10:46.9	30	Ofpe/WN9	30	–
84-1	MDM11 32, DBS03 179 #20	17:11:33.037	-39:10:40.05	5	WN9	0	6.3±1.0
84-3	SFZ12 1181-81L	17:11:36.12	-39:11:07.9	10	WC8	10	–
84-4	SFZ12 1181-211L	17:11:46.133	-39:20:27.78	10	WN7ha	0	16.5±3.0
84-11	KSF14 1176-B49	17:12:34.87	-40:37:13.8	27	WN9h	27	–
84-5	SFZ12 1189-110L	17:14:09.551	-38:11:20.90	10	WC9	10	9.0±1.9
84-8	VVV CL099-4	17:14:24.71	-38:09:49.35	23	WN6+O	23	–
84-9	VVV CL099-5	17:14:25.42	-38:09:50.40	23	WN6	23	–
84-10	VVV CL099-7	17:14:25.66	-38:09:53.72	23	WC8	23	–
85-1	KSF14 1198-6EC8	17:15:55.9	-37:12:12.0	27	WC6:	27	–
91-1	SMG09 1222_15	17:22:40.741	-35:04:52.95	1	WC7	0	4.7±0.8
94-1	SFZ12 1245-23L	17:33:33.220	-32:36:16.40	10	WC9	10	3.8±0.8
98-2	KSF14 1256-1483A	17:40:59.35	-32:11:22.3	27	WN9	27	–
98-1	SFZ12 1269-166L	17:41:13.512	-30:03:40.98	10	WC8	10	6.7±1.2
100-3	SFZ12 1275-184L	17:44:06.89	-30:01:13.2	10	WN8	10	–
100-2	MCD10 2	17:45:06.91	-29:12:02.1	12	WC9?d	12	–
100-1	J174508.9-291218	17:45:08.900	-29:12:18.00	11	WN7b	0	8.7±1.4
101-7	MCD10 4	17:45:09.74	-29:14:14.6	12	WC9?d	12	–
101-2	J174516.1-284909	17:45:16.10	-28:49:09.0	11	WN9	11	–
101-3	J174516.7-285824	17:45:16.726	-28:58:25.10	11	WN8o	0	7.5±1.3
101-4	J174519.1-290321	17:45:19.16	-29:03:21.78	11	WC9d	11	–
101-8	MCD10 3	17:45:21.870	-29:11:59.43	12	WC9	12	9.2±1.9
101-5	J174522.6-285844	17:45:22.600	-28:58:44.00	11	WN6b	0	5.5±1.0
101-6	J174528.6-285605	17:45:28.60	-28:56:05.0	11	WN8-9h	11	–
101-9	MCD10 8	17:45:32.518	-29:04:57.93	12	WC9	12	4.5±1.0
101-1	Edd-1, J174536.1-285638	17:45:36.120	-28:56:38.70	31	WN9h	0	7.4±1.1
102-12	MCD10 11	17:45:48.617	-28:49:42.64	12	WN8–9h	12	7.1±1.2
102-4	J174550.2-284911	17:45:50.20	-28:49:11.0	11	WN8-9h	11	–
102-13	MCD10 19	17:45:50.29	-28:57:26.2	12	WC9	12	–
102-5	J174550.6-285617	17:45:50.60	-28:56:17.00	11	WN7	11	–
102-14	MCD10 12	17:45:53.18	-28:49:36.0	12	WN8-9h	12	–
102-6	J174555.3-285126	17:45:55.300	-28:51:26.00	11	WN5–6b	11	
102-15	MCD10 14	17:46:02.48	-28:54:12.8	12	WC9	12	–
102-2	LHO09 76	17:46:14.15	-28:49:35.4	14	WC9d	14	

Table A1. (Continued)

WR	Alias	RA (hh:mm:ss)	Dec (±dd:mm:ss)	Ref	Sp Type	Ref	Distance kpc
102-3	LHO09 79, qF250	17:46:15.39	-28:49:34.6	14	WC9d	14	
102-16	MCD10 16	17:46:17.57	-28:53:03.7	12	WN8-9h	12	–
102-7	J174617.7-285007	17:46:17.70	-28:50:07.0	11	WC9d	11	–
102-17	MCD10 17	17:46:23.838	-28:48:11.26	12	WN6b	0	7.7±1.3
102-1	J174645.3-281546	17:46:45.34	-28:15:46.10	32	(WC)	32	–
102-8	J174656.3-283232	17:46:56.295	-28:32:32.50	11	WN9h	0	7.3±1.2
102-18	MCD10 15	17:46:09.73	-28:55:31.9	12	WN8-9h	12	–
102-9	J174711.4-283006	17:47:11.471	-28:30:06.99	11	WN9h	0	6.4±1.0
102-10	J174712.2-283121	17:47:12.250	-28:31:21.56	11	WN8o	0	5.5±0.9
102-11	J174713.0-282709	17:47:13.00	-28:27:09.00	11	WN7–8h	11	–
102-19	SFZ12 1322-220L	17:55:20.211	-24:07:38.41	10	WN5	10	5.1±0.8
102-23	KSF14 1319-3BC0	17:57:16.87	-25:23:13.8	27	WC7: 27	–	
102-22	FSZ14 WR1327-14AF	17:59:02.27	-24:17:00.1	33	WC7	33	–
102-20	SFZ12 1327-25L	17:59:02.897	-24:20:50.61	10	WC9	10	5.2±1.3
102-24	KSF14 1338-2B3	17:59:07.99	-22:36:43.0	27	WN9	27	–
102-21	SFZ12 1342-208L	17:59:48.22	-22:14:52.4	10	WN6	10	–
104-1	KSF14 1343-69E	18:02:22.35	-22:38:00.3	27	WN8–9	27	–
105-1	FSZ14 WR1343-193E	18:02:46.23	-22:36:39.7	33	WN6	33	–
105-2	KSF14 1343-284	18:03:28.37	-22:22:58.9	27	WN8–9	27	–
108-2	KSF14 1353-160A	18:05:35.60	-21:04:23.3	27	WC8–9	27	–
108-3	KSF14 1366-438	18:05:55.27	-19:29:44.1	27	WN7–8	27	–
108-1	FSZ14 WR1361-1583	18:07:05.16	-20:15:16.1	33	WN9	33	–
111-8	KSF14 1367-638	18:09:06.22	-19:54:27.2	27	WN9	27	–
111-1	HDM07 7	18:09:45.057	-20:17:10.35	2	WN6o	2	6.4±1.3
111-9	KSF14 1381-19L	18:12:02.0	-18:06:55.0	27	WC9	27	–
111-5	MDM11 33	18:12:41.102	-18:26:30.46	5	WN9	0	15.3±2.4
111-6	SFZ12 1381-20L	18:12:57.580	-18:01:24.36	10	WC9	10	4.2±0.9
111-2	HDM07 8, MDF11 #4	18:13:14.200	-17:53:43.50	2	WN7b	2	3.6±0.7
111-4	MDM11 34, MDF11 #7	18:13:22.480	-17:53:50.30	5	WN7	0	3.6±0.7
111-3	SMG09 1385_24	18:13:42.476	-17:28:12.21	1	WC8	1	2.8±0.5
111-10	KSF14 1389-4AB6	18:14:14.09	-17:21:02.6	27	WC7	27	–
111-11	KSF14 1389-1F5D	18:14:17.37	-17:21:54.2	27	WN8	27	–
111-7	SFZ12 1395-86L	18:16:02.36	-16:53:59.4	10	WC8	10	–
113-1	HDM07 9	18:19:22.194	-16:03:12.38	2	WN7o	2	2.9±0.6
113-3	KSF14 1430-AB0	18:21:02.92	-12:27:45.8	27	WN4-7	27	–
113-2	SMG09 1425_47	18:23:03.42	-13:00:00.4	1	WC5-6	1	–
114-2	SFZ12 1434-43L	18:23:32.333	-12:03:58.57	10	WC8	10	11.4±2.1
114-1	HDM07 10, KSF14 1446-B1D	18:25:00.241	-10:33:23.63	2	WN7b	2	12.2±1.9
115-1	HDM07 11	18:25:53.094	-13:28:32.41	2	WN6o	2	4.1±0.8
115-2	MDM11 35, SFZ12 1431-34L	18:25:53.617	-12:50:03.19	5	WN8	5	7.4±1.2
115-3	MDM11 36	18:26:06.116	-13:04:10.47	5	WN7	5	3.7±0.7
116-1	J18281180-1025424	18:28:11.80	-10:25:42.4	3	WC9+OBI	3	–
116-4	KSF14 1443-760	18:28:33.39	-11:46:44.2	27	WN9h	27	–
116-2	SMG09 1462_54	18:29:33.847	-08:39:02.10	1	WN5o	1	9.3±1.5
116-3	MDM11 37	18:30:53.206	-10:19:37.09	5	WN6ha	0	14.5±2.4
117-2	KSF14 1457-673	18:31:06.65	-09:48:01.4	27	WC9	27	–
117-1	MWC10-XGPS14, MDM11 38	18:31:16.531	-10:09:25.01	20	WN7	5	2.6±0.5
118-4	MDM11 39, SFZ12 1463-7L	18:33:47.637	-09:23:07.71	5	WC8	5,10	3.9±0.7
118-7	SFZ12 1477-55L	18:35:47.658	-07:17:50.07	10	WC9	10	4.4±0.9
118-1	MDI09 Quartet 5	18:36:16.33	-07:05:17.0	15	WC9d	15,0	
118-2	MDI09 Quartet 2	18:36:16.69	-07:04:59.50	15	WN9	15	–
118-3	MDI09 Quartet 1	18:36:17.29	-07:05:07.30	15	WN9	15	–
118-10	KSF14 1485-6C4	18:36:55.53	-06:31:02.1	27	WN6	27	–
118-5	MDM11 40	18:37:51.49	-06:08:41.7	5	WC9d	5	–
118-11	KSF14 1485-844	18:37:51.82	-06:31:19.1	27	WN8	27	–
118-8	SFZ12 1487-80L	18:38:00.479	-06:26:46.23	10	WC9	10	5.5±1.2
118-6	MDM11 41, SFZ12 1483-212L	18:38:27.169	-07:10:44.79	5	WN7	5, 10	7.2±1.4
118-9	SFZ12 1489-36L	18:38:38.931	-06:00:16.01	10	WC9	10	5.5±1.2
119-2	MDM11 42, SFZ12 1493-9L	18:39:34.581	-05:44:23.08	5	WC8	5, 10	4.9±0.9

Table A1. (Continued)

WR	Alias	RA (hh:mm:ss)	Dec (±dd:mm:ss)	Ref	Sp Type	Ref	Distance kpc
119-4	KSF14 1495-1D8A	18:39:40.60	-05:35:17.6	27	WC8–9	27	–
119-5	KSF14 1495-705	18:39:41.19	-05:57:36.3	27	WN8	27	–
119-3	SFZ12 1487-212L	18:39:42.533	-06:41:46.37	10	WN7	10	7.5±1.5
119-1	HDM07 12	18:40:08.66	-03:29:31.10	2	WN7o	2	–
120-16	KSF14 1514-AA0	18:41:06.79	-02:56:01.0	27	WC8	27	–
120-1	HDM07 13	18:41:10.70	-04:51:27.0	2	WC9	2	–
120-11	SFZ12 1495-32L	18:41:23.348	-05:40:58.39	10	WC8	10	7.0±1.2
120-7	MDM11 43, SFZ12 1503-160L	18:41:34.071	-05:04:01.26	5	WN7	5, 10	3.7±0.7
120-2	SMG09 1509_29, SCB12 2w01	18:41:48.49	-04:00:12.4	1	WC7	1, 34	–
120-8	MDM11 44	18:42:02.551	-03:56:26.37	5	WN9	0	8.0±1.3
120-3	WMD47, WR120bb	18:42:06.308	-03:48:22.48	13	WN9h	13, 37	6.9±1.1
120-4	WMD48, WR120bc	18:42:08.271	-03:51:02.91	13	WN9h	13, 37	7.6±1.2
120-5	J18420846-0349352, SCB12 2w02	18:42:08.467	-03:49:35.22	13	WC8	13	4.9±0.9
120-14	SCB12 2w03	18:42:22.17	-03:05:39.6	34	WC8	34	–
120-17	KSF14 1509-2E64	18:42:26.61	-03:56:36.0	27	WC9	27	–
120-6	WMD10 50, PN G029.0+0.04	18:42:46.921	-03:13:17.25	9	WN6o	9	19.9±3.9
120-15	SCB12 2w04	18:43:17.23	-03:08:56.6	34	WC8	34	–
120-12	SFZ12 1513-111L, SCB12 2w05	18:43:17.28	-03:20:23.7	10	WC8	34	–
120-9	MDM11 45	18:43:32.575	-04:04:19.02	5	WN7ha	0	19.7±3.8
120-13	SFZ12 1522-55L	18:43:39.65	-02:29:35.9	10	WC9	10	–
120-10	MDM11 46, SFZ12 1517-138L	18:43:58.034	-02:45:17.22	5	WN7	5	3.9±0.8
121-2	MDM11 47	18:44:51.576	-03:21:49.61	5	WN7	5	9.3±1.8
121-3	MDM11 48	18:44:51.610	-03:27:43.75	5	WN7	5	7.7±1.5
121-11	KSF14 1525-2352	18:45:14.63	-02:05:05.7	27	WC8:	27	–
121-7	SCB12 2w06, KSF14 1519-E43	18:45:49.90	-02:59:56.3	34	WC7-8	34, 27	–
121-12	KSF14 1530-8FA	18:46:00.97	-01:14:35.0	27	WN5	27	–
121-5	SFZ12 1527-13L, SCB12 2w07	18:47:38.33	-02:06:38.9	10	WC8	10, 34	–
121-8	SCB12 2w08	18:47:57.34	-01:27:36.9	34	WC8	34	–
121-9	SCB12 2w09	18:48:24.50	-02:06:16.2	34	WC8	34	–
121-1	WR121b, WMD10 52	18:49:27.336	-01:04:20.79	16	WN7h	16	6.1±1.2
121-4	MDM11 49, SFZ12 1528-15L	18:49:32.305	-02:24:27.08	5	WC7	0	6.9±1.2
121-10	SCB12 2w10, KSF14 1541-3C8	18:50:02.77	-00:32:08.1	34	WC8	34, 27	–
121-13	KSF14 1541-197C	18:50:37.54	-00:01:21.1	27	WC8	27	–
121-6	SFZ12 1536-180L	18:51:10.77	-01:30:03.4	10	WN5	10	–
121-14	KSF14 1547-E0B	18:51:33.07	-00:13:41.3	27	WN4	27	–
121-15	KSF14 1544-FA4	18:51:33.08	+00:13:41.2	27	WN5	27	–
121-16	KSF14 1547-1DF2	18:51:38.98	-00:10:08.1	27	WN8:	27	–
122-6	SFZ12 1551-19L	18:52:32.97	+00:14:26.8	10	WC8:	10	–
122-12	KSF14 1553-9E8	18:52:33.12	+00:47:41.8	27	WN9h	27	–
122-2	MDM11 51	18:52:43.699	+00:08:41.58	5	WN9	0	8.3±1.3
122-13	KSF14 1547-1488	18:52:57.20	+00:02:54.1	27	WN5	27	–
122-14	KSF14 1553-15DF	18:53:02.56	+01:10:22.7	27	WC8	27	–
122-3	MDM11 52	18:54:03.125	+01:24:50.84	5	WN6	0	4.7±0.9
122-7	SFZ12 1563-66L	18:55:44.44	+01:36:43.9	10	WC8: 10	–	
122-8	SFZ12 1563-89L	18:56:02.04	+01:36:32.9	10	WC7:	10	–
122-9	SFZ12 1567-51L	18:56:07.90	+02:20:49.0	10	WC7:	10	–
122-11	FSZ14 WR1583-B73	19:00:05.09	+03:47:27.1	33	WN6	33	–
122-1	J190015.86+000517.3	19:00:15.86	+00:05:17.3	35	WC8	35	–
122-10	SFZ12 1583-64L	19:00:59.99	+03:55:35.6	10	WC7:	10	–
122-4	MDM11 53, SFZ12 1583-48L	19:01:26.614	+03:51:55.34	5	WC8	5, 10	8.1±1.4
122-5	MDM11 54, SFZ12 1583-47L	19:01:27.119	+03:51:54.22	5	WC8	5, 10	7.6±1.4
122-15	KSF14 1602-9AF	19:02:42.32	+06:54:44.4	27	WN6	27	–
123-6	KSF14 1603-11AD	19:04:20.14	+06:07:52.2	27	WN5	27	–
123-4	SFZ12 1603-75L	19:04:33.490	+06:05:18.50	10	WC8	10	33.2±6.4
123-7	KSF14 1609-1C95	19:06:10.68	+07:19:13.3	27	WC9	27	–
123-8	KSF14 1626-4FC8	19:06:33.66	+09:07:20.8	27	WC6	27	–
123-2	SMG09 1613_21	19:06:36.53	+07:29:52.40	1	WCE	1	–
123-1	HDM07 14	19:08:17.975	+08:29:10.56	2	WN6	2	3.2±0.6
123-3	MDM11 55	19:08:38.093	+09:28:21.06	5	WN8	5	9.8±1.6

Table A1. (Continued)

WR	Alias	RA (hh:mm:ss)	Dec (±dd:mm:ss)	Ref	Sp Type	Ref	Distance kpc
123-9	KSF14 1629-14D6	19:10:06.40	+09:45:25.7	27	WN9h	27	–
123-5	SCB12 2w11, KSF14 1627-A6D	19:10:11.53	+08:58:39.6	34	WC7	34, 27	–
124-1	MDI09 Glimpse 20-6	19:12:24.140	+09:57:29.10	15	WC8	0	4.4±0.7
124-13	KSF14 1635-AD8	19:13:19.19	+09:55:29.0	27	WN6	27	–
124-8	SFZ12 1650-96L	19:13:23.731	+11:43:26.81	10	WN6	10	2.8±0.6
124-14	KSF14 1653-FFE	19:14:40.73	+11:54:15.4	27	WN5–6	27	–
124-15	KSF14 1651-BB4	19:15:37.26	+11:25:26.3	27	WN5	27	–
124-16	KSF14 1647-1E70	19:15:52.52	+11:12:59.7	27	WC8:	27	–
124-3	MDM11 56, SFZ12 1657-51L	19:16:18.383	+12:46:49.36	5	WC7	0	9.5±1.6
124-17	KSF14 1659-212	19:17:22.20	+12:13:09.2	27	WN9	27	–
124-9	SFZ12 1670-57L	19:17:32.805	+14:08:27.98	10	WC6:	10	13.2±4.1
124-4	MDM11 57, SFZ12 1652-24L	19:17:41.21	+11:29:18.9	5	WC7	5	–
124-18	KSF14 1669-3DF	19:18:31.35	+13:43:39.4	27	WN9h	27	–
124-10	SFZ12 1669-24L	19:18:31.705	+13:43:17.84	10	WC6:	10	9.7±3.0
124-19	KSF14 1660-1169	19:20:02.46	+12:08:20.3	27	WC6:	27	–
124-5	MDM11 58	19:20:29.32	+14:12:06.1	5	WC8-9d?	5	–
124-2	SMG09 1671_5	19:20:40.38	+13:50:35.2	1	WC8	1	–
124-12	FSZ14 WR1667-D00	19:20:50.59	+13:18:41.1	33	WN7	33	–
124-6	MDM11 59, SFZ12 1675-17L	19:22:53.616	+14:08:49.82	5	WC6	0	4.6±1.4
124-7	MDM11 60, SFZ12 1675-10L	19:22:54.462	+14:11:28.01	5	WC8	0	3.8±0.7
124-11	SFZ12 1698-70L	19:24:46.914	+17:14:25.18	10	WN6b	0	7.8±1.3
124-20	KSF14 1697-38F	19:25:18.12	+17:02:15.9	27	WC9	27	–
124-21	KSF14 1702-23L	19:26:08.00	+17:46:23.0	27	WC8	27	–
124-22	KSF14 1695-2B7	19:27:17.98	+16:05:24.6	27	WC9	27	–
125-4	MDM11 61	19:30:05.304	+17:46:01.10	5	WC8d	5	6.5±1.3
125-3	HKB10 2, Mercer 23 #2	19:30:13.820	+18:32:00.33	17	WN7ha	0	6.5±0.3
125-2	J193038.84+183909.8	19:30:38.84	+18:39:09.8	35	WN8-9	35	–
125-1	HMD07 15	19:33:44.016	+19:22:47.54	2	WC8	2	5.1±0.9
138-1	WR138a, HBHA 4202-22	20:17:08.12	+41:07:27.0	36	WN8-9h	36	–
142-1	HBHα 4203-27	20:28:14.552	+43:39:25.74	18	WN6o	18	1.7±0.3

(0) This work, (1)Shara et al. (2009), (2)Hadfield et al. (2007), (3)Mauerhan, van Dyk & Morris (2009), (4)Kurtev et al. (2007), (5)Mauerhan et al. (2011), (6)Davies et al. (2012a), (7)Roman-Lopes (2011b), (8)Roman-Lopes (2011c), (9)Wachter et al. (2010), (10)Shara et al. (2012), (11)Mauerhan et al. (2010a), (12)Mauerhan et al. (2010c), (13)Mauerhan et al. (2010b), (14) Liermann et al. (2009), (15)Messineo et al. (2009), (16)Gvaramadze et al. (2010), (17)Hanson et al. (2010), (18)Littlefield et al. (2012). (19) Roman-Lopes et al. (2011a), (20) Motch et al. (2010) (21)Roman-Lopes (2012), (22)Roman-Lopes (2013), (23)Chené et al. (2013), (24) Rahman, Moon, & Matzner (2011), (25) Anderson et al. (2011), (26) Marston et al. (2013), (27) Kanarek et al. (2014), (28) Davies et al. (2012), (29) de La Fuente, Najarro, Davies, & Figer (2013), (30) Borissova et al. (2012), (31) Mikles et al. (2006), (32) Hyodo et al. (2008), (33) Faherty et al. (2014) (34) Smith et al. (2012), (35) Corradi et al. (2010), (36) Gvaramadze et al. (2009), (37) Burgemeister et al. (2013)

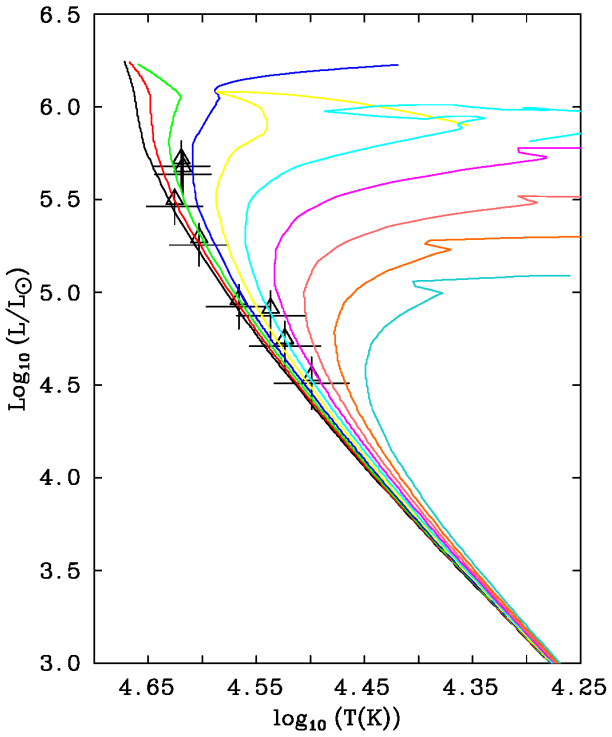

Figure B1. Hertzsprung-Russell diagram showing positions of the 8 brightest (V-band, Massey et al. 2001a) O-stars in the Pismis 24 open cluster (triangles). Stars are individually dereddened and shown at a distance modulus of 11.5, with Z=0.02 iochrones (Lejeune & Schaerer 2001) for ages (from left to right) 6.00, 6.09, 6.19, 6.30, 6.40, 6.50, 6.59, 6.69, 6.80, and 6.90 Myr (left to right, solid lines).

APPENDIX B: WR STARS AND CLUSTERS WITH DISTANCE AMBIGUITY

B0.1 Pismis 24 and WR 93

The open cluster Pismis 24 (Pi 24) contains the WC7+O binary system WR 93, and has conflicting distance meaurements in the literature, i.e., 2.56 ± 0.10 kpc (Massey, DeGioia-Eastwood & Waterhouse 2001a) and 1.7 ± 0.2 kpc (Fang et al. 2012). In Figure B1 we plot Lejeune & Schaerer (2001) isochrones along with the positions of the 8 brightest O-stars in Pi 24. We take photometry and spectral types for these O-stars from Massey et al. (2001a) except for Pi 24–1, which has since been resolved into two components, Pi 24–1 NE and Pi 24–1 SW (Maíz Apellániz et al. 2007), with an optical/near ultraviolet $\Delta m \sim 0.1$. We adjust the Massey et al. photometry for Pi 24–1 to account for its binary nature, and adopt spectral types of O3.5If* and O4III(f+) for Pi 24–1 NE and Pi 24–1 SW respectively (Maíz Apellániz et al. 2007). To calculate an extinction to each of the 8 O-stars, we evaluate the E_{B-V} colour excess assuming Martins & Plez (2006) intrinsic colours and an R_V=3.1 extinction law. Finally, by taking O-star temperatures and bolometric corrections from Martins, Schaerer & Hillier (2005), we see that best agreement with the isochrones is found at a distance modulus of 11.5 ± 0.2, corresponding to $d = 2.00^{+0.19}_{-0.17}$ kpc.

B0.2 Westerlund 2

The distance to the young massive open cluster Westerlund 2 - probable host of the O3If*/WN6+O3If*/WN6 binary WR 20a (Rauw, Sana & Nazé 2011) and WR 20b (WN6ha) - remains controvertial. Literature values range from 2.5 kpc to 8 kpc, bringing the membership of the very luminous WR 20a into doubt. Rauw et al. (2007) used the light curve of WR 20a and the knowledge that both stars are of identical spectral type to derive a distance of 8.0 ± 1.0 kpc for this binary system. These authors also derive a distance to the Westerlund 2 cluster of 8.0 ± 1.4 kpc from spectrophotometry of cluster O-stars and use this agreement as evidence for membership of WR 20a. However, these distances are derived on the asumption of an $R_V = 3.1$ extinction law, yielding an average $A_V = 4.68$ for the cluster. Carraro et al. (2012) have claimed an anomalous extinction law along this line of sight with an average $R_V = 3.8 \pm 0.2$. These authors use the spectra of Rauw et al. to obtain $A_V = 7.1 \pm 1.2$, corresponding to a much smaller distance of 3.02 ± 0.52 kpc. The membership of WR 20a as two $\sim 80\,M_\odot$ stars is unfeasible at such a small distance.

WR 20b showns no evidence of binarity in the spectroscopic and photometric monitoring of Rauw et al. (2007). The asssumed intrinsic near-IR colour of WN6ha stars (Table 4) provides $A_{K_S} = 0.75 \pm 0.05$ ($A_V \sim 6.8$), favouring the higher extinction and lower distance estimate for Westerlund 2. Until the issue of the form of the extinction law to Westerlund 2 is settled, we consider neither WR 20a or WR 20b as members of the cluster. We include the stars of WR 20a in our calibration at the binary orbit-derived distance of 8.0 kpc.

B0.3 The Galactic Centre

The Arches and Quintuplet clusters are found 11.6′ and 13.1′ from Sgr A* respectively, which is itself surrounded by a cluster of massive stars. The distance to the GC (R_o), and these three clusters by association, has been the subject of considerable study. The first direct parallax measurement of a GC object - the star forming region Sgr B2 - was presented by Reid et al. (2009) giving a distance of 7.9 ± 0.8 *kpc*; from kinematic arguments Sgr B2 is estimated to be 0.13 kpc nearer than the GC. The most recent determinations of R_o are summerised by Gillessen et al. (2013), and are converging on 8 kpc. Acknowledging the spread in measurements that still remains, we assume a distance of 8.0 ± 0.25kpc for these three clusters.

B0.4 The G305 complex

There are 9 currently identified WR stars located within the boundary of the giant HII region G305.4+0.1, of which only 4 reside in the two central clusters Danks 1 & 2 (see Figure 16 of Mauerhan et al. 2011, and Davies et al. 2012a). This is rather surprising, as one may expect to find these stars - as descendants of massive progenitors - at the centre of these star clusters due to relaxation of their orbits. However, in the dense environment of a cluster a massive star is more likely to encounter other massive stars or binaries, resulting in possible ejection. The apparent concentration of these 5 non-cluster WR stars in G305 around the younger Danks 1

cluster (Davies et al. 2012a) supports a dynamical ejection scenario.

Located only $\sim$2.3′ from the Danks 1 cluster, WR 48–4 is the faintest WR star located within G305. Mauerhan et al. (2011) note that by assuming a WC7 spectral type and applying the K_S-band absolute magnitude-subtype calibations of Crowther et al. (2006b), this star appears to be twice as distant as the two central clusters yet is reddened by a similar amount. We consider the high IR-derived distance to WR48–4 as insignificant evidence for a chance superposition with G305, and included these 9 WRs in the calibration sample at the distance derived for the two central clusters.

APPENDIX C: SINGLE WR STAR EMISSION LINE STRENGTHS

In Table C1 we present average strengths for the most prominent lines in the spectra of each WR spectral type, gathered from published spectra of single WR stars. We use these values to calculate J and K_S-band continuum flux ratios in cases where WR emission lines are diluted by an unknown companion. An uncertainty of 0.1 dex is assumed on each averaged equivalent width, in accordance with the majority of studies from which individual measurements are taken.

Table C1: Emission line strengths (Equivalent widths, Å) in (apparently) single WR stars.

Spectral type	Star (WR#)	Equivalent width (Å)	ref	Average (Å)
		He II 1.012μm		
WN7	55	109.5	a,b	**89**
	82	75.9	b	
	84	134.6	b	
	120	70.8	c,d	
WN6	115	126	c,d	**119**
	85	112	a	
WN4-5	83	192.4	b	**221**
	54	236.2	b	
	61	243.8	b	
	149	234	a	
	129	200	a	
WN4b	1	377	e	**412**
	18	447	a	
WN5-6b	75	327	b	**375**
	110	423	a,d	
WN7b	77sc	280	f	
WC8	135	93	e	**93**
	57	121.7	b	
	60	111.1	b	
	118-4	80	g	
	119-2	93	g	

Continued...

Table C1 continued

Spectral type	Star (WR#)	Equivalent width (Å)	ref	Average (Å)
	53	61.7	a	
WC7	56	143.8	b	**147**
	64	145.8	b	
	90	162	b	
	124-3	138	g	
WC6	154	205	e	**179**
	107a	182	b	
	23	151	a	
WC4-5	111	218	e	**225**
	17	263	a	
	52	234	b	
	150	186	a	
		He I 1.083μm		
WN8	116	480	e	**308**
	130	200	e	
	16	245	d	
WN7	55	296	b	**291**
	82	309	b	
	84	267	b	
WN6	115	170	d	**170**
WN4-5	83	95	b	**114**
	54	106	b	
	61	142	b	
WN7b	77sc	930	f	**930**
WN5-6b	75	661	b	**712**
	110	763	d	
WN4b	1	452	e	
WC8	57	221	b	**412**
	60	353	b	
	118-4	537	g	
	119-2	600	g	
	135	344	e	
WC7	56	221	b	**227**
	64	171	b	
	90	301	b	
	124-3	215	g	
WC6	5	276	e	**232**
	107a	200	b	
	154	220	e	
WC4-5	52	149	b	**169**
	111	189	e	
		He I-II 2.164μm		
WN8-9	16	75	d	**73**
	105	63	d	
	116	106	e	
	130	46	e	
WN7	55	33	b	**43**
	120	52	d	
WN6	24	34	d	**35**
	115	36	d	
WN4-5	129	50	h	**53**

Continued...

Table C1 continued

Spectral type	Star (WR#)	Equivalent width (Å)	ref	Average (Å)
	149	55	h	
WN7b	77sc	85	f	
WN6b	75	74	b	
WN4b	1	54	e	
		He II 2.189μm		
WN7	120	39	d	**35**
	55	31	b	
WN6	115	58	d	**42**
	24	25	d	
WN4-5	129	110	h	**105**
	149	99	h	
		C IV 2.071–2.084μm		
WC8	48-2	581	b	**466**
	77g	430	f	
	118-4	303	g	
	119-2	433	g	
	135	583	e	
WC7	67-2	783	i	**937**
	90	825	b	
	124-3	1202	g	
WC6	5	1339	e	**1530**
	48-4	1862	b	
	154	1388	e	
WC4-5	52	1169	b	**1391**
	111	1613	e	
		C III 2.104–2.115μm		
WC8	48-2	220	b	**209**
	77g	198	f	
	118-4	173	g	
	119-2	260	g	
	135	192	e	
WC7	67-2	234	i	**293**
	90	224	b	
	124-3	422	g	
WC6	5	228	e	**301**
	48-4	385	b	
	154	289	e	
WC4-5	52	277	b	**290**
	111	302	e	

(a)Conti, Massey & Vreux (1990), (b)P.A. Crowther, (priv. comm.), (c)Howarth & Schmutz (1992), (d)Crowther & Smith (1996), (e)W.D. Vacca, (priv. comm.), (f)Crowther et al. (2006b), (g)Mauerhan et al. (2011), (h)Figer, McLean & Najarro (1997), (i)Roman-Lopes (2011c)

APPENDIX D: A VOLUME-LIMITED SAMPLE OF WR STARS

We present a volume-limited ($d < 3$ kpc) sample of Galactic Wolf-Rayet stars in Table D1, in which distances are either from this work, or are derived by adopting M_v (by subtype) and A_v from van der Hucht (2001).

Table D1: Closest ($d < 3$kpc) WR stars listed in ascending heliocentric distance. In the fourth column we class each system as WR-dominated ($m_K^{\rm WR} - m_K^{sys} > 0.4$; WR), companion-dominated (C), or dust-producing (D). References are given for spectral types of stars not appearing in Tables 1–3 or 8 (online).

WR#	Spectral type	Distance (kpc)	Class
11	WC8+O7.5III	0.34 ± 0.08	C
147	WN8(h)+OB	0.73 ± 0.12	WR
94	WN5	0.78 ± 0.12	WR
90	WC7	1.15 ± 0.19	WR
136	WN6b(h)	1.3 ± 0.2	WR
137	WC7+O9	1.3 ± 0.2	D
139	WN5+O6III-V	1.3 ± 0.2	C
141	WN5+O5III-V	1.3 ± 0.2	C
143	WC4+Be	1.33 ± 0.33	C
138	WN5+OB	1.38 ± 0.26	C
144	WC4	1.40 ± 0.08	WR
52	WC4	1.54 ± 0.23	WR
110	WN5b	1.55 ± 0.24	WR
9	WC5+O7*	$1.57 \pm 0.58^\star$	C
15	WC6	1.57 ± 0.49	WR
81	WC9	1.64 ± 0.34	WR
78	WN7	1.64 ± 0.03	WR
79	WC7+O5-8V	1.64 ± 0.03	C
79a	WN9ha	1.64 ± 0.03	WR
140	WC7pd+O5fcIII-I[1]	1.67 ± 0.03[2]	D
142-1	WN6	1.70 ± 0.34	WR
6	WN4b	1.80 ± 0.27	WR
121	WC9d*	$1.8 \pm 0.4^\star$	D
142a	WC7	1.83 ± 0.31	WR
105	WN9	1.9 ± 0.2	WR
111	WC5	1.9 ± 0.2	WR
134	WN6b	1.9 ± 0.2	WR
135	WC8	1.9 ± 0.2	WR
86	WC7+B0III	1.97 ± 0.47	WR
113	WC8d+O8-9*	2.0 ± 0.2	D
14	WC7	2.0 ± 0.1	WR
93	WC7+O7-9	2.0 ± 0.2	WR
114	WC5	2.05 ± 0.09	WR
115	WN6	2.05 ± 0.09	WR
70	WC9vd+B0I*	$2.1 \pm 0.4^\star$	D
47	WN6+O5.5	2.13 ± 0.44	WR
133	WN5+O9I	2.14 ± 0.07	C
70-5	WC9	2.17 ± 0.45	WR
48	WC6+O6-7V[3]...	$< 2.3^\star$	C

Continued...

Table D1 continued

WR#	Spectral type	Distance (kpc)	Class
	...+O9.5/B0Iab*		
1	WN4b	2.3 ± 0.5	WR
103	WC9d*	$2.3 \pm 0.5^\star$	D
59	WC9d*	$2.3 \pm 0.5^\star$	D
2	WN2b+B[4]	2.4 ± 0.8	WR
106	WC9d*	$2.4 \pm 0.6^\star$	D
19a	WN7	2.41 ± 0.47	WR
101	WC8	2.46 ± 0.43	WR
40	WN8h	2.48 ± 0.41	WR
95	WC9d*	2.5 ± 0.5	D
60	WC8	2.55 ± 0.45	WR
155	WN6+O9II-Ib	2.56 ± 0.56	WR
117-1	WN7	2.59 ± 0.50	WR
18	WN4b	2.6 ± 0.2	WR
22	WN7ha+O9III-V	2.6 ± 0.2	WR
23	WC6	2.6 ± 0.2	WR
24	WN6ha	2.6 ± 0.2	WR
25	O2.5If*/WN6[5]+OB	2.6 ± 0.2	C
104	WC9d+B0.5V*	2.6 ± 0.7	D
88	WC9	2.67 ± 0.54	WR
4	WC5	2.69 ± 0.49	WR
5	WC6	2.69 ± 0.84	WR
72-1	WC9	2.73 ± 0.56	WR
16	WN8h	2.77 ± 0.46	WR
85	WN6	2.8 ± 1.1	WR
111-3	WC8	2.80 ± 0.49	WR
69	WC9d+OB*	$2.8 \pm 0.6^\star$	D
75b	WC9	2.82 ± 0.58	WR
124-8	WN6	2.84 ± 0.56	WR
113-1	WN7	2.88 ± 0.56	WR
151	WN4+O5V	2.93 ± 0.65	WR
42	WC7+O7V	2.96 ± 0.53	C
57	WC8	2.97 ± 0.52	WR
75a	WC9	2.98 ± 0.60	WR

*van der Hucht (2001),
(1) Fahed et al. (2011),
(2) Monnier et al. (2011),
(3) Hill et al. (2002),
(4) Chené et al. (2014),
(5) Crowther & Walborn (2011).

This paper has been typeset from a TEX/ LATEX file prepared by the author.